

# Flexible perovskite solar cells: Material selection and structure design

Cite as: Appl. Phys. Rev. **9**, 021307 (2022); doi: [10.1063/5.0084596](https://doi.org/10.1063/5.0084596)

Submitted: 8 January 2022 · Accepted: 20 April 2022 ·

Published Online: 12 May 2022



[View Online](#)



[Export Citation](#)



[CrossMark](#)

Yumeng Xu,<sup>1</sup> Zhenhua Lin,<sup>1</sup> Jincheng Zhang,<sup>1,2</sup> Yue Hao,<sup>1</sup> Jianyong Ouyang,<sup>3</sup>  Shengzhong Liu,<sup>4</sup>  and Jingjing Chang<sup>1,2,a)</sup> 

## AFFILIATIONS

<sup>1</sup>State Key Discipline Laboratory of Wide Band Gap Semiconductor Technology, School of Microelectronics, Xidian University, 2 South Taibai Road, Xi'an 710071, China

<sup>2</sup>Advanced Interdisciplinary Research Center for Flexible Electronics, Xidian University, 2 South Taibai Road, Xi'an 710071, China

<sup>3</sup>Department of Materials Science and Engineering, National University of Singapore, 7 Engineering Drive 1, Singapore 117574, Singapore

<sup>4</sup>Key Laboratory of Applied Surface and Colloid Chemistry, Ministry of Education, Institute for Advanced Energy Materials, School of Materials Science and Engineering, Shaanxi Normal University, Xi'an 710119, China

Note: This paper is part of the special collection on Flexible and Smart Electronics.

<sup>a)</sup>Author to whom correspondence should be addressed: [jjingchang@xidian.edu.cn](mailto:jjingchang@xidian.edu.cn)

## ABSTRACT

With the rapid development of the Internet of Things, convenient and portable self-powered devices are in great need. Among all substitutes that could provide clean and sustainable power, the flexible perovskite solar cells (FPSCs) are the most attractive with the characteristics of flexibility, lightweight, high power conversion efficiency, and low cost. In this review, the recent advances of FPSCs are summarized, focusing on the materials' assessment of flexible and durable substrate, transparent electrode, low-temperature processed charge transporting layer, and mechanically robust perovskite film, with device design interspersed in each part. Finally, the challenges of FPSCs in terms of higher efficiency, higher flexibility, higher stability, and scalable fabrication are summarized.

Published under an exclusive license by AIP Publishing. <https://doi.org/10.1063/5.0084596>

## TABLE OF CONTENTS

I. INTRODUCTION .....	2	A. TiO <sub>2</sub> .....	9
II. FLEXIBLE SUBSTRATES.....	4	B. ZnO .....	10
A. Flexible polymer substrates .....	5	C. SnO <sub>2</sub> .....	12
B. Biomass substrates .....	5	D. Other ETLs .....	13
C. Metallic substrates .....	5	V. LOW-TEMPERATURE PROCESSED HTL .....	14
D. Other materials .....	6	A. Organic HTL .....	14
III. FLEXIBLE ELECTRODES .....	7	B. Inorganic HTL .....	16
A. Transparent conductive oxide .....	7	C. HTL-free FPSCs .....	17
B. Conductive polymer .....	7	VI. FLEXIBLE PEROVSKITE .....	18
C. Carbon materials .....	7	A. Additive doping .....	18
D. Metallic nanostructures .....	8	B. Other methods .....	19
1. AgNWS .....	8	VII. CHALLENGES .....	20
2. Metal mesh .....	9	A. Higher efficiency .....	20
3. Ultra-thin metal films .....	9	B. Higher flexibility .....	21
E. Flexible opaque electrodes .....	9	C. Higher stability .....	21
IV. LOW-TEMPERATURE PROCESSED ETL .....	9	D. Scalable fabrication .....	23
		VIII. SUMMARY AND FUTURE PERSPECTIVES .....	24

## I. INTRODUCTION

Solar photovoltaic (PV), among the renewable power, is taking an increasingly important role for an estimated total of 760 gigawatts (GW) over the world, adding about 139 GW in 2020, which takes over half of the annual addition of renewable power.<sup>1</sup> It has been estimated that over 50% of the total electricity generation will be provided by solar energy in 2050. According to the carbon neutrality goal, China aims to reach 1200 GW of solar power and wind power in 2030.<sup>2</sup> Among different solar cells, perovskite solar cells (PSCs) are regarded as a promising PV technology due to their low cost and high efficiency, which complements mainstream silicon solar cells. Thanks to the similar manufacturing process to organic photovoltaic (OPV) and dye-sensitized solar cells (DSSCs), PSCs have quickly entered commercialization. Companies such as Oxford PV, Greatcell, Solliance, GCL, and Microquanta are developing PSCs, some of which are even researching flexible perovskite solar cells (FPSCs) through roll-to-roll printing strategies. For instance, Oxford PV is going to manufacture commercial perovskite-on-silicon tandem solar cells in 2022.<sup>3</sup> Recently, PSCs have been rapidly developed, and the efficiency of the state-of-art device has reached 25.7%.<sup>4</sup> The perovskite materials with low-temperature processability and high flexibility are attractive in the application of various flexible devices.<sup>5–7</sup> FPSCs have the advantages of flexibility and high power-per-weight, which are favorable for the application of building PV, vehicle PV, the unmanned aerial vehicle, and aerospace craft (Fig. 1), which are high-value markets where silicon panels are not suitable due to the weight and instability in space.<sup>8</sup> Compared to the rigid devices, FPSCs could further lower the fabrication cost via the roll-to-roll method and reduce the transportation and installation costs due to their lightweight. Other types of flexible solar cells, including silicon solar cells, OPV, DSSCs, copper indium gallium selenide solar cells (CIGS), cadmium telluride solar cells (CdTe), and so on, show either low efficiency, high cost, or insufficient flexibility (see Ref. 9). In comparison, FPSCs are more suitable in the application of wearable and portable electronics due to their high efficiency, low cost, and lightweight. Nonetheless, stability issues and reduced efficiency over large areas are hurdles on the road to commercialization. In addition, by applying proper material and fabrication methods, FPSCs are also attractive in terms of biocompatibility, biodegradability,

stretchability, self-healing properties, implying broad application prospects in portable and wearable electronics as energy harvesting parts that make it convenient to use electricity for outdoor workers and rescue teams in emergency situations. Lately, FPSCs have made significant progress in flexibility, stability, and efficiency, with the power conversion efficiency (PCE) exceeding 20%<sup>10–12</sup> from 2.62% in 2013.<sup>13</sup> [Fig. 2(a)].

The rigid PSCs normally include planar structures and mesoporous structures as shown in Figs. 2(b) and 2(c). The difference between the two structures is that mesoporous structures have a mesoporous scaffold layer, which could effectively enhance the perovskite growth and induce lower series resistance and higher shunt resistance. Conventionally, the PSCs with mesoporous architecture requires a high temperature ( $>450^{\circ}\text{C}$ ) sintering process for the scaffold layer, which is not cost-effective and incompatible with flexible plastic substrates. The state-of-the-art FPSCs take planar structure to simplify their fabrication and exclude the high temperature-processed scaffold layers. Nevertheless, there are a few reports about flexible mesostructured PSCs by using low-temperature solution methods to prepare scaffold layers, such as UV exposure,<sup>14–17</sup> O<sub>2</sub> plasma,<sup>16</sup> and intense pulsed light curing.<sup>16</sup> Giacomo and co-workers constructed scaffold FPSCs with a UV-irradiated scaffold layer and a plasma-enhanced atomic layer deposition (PEALD) compact TiO<sub>2</sub> layer on indium tin oxide (ITO)/polyethylene terephthalate (PET) substrates. They achieved an efficiency of 8.4% for single cells and further improved to 9.2% with the same strategy.<sup>14,15</sup> Furthermore, they explored several alternative curing techniques for the mesoporous TiO<sub>2</sub> layer in scaffold PSCs, including UV/O<sub>3</sub> treatment, O<sub>2</sub> plasma treatment, and intense pulsed light sintering treatment. They revealed that UV/O<sub>3</sub> treatment and O<sub>2</sub> plasma treatment showed a similar effect in removing the binder of TiO<sub>2</sub> paste but required much more time compared to high-temperature sintering. Additionally, intense pulsed light sintering treatment within a few seconds proves to be effective for the binder-free TiO<sub>2</sub> film and suitable for roll-to-roll manufacturing, achieving a stabilized efficiency of 12.3% on ITO/polyethylene naphthalate (PEN) substrates.<sup>16</sup> Recently, a combination of SnO<sub>2</sub> and mesoporous-TiO<sub>2</sub> was developed as the electron transport layer (ETL) via spin coating and followed by annealing at 140–150 °C and UV-light irradiation

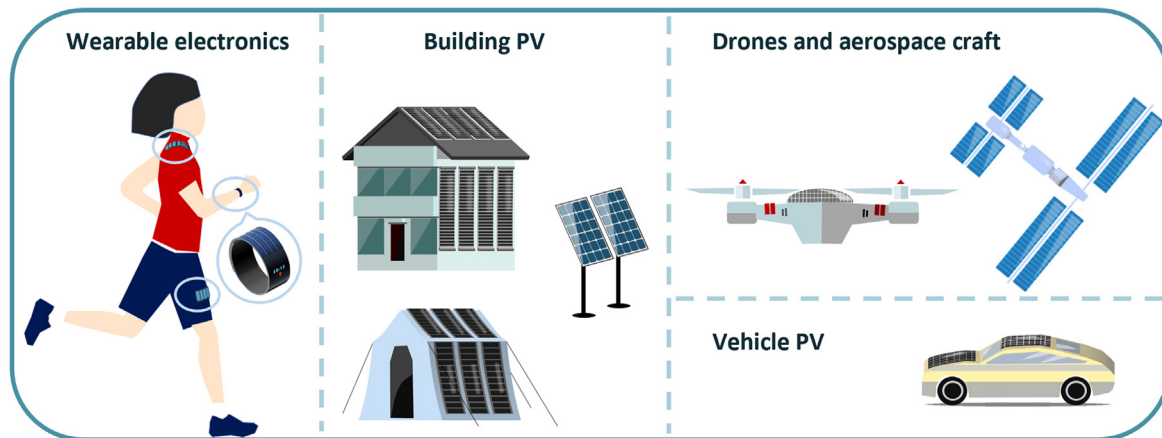
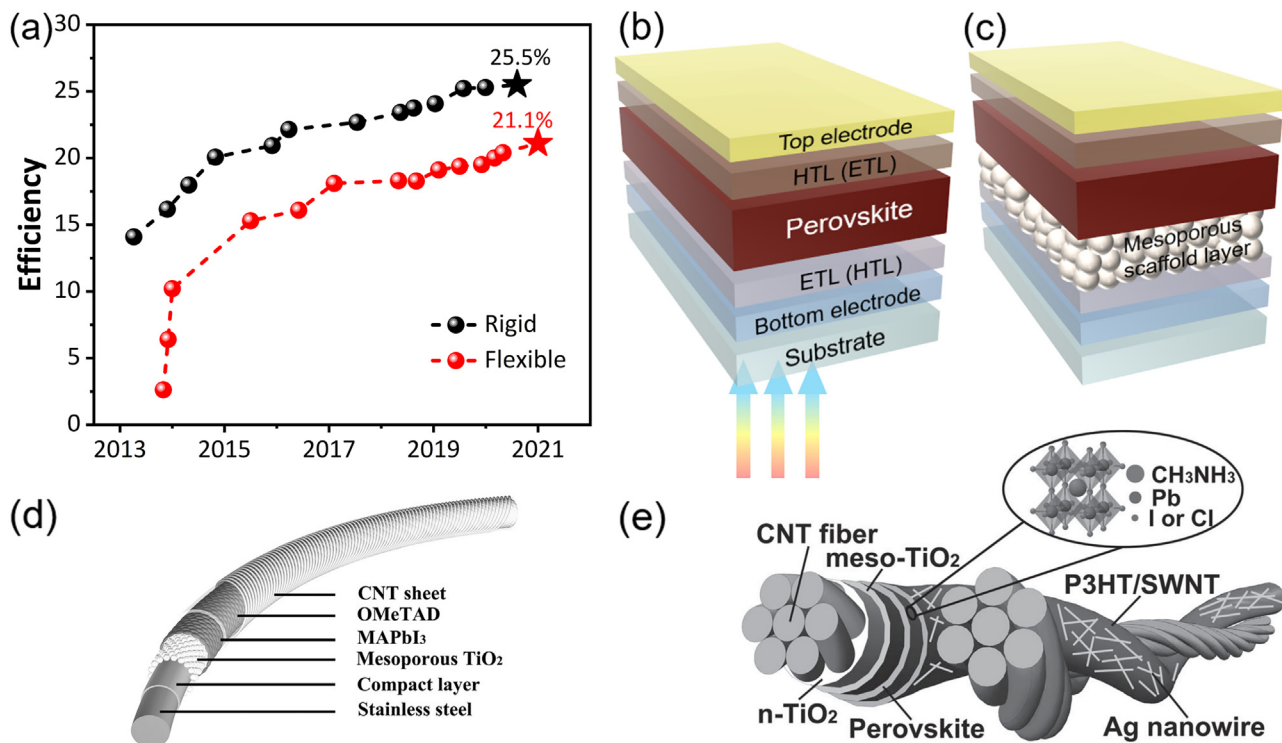


FIG. 1. Applications areas of FPSCs.



**FIG. 2.** (a) Chronological evolution of the PCE of PSCs and FPSCs since 2013. (The data of flexible devices referred to 2013,<sup>13,109</sup> 2014,<sup>140</sup> 2015,<sup>98</sup> 2016,<sup>190</sup> 2017,<sup>208</sup> 2018,<sup>85,108</sup> 2019,<sup>156–158</sup> 2020,<sup>66,67</sup> and 2021.<sup>11</sup> The data of rigid PSCs are derived from the NREL.<sup>4</sup>) Schematics of planar PSCs (b) and mesoporous PSCs (c). (d) Structure of coaxial fiber-shaped PSCs. Reproduced with permission from Qiu *et al.*, *Angew. Chem., Int. Ed.* **53**, 10425 (2014). Copyright 2014 Wiley-VCH. (e) Structure of double-twisted fibrous FPSCs. Reproduced with permission from Li *et al.*, *Adv. Mater.* **27**, 3831 (2015). Copyright 2015 Wiley-VCH.

treatment. Based on this fully solution-processed ETL, a maximum PCE of 14.8% was achieved on the ITO/PET substrate with  $0.1\text{ cm}^2$  area and 8.8% with  $12\text{ cm}^2$ .<sup>17</sup> In addition, metal substrates have also been adopted to fabricate mesoporous FPSCs for good heat resistance.<sup>18</sup> It is obvious that the mesostructured FPSCs have inferior performance to the planar counterparts, which now have a high efficiency of 21.05%.<sup>10,11</sup> In addition, the complicated processes and high cost of the scaffold structure limit their development in FPSCs.

In addition, there are fiber-shaped PSCs, which is first reported by Qiu *et al.* in 2014.<sup>19</sup> The fiber-shaped PSCs could be divided into coaxial fiber-shaped PSCs and double-twisted fibrous PSCs, as shown in Figs. 2(d) and 2(e). The former usually adopts metal wires such as Ti and stainless steel as the core and electrode. Electrochemical deposition, anodization, vapor assisted deposition, or dip-coating process are used to fabricate function layers, and the transparent electrodes are prepared by wrapping the CNT sheet, coating silver nanowire (AgNW) solution, or sputtering noble metal thin films.<sup>20–24</sup> The latter additionally entwisted a conductive wire such as CNT fiber to adjunctively transfer electric current to external circuits.<sup>25</sup> For the fiber-shaped PSCs, insufficient flexibility and poor corrosion resistance are mainly caused by the metal wires, limiting their performance. Other alternative materials such as CNT fibers and PEN/ITO strips are favorable to realize ultra-flexible devices.<sup>25,26</sup> To make a further step in wearable electronics, Qiu *et al.* assemble the PSC fibers based on electrospun perovskite composite nanofibers into the fabric. However, it

demonstrated severe damage during weaving and very low efficiency.<sup>27</sup> In comparison, there are reports about planar type flexible devices directly fabricated on the textile by mechanically attaching to the textile<sup>28</sup> or coating the polyurethane layer on textile before all the fabrication steps to form a smooth surface, which is vital to the quality of subsequent films.<sup>29</sup> Nonetheless, the fiber-shaped PSCs suffer from poor efficiency (see Table I) and complicated fabrication processes, which are difficult to control the thickness and quality of functional films, inhibiting their further development. Overall, the vast majority of FPSCs is fabricated in a planar geometry, and this review primarily focuses on the constituent materials and challenges of planar FPSCs.

Generally, standard planar FPSCs comprise the flexible substrate, bottom electrode, ETL, perovskite film, hole transport layer (HTL), and top electrode as shown in Fig. 2(b). Usually, the rigid device could be flexible only by changing the substrate to a flexible one. A variety of materials have been chosen as flexible substrates such as polymers, metals, papers, and other novel substrates. Polymer substrates such as PET and PEN are most popular in advanced FPSCs, considering the high transparency, favorable flexibility, and low cost. Among the components in FPSCs, an outstanding transparent conductive electrode with excellent electrical, optical, and mechanical properties is vital to the development of highly efficient FPSCs. Since the light crosses over the transparent electrode before being absorbed by active materials and the photogenerated charges are finally collected by this transparent electrode, the optical transparency and electrical conductivity of

**TABLE I.** Summary of non-mainstream types of FPSCs.

Type	Configuration	PCE (%)	References
Mesoporous FPSCs	PET/ITO/ (ALD) compact TiO <sub>2</sub> /(UV irradiation) mesoporous TiO <sub>2</sub> /CH <sub>3</sub> NH <sub>3</sub> PbI <sub>3-x</sub> Cl <sub>x</sub> /Spiro-OMeTAD/Au	8.4	14
	PEN/ITO/(e-beam) compact TiO <sub>2</sub> /(intense pulsed light) mesoporous TiO <sub>2</sub> / Perovskite/Spiro-OMeTAD/Au	12.3	16
Fiber-shaped FPSCs	PET/ITO/SnO <sub>2</sub> /mesoporous TiO <sub>2</sub> (UV irradiation)/CH <sub>3</sub> NH <sub>3</sub> PbI <sub>3</sub> /Spiro-OMeTAD/Au	14.8	17
	Stainless steel/compact layer/mesoporous TiO <sub>2</sub> /CH <sub>3</sub> NH <sub>3</sub> PbI <sub>3</sub> /Spiro-OMeTAD/CNT sheet	3.3	19
	Ti wire/compact TiO <sub>2</sub> /mesoporous TiO <sub>2</sub> /CH <sub>3</sub> NH <sub>3</sub> PbI <sub>3</sub> /Spiro-OMeTAD/AgNWs	3.85	23
	Stainless steel/ZnO nanorod/CH <sub>3</sub> NH <sub>3</sub> PbI <sub>3</sub> /Spiro-OMeTAD/CNT	3.8	22
	Ti/compact TiO <sub>2</sub> /mesoporous TiO <sub>2</sub> /CH <sub>3</sub> NH <sub>3</sub> PbI <sub>3-x</sub> Cl <sub>x</sub> /Spiro-OMeTAD/Au	5.35	20
	Ti/compact TiO <sub>2</sub> /TiO <sub>2</sub> nanotubes/Perovskite/CNTs	7.1	21
	CNT/compact TiO <sub>2</sub> /mesoporous TiO <sub>2</sub> /CH <sub>3</sub> NH <sub>3</sub> PbI <sub>3-x</sub> Cl <sub>x</sub> /P3HT/SWNT/Ag nanowire/CNT	3.03	25
	Ti wire/compact TiO <sub>2</sub> /mesoporous TiO <sub>2</sub> /CH <sub>3</sub> NH <sub>3</sub> PbI <sub>3-x</sub> Cl <sub>x</sub> (vapor-assisted deposition)/Spiro-OMeTAD/Au/Au wire	10.79	24
	Ag yarn/P3HT/CH <sub>3</sub> NH <sub>3</sub> PbI <sub>3</sub> -PVP nanofibers (electrospinning)/PC <sub>61</sub> BM-SnO <sub>2</sub> /carbon nanofiber (double-twisted fibrous PSC)	15.7	27
	PEN/ITO (strip) /TiO <sub>2</sub> /CH <sub>3</sub> NH <sub>3</sub> PbI <sub>3</sub> /CNT	9.49	26
Textile-based planar FPSCs	PEN/ITO/SnO <sub>2</sub> /PCBM/CH <sub>3</sub> NH <sub>3</sub> PbI <sub>3</sub> /Spiro-OMeTAD/Au/ductile elastomer/textile (simply attached)	14.3	28
	Polyester fabric/polyurethane/PEDOT:PSS-CNT/ PEDOT:PSS /CH <sub>3</sub> NH <sub>3</sub> PbI <sub>3</sub> /PCBM/Ag	5.72	29

the transparent electrode directly impact the device performance of PSCs.<sup>30</sup> Additionally, the damage to FPSCs during bending is usually caused by the fracture of ITO, which is the mostly used bottom electrode in FPSCs. Therefore, the challenge remains in the development of highly flexible transparent electrodes with low sheet resistance and high transparency. Efforts have been made to replace the fragility and expensive ITO with other superflexible and low-cost materials such as conductive polymers, carbon materials, metal nanomaterials, and composite materials. Depending on the direction of incident light transportation, the PSCs are classified into n-i-p and p-i-n structures. Specifically, for n-i-p type devices, the incident light successively crosses over the cathode, ETL, and reaches the perovskite, whereas the light will pass through the anode and HTL before being absorbed by the active layer in p-i-n type devices.<sup>31</sup> For the charge transporting layers, a low processing temperature is necessary because the mostly used flexible substrates are sensitive to temperature. As for the perovskites, a moderate flexing could be sustained due to the relatively low Young's moduli ranging 10–20 GPa.<sup>32</sup> Further improvements in the flexibility and stability of perovskite film are undergoing.

In this review, we start with a brief introduction of different types of FPSC, in which planar FPSC is mainly studied in the whole review. Then, the FPSCs are summarized and assessed critically from the views of material selection and structure design for different functional layers of planar FPSCs, including the flexible substrate, the transparent electrode, charge transporting layers, and the more flexible perovskite layer. Following this, the current challenges faced by the FPSCs will be categorized and discussed, mainly concentrating on the improvement of efficiency, flexibility, stability, and scalable fabrication. In the end, challenges and summary of FPSCs are provided.

## II. FLEXIBLE SUBSTRATES

For the PSCs, the key factor to realizing flexibility lies in the substrate. The conventional substrate in PSCs is glass, which is highly transparent and robust. However, the rigid property does not suit the application of FPSCs. Generally, the flexible substrates must meet the requirements of flexible devices in several aspects. (1) Mechanical properties: the substrates should be robust enough to sustain the subsequent process steps and wear during daily use. In addition, the substrates should be flexible enough to withstand the deformation during the bending process. Moreover, stretchability is an additional advantage in realizing twistable and stretchable PSCs. (2) Optical transmittance: high optical transparency ensures that as many incident photons as possible could reach the perovskite layer and be absorbed. The special case is that for opaque substrates such as metal foils, top illumination is feasible by using the transparent top electrode. In addition, the high haze of substrates is beneficial for light utilization. (3) Chemical stability: the flexible substrate should be inert for the solvents that are frequently used in PSCs. (4) Thermal stability: to avoid shape deformation and substrate damage, the flexible substrate must sustain the highest processing temperature during the preparation of functional layers. Moreover, the thermal expansion coefficient of the substrate should be consistent with the adjacent layer to prevent mechanical stress and cracking during the variation of temperature. (5) Surface roughness: the optoelectrical performance of subsequent layers especially the bottom electrode is heavily dependent on the surface morphology of the substrate. (6) Hermeticity: the water vapor and oxygen transmission will lead to fast device degradation. Thus, the substrate with low gas permeability helps to obtain a stable device. (7) Environmentally friendly: environmental issues have received serious attention, and there is a great need for renewable and bio-degradable materials for substrates. In addition to the widely used polymer

**TABLE II.** Property parameters for flexible transparent substrates.

Substrate	Optical transmittance (average) (%)	Max temperature (°C)	Modulus (GPa)	WVTR (g/m <sup>2</sup> ·day)	CTE (ppm/°C)
PET	91.8 <sup>43</sup>	150 <sup>33</sup>	2–4.1 <sup>314</sup>	1.1 <sup>48</sup>	15–33 <sup>314</sup>
PEN	87.2 <sup>43</sup>	180 <sup>33</sup>	0.1–0.5 <sup>314</sup>	4 <sup>303</sup>	20 <sup>314</sup>
Flexible glass	>90 <sup>48</sup>	700 <sup>48</sup>	...	<7 × 10 <sup>-6</sup> <sup>48</sup>	2.5 ppm/°C
PI	49.2 <sup>43</sup>	400 <sup>314</sup>	2.5 <sup>314</sup>	...	8–20 <sup>314</sup>
Colorless PI	87.9 <sup>43</sup>	>350 <sup>315</sup>	2.8–4.5 <sup>316</sup>	...	29.2 <sup>315</sup>
Nanopaper	90 <sup>36</sup>	300 <sup>36</sup>	7.4–14 <sup>317</sup>	...	12–28.5 <sup>317</sup>
ChNF paper <sup>a</sup>	91.7 <sup>43</sup>	150 <sup>43</sup>	4.3 <sup>43</sup>	...	17.5 <sup>43</sup>
Mica	>90 <sup>53</sup>	600 <sup>53</sup>	...	...	1 ppm/°C

<sup>a</sup>WVTR: water vapor transmission rate, CTE: coefficient of thermal expansion, PET: polyethylene terephthalate, PEN: polyethylene naphthalate, PI: polyimide, ChNF paper: Chitin nanofibers paper.

substrates, novel materials such as paper, cellulose, and photoresist are also developed to realize ultra-flexible and bio-friendly devices. Table II summarizes the properties of flexible transparent substrates.

### A. Flexible polymer substrates

Polymeric materials such as PET and PEN are popular in the application of flexible substrates due to the advantages of low cost, high optical transmittance, favorable flexibility, and so on. However, the large coefficient of thermal expansion of polymer substrates does not match with other functional layers and the limited processing tolerance temperature restrains their applications. In terms of the deformation of plastic substrates under heating, PET and PEN have no obvious deformation below 150 and 180 °C, respectively. The higher temperature tolerance of PEN is associated with the naphthalene rings instead of benzene in PET.<sup>33</sup> For the polymer/ITO substrates, their original sheet resistance values can be maintained until the temperature rises to 200 and 250 °C for PET and PEN substrates, respectively [see Fig. 3(a)]. However, generally, the temperature exceeding 100 °C will induce a slight deformation curvature as illustrated in Figs. 3(b) and 3(c), which is mainly arising from the residual stresses during the deposition of the ITO film.<sup>33</sup> Therefore, it is quite necessary to lower the processing temperature when fabricating functional layers upon polymer substrates. By comparison, polyimide (PI) is more thermal stable with a higher glass transition temperature of over 350 °C, but the faint yellow film has an inferior optical transmittance.<sup>34</sup> Colorless polyimide (CPI) has high transparency in the visible region with a UV-cut off at 400 nm.<sup>30</sup> In addition, the vapor penetration of polymer substrates is not satisfying for the long-term stability of flexible devices.

### B. Biomass substrates

Considering the environmental pollution of the plastic substrate, various biomass substrates that are biodegradable, renewable, and biocompatible have been explored in the fields of FPSCs. Paper substrates that have advantages of high thermal stability exceeding 200 °C, high flexibility even foldability [see Fig. 3(d)], and low production cost exhibit the possibility of portable and disposable applications in flexible green electronics. In addition, these paper-based devices can be trimmed by scissors or hand easily and disposed by incineration.<sup>35–39</sup>

A variety of paper substrates, including opaque cellulose paper, transparent nanopaper, and cellophane paper, have been used in PSCs and most are commercially available. The opaque cellulose paper substrates offer advantages of low cost and bio-friendly nature, but with high surface roughness, leading to the lower efficiency for flexible devices.<sup>35,38</sup> On the contrary, the nanopaper has a high optical transmittance of nearly 90% with a high haze [Fig. 3(e)], which is advantageous for light utilization in solar cells. In addition, the nanopaper demonstrated excellent thermal stability up to 300 °C, a low thermal expansion coefficient of about 12–28.5 ppm/K, and a smooth surface (root mean square (RMS) roughness of 6.98 nm), which is attractive in the fabrication of high-quality functional layers.<sup>36</sup> With advantages of high flexibility, high foldability, and high smoothness (RMS roughness of 8.89 nm), the cellophane paper-based FPSCs realized ultra-flexibility, preserving 97.6% of the original PCE after bending with a radius of 0.3 mm and excellent foldability, which enabled the devices to have properties of size compactness and shape transformation.<sup>37,39</sup>

Interestingly, Zou's research group has explored several biomass materials, including bamboo-derived cellulose nanofibrils,<sup>40</sup> polylactic acid,<sup>41</sup> and silk,<sup>42</sup> which are ultra-flexible and highly transparent along with biocompatible and comfortable to human skin [see Figs. 3(f) and 3(g)]. The corresponding FPSCs demonstrated efficiencies of around 11%.<sup>40,41</sup> In addition, the malleable and pliable silk-derived electrodes demonstrated reversible plasticization with the help of water vapor, enabling the fabrication of deformable and stretchable PSCs.<sup>42</sup> Moreover, chitin is also promising in fabricating transparent paper substrates for flexible devices. The mechanical robust and biofriendly chitin nanofiber transparent paper has excellent transmission properties at entire visible wavelengths [91.7% at 550 nm, see Fig. 3(h)] and good thermal stability with no noticeable thermal decomposition up to 170 °C by thermogravimetric analysis. Additionally, it also demonstrated a small coefficient of thermal expansion of 17 ppm/K without T<sub>g</sub> and an elastic modulus of 4.3 GPa.<sup>43</sup>

### C. Metallic substrates

Metallic foils, such as Ti and Cu, with a thickness of more than 100 μm are also employed as flexible substrates in FPSCs, owing to the low cost, excellent mechanical ductility, and outstanding barrier

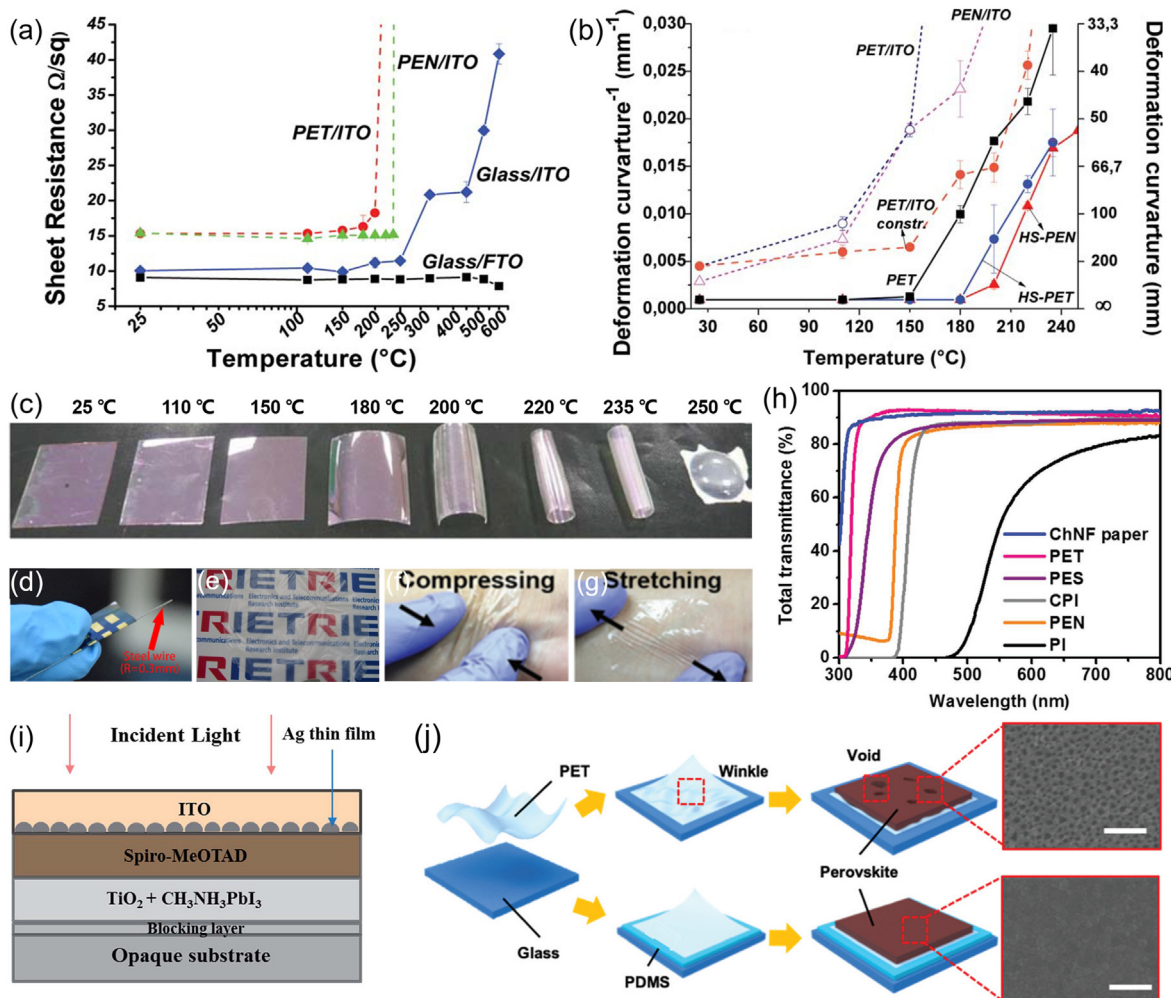


**FIG. 3.** (a) Sheet resistances of flexible substrates and glass substrates after thermal treatment for 30 min at different temperatures. (b) Deformation curvature of different polymer films and polymer/ITO substrates after treating under different temperatures. (c) Photos of PET/ITO foils after thermal treatment. (a)–(c) Reproduced with permission from Zardetto *et al.*, *J. Polym. Sci., Part B* **49**, 638 (2011). Copyright 2011 Wiley-VCH. (d) Image of FPSCs based on the cellophane substrate in a bending radius of 0.3 mm. Reproduced with permission from Li *et al.*, *Sol. Energy* **188**, 158 (2019). Copyright 2019 Elsevier. (e) Image of the nanopaper substrate. Reproduced with permission from Jung *et al.*, *Sol. Energy* **139**, 458 (2016). Copyright 2016 Elsevier. Demonstration of compressing (f) and stretching (g) of the chitin paper that is attached to human skin. (h) Transmittance spectra of the chitin nanofiber paper compared to other polymers. (f)–(h) Reproduced with permission Jin *et al.*, from *Adv. Mater.* **28**, 5169 (2016). Copyright 2016 Wiley-VCH. (i) Structure of FPSCs based on the Ti substrate and Ag/ITO top electrode. Reproduced with permission from Lee *et al.*, *J. Mater. Chem. A* **3**, 14592 (2015). Copyright 2015 Royal Society of Chemistry. (j) Illustration of the dependence of film quality based on different preparation methods. Reproduced with permission from Lee *et al.*, *Energy Environ. Sci.* **12**, 3182 (2019). Copyright 2019 Royal Society of Chemistry.

property.<sup>18,44–46</sup> Moreover, the smoother surface of metal foils compared to other flexible substrates is favorable in obtaining a flatter functional layer and suppressing charge recombination. In addition, the highly conductive metal foils could also play the role of the bottom electrode. The inherently high thermal resistance and mechanical stability of metallic substrates enable the direct deposition of charge transport layers, such as  $\text{TiO}_2$  and  $\text{NiO}_x$ , which need a high-temperature crystallization process.<sup>44</sup> In addition, due to the opaque nature of metal foils, transparent top electrodes, such as ITO, transparent metal nanomaterials, or carbon nanomaterials, are needed to let photons in as shown in Fig. 3(i).<sup>44,45,47</sup>

#### D. Other materials

Willow glass, also known as flexible glass, is a flexible and highly transparent substrate with advantages of low coefficient of thermal expansion, low surface roughness, favorable hermeticity with neglectable water vapor transmission rate, good dimensional, and thermal stability with the temperature resistance up to 700 °C.<sup>48,49</sup> Moreover, as the thickness of willow glass is below 200  $\mu\text{m}$  and usually 50  $\mu\text{m}$ , it is suitable for the roll-to-roll process such as screen printing, slot die coating, and lamination.<sup>50,51</sup> Additionally, according to the research by Burst *et al.*, ITO/willow glass has excellent mechanical durability with no appreciable change in sheet resistance after 25–50 k bending

cycles, while the commercial ITO/PET suffers ~50%–100% increase in sheet resistance and obvious degradation in light transmittance.<sup>48</sup> However, the bending radius of willow glass is at the scale of centimeters because of its intrinsically brittle property. In addition, willow glass is notably more expensive than polymer materials. To sum up, willow glass, which combines the advantages of glass substrates and plastic substrates, is suitable for applications that have less requirement for small radius bending.

Additionally, photoresist Norland Optical Adhesive 63 (NOA63) is favorable to the fabrication of shape recoverable devices due to the shape memory characteristic. In particular, it has high-temperature resistance and better mechanical durability with a bending curvature radius as low as 0.7 mm compared to PET and PEN substrates.<sup>52</sup> Muscovite mica, which has high optical transmittance over 90% in the visible range, ultra-flatness at an atomic level, high-temperature tolerance up to 600 °C, and extraordinary impermeability against water and oxygen, is also used in FPSCs as the flexible transparent substrate, and the related devices show the best efficiency of 9.67%.<sup>53</sup> In addition, stretchable polydimethylsiloxane (PDMS) substrate is beneficial in realizing wearable electronics, with a high efficiency of 19.15% achieved by Chen *et al.*<sup>54,55</sup>

By adopting polymer substrates within a few micrometers thick, ultra-thin and lightweight FPSCs with high power-per-weight could be fabricated. However, the ultrathin substrates usually suffer from technical difficulties such as handling problems and distortion including wrinkling and warping during the coating process. The generally adopted method is physically adhered to the ultrathin substrate through van der Walls force onto the planar rigid support to enable all subsequent procedures. After completing the devices, the support could be peeled off without causing any damage. Directly placing ultrathin films onto rigid glass substrates would inevitably cause wrinkles on the flexible substrates and further result in inferior surface morphology of perovskite films. Choi *et al.* introduced the PDMS layer to form conformal contact between 2.5 μm thick PET and glass substrate, realizing a smooth PET film and a high-quality perovskite layer as illustrated in Fig. 3(j).<sup>56</sup> Feng *et al.* fabricated FPSCs on the thin photoresist substrates, which are spin-coated and solidified on the hydrophobic glass substrates.<sup>57</sup> Yang *et al.* laminated thin and flexible substrates onto 100 μm thick hardened PET protection film.<sup>58</sup> Kang *et al.* employed a planar PDMS film as supporting for the 1.3 μm thick PEN substrate.<sup>59</sup> Jin *et al.* spin-coated NOA63/CPI as substrates on the glass slide by applying polymethyl methacrylate (PMMA) film as a detachment-promoting layer.<sup>52</sup>

### III. FLEXIBLE ELECTRODES

The transparent conductive electrode is an essential component in the PSCs since the transparent electrode is the optical window to let photons in before being absorbed by the perovskite film and collects the finally generated carriers.<sup>30</sup> Generally, the degradation and failure of FPSCs at a small bending radius originate from the breakage of metal oxide electrodes.<sup>60–63</sup> Therefore, it is indispensable to develop a highly flexible transparent electrode with good electrical, optical, and mechanical properties to attain efficient and stable FPSCs. In this section, broadly used flexible transparent electrodes will be discussed, including metal oxides, also known as transparent conducting oxide (TCO), poly(3,4-ethylenedioxythiophene):poly(styrenesulfonate) (PEDOT:PSS), carbon nanotubes (CNTs), graphene, AgNW, ultra-thin metal films

(UTMFs, ~10 nm thick), metal meshes, and so on. In addition, flexible opaque electrodes, including metal films (60–100 nm thick) and carbon pastes, will also be summarized.

#### A. Transparent conductive oxide

TCO coated on the polymer substrate is the most frequently used bottom electrode in PSCs, including ITO, fluorine-doped tin oxide (FTO),<sup>64,65</sup> indium zinc oxide (IZO),<sup>49</sup> aluminum-doped zinc oxide (AZO),<sup>49</sup> and so on. Due to the low-temperature fabrication process, good chemical stability, and excellent device performance, ITO is the most popular transparent electrode in FPSCs with a recorded PCE of over 20%.<sup>11,66–68</sup> However, high material cost and vacuum deposition method limit its wide commercial application in FPSCs. In addition, the fragile ITO could not satisfy the needs of flexible devices, and the cracks that emerged during bending at a small curvature radius of less than 10 mm will lead to severe device deterioration as shown in Fig. 4(a). By reducing the thickness of ITO films, the mechanical flexibility of ITO-based devices could be improved.<sup>69</sup> In addition, the light absorption of ITO film at a long wavelength restricts solar energy utilization.

#### B. Conductive polymer

Replacing the brittle ITO electrode with conductive polymer PEDOT:PSS in flexible devices [Fig. 4(b)] is a good choice due to the superflexible properties of PEDOT:PSS, which is also advantageous for excellent light transmittance, low cost, and roll-to-roll processability. The tunable work function of PEDOT:PSS enables good energy level alignment and can be used as an anode or cathode. Although it has low pristine electrical conductivity, many modification methods have been developed to lift its conductivity to 4000 S/cm by removing the insulating PSS or phase separation.<sup>70</sup> Strong acid treatment is effective in enhancing the electrical conductivity of PEDOT:PSS but will damage polymer substrates. This problem can be solved by replacing strong acid with mild acid or applying the acid-assisted transfer-printing method to avoid direct contact.<sup>71,72</sup> Moreover, the commonly used acid-free strategies, including additive doping such as dimethyl sulfoxide, ethylene glycol, Zonyl FS-300, Zn(TFSI)<sub>2</sub>, and post-treatment such as oxygen-plasma treatment, are effective in conductivity enhancement of PEDOT:PSS.<sup>8,70,73–75</sup>

#### C. Carbon materials

Owing to the cheap raw materials, excellent mechanical flexibility, and inertness to different physical and chemical environments, carbon materials such as CNTs and graphene are appealing candidates for flexible transparent electrodes [Fig. 4(c)].

CNTs are classified into single-walled carbon nanotubes, double-walled carbon nanotubes, and multi-walled carbon nanotubes according to the number of graphene cylinders.<sup>76</sup> Being regarded as an efficient electrode candidate to replace ITO electrodes, CNT film has the advantages of low cost, good thermal stability, high optical transparency, ultra-flexibility, and so on. However, the rougher surface morphology of CNT film will result in insufficient contact and many shunt paths, which could be solved by laminating CNT film before depositing the charge transporting layer.<sup>77,78</sup> In addition, the low electrical conductivity and hydrophobic surface of CNT film could be improved by proper doping such as diluted nitric acid, PEDOT:PSS,

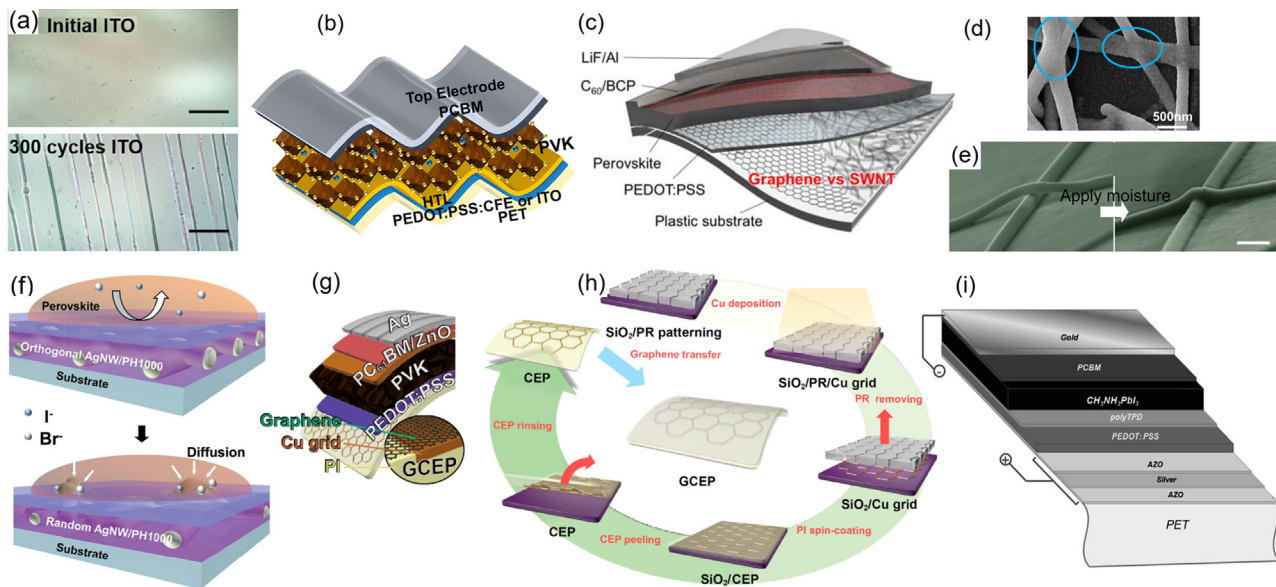


**FIG. 4.** (a) Optical images of the PET/ITO electrode before and after the bending process. (b) Device configuration of FPSCs based on the PEDOT:PSS electrode. (a) and (b) Reproduced with permission from Hu *et al.*, Joule **3**, 2205 (2019). Copyright 2019 Elsevier. (c) Device configuration of FPSCs based on the graphene or CNT electrode. Reproduced with permission from Jeon *et al.*, J. Phys. Chem. Lett. **8**, 5395 (2017). Copyright 2017 American Chemical Society. (d) SEM images of AgNW/FZO welded composite electrodes. Reproduced with permission from Han *et al.*, J. Mater. Chem. A, **3**, 5375 (2015). Copyright 2015 Royal Society of Chemistry. (e) SEM images of Ag wire-wire junctions before and after moisture treatment. Reproduced with permission from Liu *et al.*, Nano Lett. **17**, 1090 (2017). Copyright 2017 American Chemical Society. (f) Schematic of silver halide formation in PSCs fabricated on orthogonal (upper) and random (bottom) AgNW electrodes. Reproduced with permission from Kang *et al.*, J. Mater. Chem. A **7**, 1107 (2019). Copyright 2019 Royal Society of Chemistry. (g) Structure of FPSCs based on the Cu mesh electrode. (h) Fabrication process of a Cu mesh/graphene composite electrode. (g) and (h) Reproduced with permission from Jeong *et al.*, Nano Lett. **20**, 3718 (2020). Copyright 2020 American Chemical Society. (i) Structure of FPSCs based on the AZO/Ag/AZO electrode. Reproduced with permission from Roldán-Carmona *et al.*, Energy Environ. Sci. **7**, 994 (2014). Copyright 2014 Royal Society of Chemistry.

and MoO<sub>3</sub>.<sup>79,80</sup> Nevertheless, the high sheet resistance of the CNT film is still the main limitation of CNT electrode in FPSCs.

Graphene, which is usually fabricated by the chemical vapor deposition method, has received much attention due to its smooth surface, high transparency, and good electrical conductivity. The high light transmittance of the graphene film, especially at the long wavelength region, could facilitate light utilization owing to the lessened absorption of incident light by the electrode.<sup>78</sup> Although graphene has theoretically high carrier mobility, the actual electrical conductivity of graphene is not satisfactory due to the poor film morphology.<sup>81</sup> Doping strategy is useful in improving the performance of graphene electrodes. MoO<sub>3</sub> and AuCl<sub>3</sub> are the common doping materials in graphene electrodes to decrease sheet resistance from more than one thousand ohms to hundreds of ohms or even tens of ohms with improved energy level alignment to facilitate transmission and collection of charge carriers.<sup>82,83</sup> In addition, increasing the number of stacked graphene layers will also help to improve the electrical performance of graphene electrodes, while at the expense of reduced optical transparency.<sup>84</sup> In addition, the chemical bonding between the graphene layer and polymer substrate by an interlayer is necessary to strengthen the adhesion of graphene sheets.<sup>85</sup>

#### D. Metallic nanostructures

Although carbon materials demonstrate superior light transmittance to other electrodes, their high sheet resistance limits their device

performance. By comparison, metallic electrodes exhibit extremely low sheet resistance. Considering high electrical conductivity and excellent flexibility, metal nanowires, UTMFs, and metal meshes are feasible substitutes for ITO electrodes in FPSCs, although the optical transmittance has slight loss due to the reflection of incident light.

#### 1. AgNWs

AgNWs with very low sheet resistance and high mechanical flexibility is a promising electrode candidate. It can be fabricated by a simple solution process and is suitable for the large-scale manufacturing process.<sup>86,87</sup> The main problem with AgNWs is the chemical stability. The chemical reaction of Ag atoms with halides would decompose the light absorbing layer and AgNW electrode, resulting in depressed efficiency and even device failure. The discontinuous and rough AgNW films are likely to induce shunting channels through the perovskite layer, resulting in current leakage and deterioration of photovoltaic performance. A proper isolation layer deposited between AgNW and perovskite film is needed to obtain a flat surface and inhibit the corrosion process, such as TCO like ITO,<sup>88</sup> ATO,<sup>61</sup> FZO,<sup>89</sup> ZnO,<sup>90</sup> conductive polymer PEDOT:PSS,<sup>41</sup> and graphene.<sup>91</sup> In addition, the coated material is also advantageous to improve the adhesion of the AgNW film to polymer substrates and weld the junction sites of nanowires by capillary force effect to reduce contact resistance as shown in Figs. 4(d) and 4(e).<sup>41,89,91,92</sup> However, although the high haze ratio can

promote light utilization, the light transmittance of the AgNW film is not ideal due to the reflection of incident light by Ag fibers and the potential light absorption of the coated isolation layer.<sup>90,93</sup> In addition, novel deposition strategy such as capillary printing also helps to acquire AgNW film with better film morphology and chemical stability as shown in Fig. 4(f).<sup>59</sup>

## 2. Metal mesh

Metal meshes, including Ag, Au, Ni, and Cu mesh, exhibit good mechanical flexibility, moderate optical transparency, and low sheet resistance, even only a few tenths of an ohm.<sup>94</sup> Similar to other metal electrodes, device stability caused by the ion migration and chemical reaction is the major problem in the metal mesh electrodes. Furthermore, the thin metal grids are fragile and easily break during the repeated bending process. Generally, composite electrode by combining metal mesh with TCO, conducting polymer or carbon nanomaterials is an effective strategy to improve chemical stability and enhance mechanical durability such as the Cu mesh/graphene electrode in Fig. 4(g).<sup>94,95</sup>

Another problem in the application of metal mesh electrodes is that the thermal conductivity between the metal mesh and the substrate is not uniform, which is not conducive to inducing the growth of uniform and high-quality perovskite film.<sup>58</sup> Moreover, the metal mesh electrodes are usually manufactured using expensive and complicated photolithography and etching processes [Fig. 4(h)].<sup>95</sup> New methods that are cheap and efficient have been developed to prepare metal mesh electrodes, for example, nano-imprinting lithography.<sup>58</sup>

## 3. Ultra-thin metal films

Contrary to the rough metal nanowires film and an uneven metal mesh electrode, the UTMFs (Au, Ag, or Cu) have the advantage of a highly smooth surface to ensure the growth of high-quality perovskite film. Its excellent mechanical ductility is quite suitable for the application of flexible devices. For the UTMFs electrode, the thickness of the metal film (generally about 10 nm thick) needs to be adjusted carefully to balance optical transparency and electrical conductivity to acquire optimized photoelectric performance.<sup>44</sup> In addition, seed layer and modification layer such as MoO<sub>3</sub>, and Cu are usually used to control the nucleation and growth kinetics of metal film to achieve uniform and high-quality metal films.<sup>96</sup> Furthermore, there are oxide/metal/oxide structured electrodes, in which the bottom and top oxides are the same such as AZO or TiO<sub>2</sub>, as shown in Fig. 4(i). The bottom oxide plays the role of the seed layer and the top oxide works as a protective layer to improve long-term stability.<sup>37,97</sup>

## E. Flexible opaque electrodes

Metal films such as Au, Ag, and Cu films with a thickness of about 50–100 nm are widely applied in advanced FPSCs as opaque top electrodes.<sup>98–100</sup> The high electrical conductivity of metal films and good electrical contact with adjacent layers lead to high efficiency in the corresponding devices. However, the poor environmental and chemical stability of metal films electrode restrict their applications.<sup>101,102</sup> Although improvements such as the insertion of a thin chromium barrier layer have been developed to suppress the device deterioration, the protective performance could not last long for years.<sup>8</sup>

In comparison, low-cost opaque carbon electrodes developed by Han *et al.* are promising candidates to substitute metal films due to the approaching work function (~5.0 eV) with Au electrode (~5.1 eV) and excellent chemical inertness and water resistance.<sup>103</sup> Carbon pastes with low-temperature processability are suitable for the application in flexible devices and typically composed of CNTs, graphite, carbon black, and additives.<sup>103,104</sup> Moreover, carbon pastes could be easily prepared by printable fabrication techniques, holding promise for mass production.<sup>61</sup> However, the inadequate electrical conductivity of opaque carbon electrodes and the poor contact with adjacent materials result in insufficient charge collection and inferior device efficiency compared to their metal film counterparts. Further development is required to improve the electrical properties of carbon paste electrodes such as adjusting the compositions or adding inter-layers.<sup>105</sup> Also, the carbon-based HTL-free FPSCs will be discussed in Sec. V C.

## IV. LOW-TEMPERATURE PROCESSED ETL

The electron transporting material is vital in selectively extracting and transporting photo-generated electrons from the active layer to the cathode. Even though ETL-free planar PSCs have been reported, their efficiencies are lower than the cells containing ETL.<sup>106,107</sup> A suitable ETL should have properties including a suitable energy level for efficient electron injection, wide bandgap to minimize parasitic light absorption, and high electron mobility to quickly transport electrons from the light absorbing layer to the electrode, avoiding charge accumulation at the interface of ETL/perovskite layer to reduce hysteresis.<sup>108</sup> When the ETL is introduced in flexible devices, the low-temperature processing ability of ETL is also necessary. The traditional electron transporting materials such as TiO<sub>2</sub>, ZnO, and SnO<sub>2</sub> are widely applied in FPSCs, and other oxides such as Zn<sub>2</sub>SnO<sub>4</sub>, Nb<sub>2</sub>O<sub>5</sub>, and organic materials are undergoing rapid development.

### A. TiO<sub>2</sub>

Originated from solid-state dye-sensitized solar cells, the commonly used electron transport material in PSCs is TiO<sub>2</sub>, which conventionally requires a high processing temperature above 450 °C to get better crystallinity and conductivity.<sup>109–111</sup> However, the *in situ* high-temperature crystallization processing is unfavorable for cost-effective manufacture, and especially not compatible with temperature-sensitive polymer substrates. There have been reports about the low-temperature processed TiO<sub>2</sub> ETL on the rigid substrates. Wojciechowski and co-workers reported a low temperature route to fabricate compact TiO<sub>2</sub> ETL by spin-coating the colloidal dispersion of TiO<sub>2</sub> particles and drying at 150 °C.<sup>112</sup> Snaith and co-workers presented the fabrication of a compact layer composed of graphene and TiO<sub>2</sub> nanoparticles below 150 °C.<sup>113</sup> Yella and co-workers adopted the chemical bath deposition technique to deposit the TiO<sub>2</sub> layer by hydrolysis of TiCl<sub>4</sub> at 70 °C.<sup>114</sup> In addition, Zhou and co-workers prepared TiO<sub>2</sub> nanocrystals from a non-hydrolytic sol–gel route at 80 °C, and then the suspension of TiO<sub>2</sub> nanocrystals was spin-coated on ITO substrates and annealed at 150 °C.<sup>115</sup> Later in 2015, this low-temperature solution method was applied in FPSCs on IZO/PET substrates and achieved an average efficiency of 10.6 ± 1.2%.<sup>116</sup> Recently, a facile sol–gel method was employed to fabricate anatase TiO<sub>2</sub> ETL on the ITO/PEN substrate at 150 °C, and the FPSCs with an optimized concentration of TiO<sub>2</sub> colloidal solution demonstrated the best PCE of 16.11%.<sup>117</sup>

Li *et al.* fabricated the  $\text{TiO}_x$  layer by immersing ITO/PET substrates into  $\text{TiCl}_4$  solution at 70 °C. The consequent device demonstrated the best PCE of 18.1% with superior mechanical stability attributed to the incorporation of a photo-crosslinked fullerene network into  $\text{MAPbI}_3$ .<sup>118</sup>

However, under this low-temperature approach, the organic additives cannot be removed completely, and the processing temperature is still close to the maximum temperature that plastic substrates can withstand.<sup>116,119,120</sup> Jeong and co-workers synthesized  $\text{TiO}_2$  nanoparticles via a non-hydrolytic sol-gel method and replaced the subsequent high-temperature sintering procedure with the UV irradiation at 45 °C.<sup>121</sup> A photocatalytic was induced in UV exposure to remove the organic compound and spontaneous coalescence of  $\text{TiO}_2$  nanoparticles, forming a uniform and dense  $\text{TiO}_2$  layer. Compared to the traditional high-temperature sintering technology, the  $\text{TiO}_2$  layer has higher transparency and a better hole blocking effect with this UV-assisted process. In addition, the photonic curing technique, also known as pulse-thermal processing technology, is used to rapidly anneal different thin films with no damage on substrates by delivering high peak sintering power during a millisecond, enabling reproducible, roll-to-roll, high-temperature processing on temperature-sensitive substrates.<sup>122</sup>

Nevertheless, traditional solution methods to process the  $\text{TiO}_2$  layer suffer from the low film quality. Advanced manufacturing techniques are suitable for fabricating  $\text{TiO}_2$  layers in FPSCs.<sup>123</sup> Atomic layer deposition (ALD) is a precise method of depositing an ultrathin, uniform, and pinhole-free  $\text{TiO}_2$  compact layer.<sup>124–126</sup> In 2015, Kim and co-workers reported an amorphous  $\text{TiO}_x$  nanolayer on ITO/PEN substrates via the PEALD method at 80 °C, realizing an efficiency of 12.2% with moderate flexibility.<sup>127</sup> Almost at the same time, Giacomo and co-workers demonstrated scaffold FPSCs with a UV-irradiated scaffold layer and a compact  $\text{TiO}_2$  ETL by PEALD on ITO/PEN substrates.<sup>14</sup> Furthermore, they investigated the thickness of ALD  $\text{TiO}_2$  and proved that a dense  $\text{TiO}_2$  layer with 5.5 nm thick can prohibit charge recombination at interfaces efficiently.<sup>15</sup> Electron beam (e-beam) evaporation is suitable for different substrates. Through this method, the layer thickness and substrate temperature can be both controlled. In addition, with neither additives nor annealing steps in the deposition process, the e-beam evaporated  $\text{TiO}_2$  can be used directly. For instance, by using e-beam induced evaporation method, Qiu and co-workers demonstrated a highly transparent, amorphous, and pinhole-free  $\text{TiO}_2$  ETL. They found that the thickness of  $\text{TiO}_2$  plays an important role in the surface morphology of perovskite. An optimized thickness of the  $\text{TiO}_2$  layer would result in fewer pinholes in perovskite film, increased light absorption, and reduced shunt resistance.<sup>120</sup> Magnetron sputtering is also an efficient way to fabricate a compact  $\text{TiO}_2$  layer and the thickness of  $\text{TiO}_2$  films can be controlled by the sputtering time.<sup>123</sup> In addition, the  $\text{TiO}_2$  film via this deposition method enables fast electron transportation and perfect isolation between the active layer and the electrode owing to its compact nature.<sup>128</sup> Shengzhong Liu and co-workers processed a dense amorphous  $\text{TiO}_2$  layer with a deeper Fermi level via magnetron sputtering at room temperature, leading to an increased electron injection and a reduced transfer resistance. The final FPSCs displayed on the ITO/PET substrates exhibited a favorable PCE of 15.07% and good mechanical stability on the large area over 10 cm<sup>2</sup>.<sup>129</sup>

However, for the ALD, e-beam evaporation, and magnetron sputtering techniques, the strict conditions of vacuum processes

increase the fabrication cost and limit the throughput. As for the low-temperature solution-processed  $\text{TiO}_2$  ETL, the inferior crystallization and interfacial property lead to lower photovoltaic performances than those with high-temperature annealing  $\text{TiO}_2$ . Meanwhile, the required annealing temperature for the solution-processed  $\text{TiO}_2$  ETL is still too high for plastic substrates.

Employing  $\text{TiO}_2$  in PSCs usually causes serious density-voltage ( $J-V$ ) hysteresis due to the unbalanced charge transport between  $\text{TiO}_2$  and the organic HTL, resulting in charge accumulation at the ETL/perovskite interface.<sup>122,130–132</sup> The hysteresis of  $\text{TiO}_2$ -based devices could be overcome by modifying or doping appropriately to increase electron mobility. The modification materials with strong electron extraction ability, such as acetylacetone,<sup>133</sup> fullerene, and its derivatives,<sup>134</sup> can promote the electron transfer, resulting in significantly reduced hysteresis. Moreover, the transport property of  $\text{TiO}_2$  can be improved by doping such as Yttrium-doped  $\text{TiO}_2$ <sup>115</sup> and Li-doped  $\text{TiO}_2$ .<sup>135</sup> In addition, there are also other explanations for the  $J-V$  hysteresis, for example, the interfacial defects and the capacitance of the  $\text{TiO}_2$  layer which are ascribed to the high dielectric constants.<sup>136</sup> Except for  $J-V$  hysteresis, the  $\text{TiO}_2$  ETL also suffers from the inherent instability upon UV exposure. During UV illumination, the desorption of molecular oxygen leaves unoccupied deep trap sites, which would trap charges, leading to reduced photocurrent and device performance.<sup>137</sup> Passivating the  $\text{TiO}_2$  surface or preventing the UV light from reaching the  $\text{TiO}_2$  film by using a UV filter can overcome this problem. Nevertheless, replacing  $\text{TiO}_2$  with less catalytically active  $\text{ZnO}$  or  $\text{SnO}_2$  materials is more efficient to circumvent this instability and display stable device performance under continuous full spectrum sunlight.<sup>137,138</sup>

## B. ZnO

With higher electron mobility than  $\text{TiO}_2$ ,  $\text{ZnO}$ -based devices can effectively avoid the  $J-V$  hysteresis. The solution and low temperature processable  $\text{ZnO}$  which has the advantage of low cost and high optical transmittance in the visible range has been applied in FPSCs as electron transport material since 2013. Most importantly,  $\text{ZnO}$  has a similar bandgap but much higher electron mobility than  $\text{TiO}_2$ , resulting in higher efficiency and less  $J-V$  hysteresis of the resultant FPSCs.<sup>13,108,139–141</sup> Various deposition methods such as electrodeposition,<sup>13</sup> chemical bath deposition,<sup>13</sup> spin coating,<sup>30,140,142</sup> sputtering,<sup>51</sup> and hydrothermal<sup>141</sup> have been applied to prepare  $\text{ZnO}$  layer in different forms, including  $\text{ZnO}$  compact layer,<sup>13</sup>  $\text{ZnO}$  nanorods,<sup>13,141,143</sup> and  $\text{ZnO}$  nanoparticles.<sup>140</sup> Kumar *et al.* first demonstrated a  $\text{ZnO}$ -based FPSC on ITO/PET substrates by employing an electrodeposited  $\text{ZnO}$  compact layer as the hole blocking layer and chemical bath deposited  $\text{ZnO}$  nanorods as the electron transport film, achieving a PCE of 2.62%.<sup>13</sup> The diameter and length of  $\text{ZnO}$  nanorods could be controlled by the precursor concentration and growth time during the chemical bath deposition.<sup>143</sup> Later Liu *et al.* adopted thin films of  $\text{ZnO}$  nanoparticles in FPSCs by a spin-coating process, and a PCE beyond 10% was achieved by controlling the thickness of  $\text{ZnO}$  at 25 nm. In addition, they ascribed the lower efficiency of flexible devices to the worse optical clarity of flexible substrates.<sup>140</sup> Kim *et al.* achieved a remarkable PCE of 16.8% for FPSCs on the spin-coated  $\text{ZnO}$  layer.<sup>144</sup> Tavakoli *et al.* employed sputtered  $\text{ZnO}$  layers as ETL on 50  $\mu\text{m}$  thick flexible glasses [see Fig. 5(a)] and achieved a PCE of 13.14%.<sup>51</sup> Continuous progress is emerging to improve the electrical properties

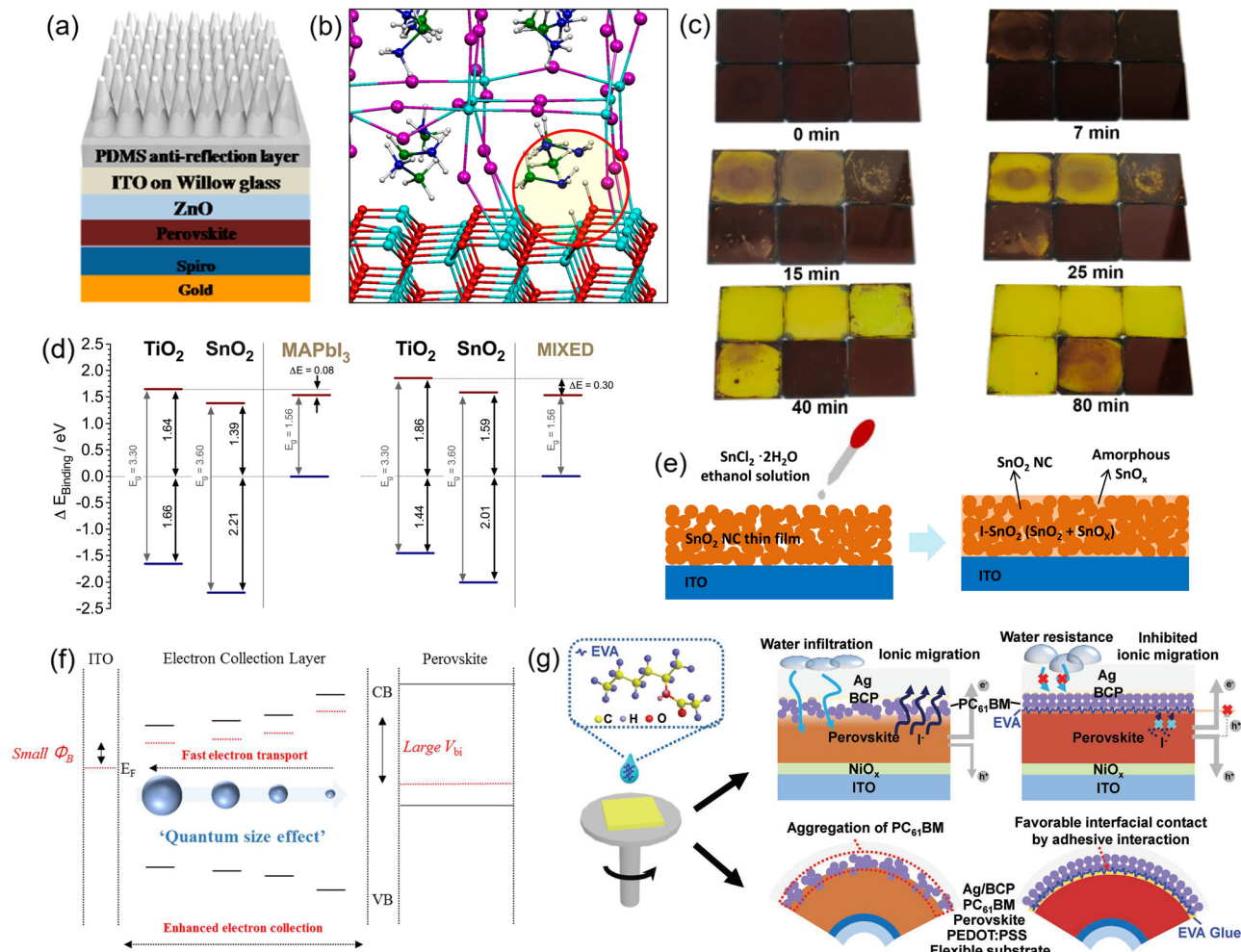
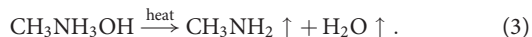


**FIG. 5.** (a) Schematic structure of FPSCs based on the PDMS/Willow glass/ITO/ZnO substrate. Reproduced with permission from Tavakoli *et al.*, ACS Nano **9**, 10287 (2015). Copyright 2015 American Chemical Society. (b) Illustration of deprotonated methylammonium cations at the ZnO/MAPbI<sub>3</sub> interface. (c) Photographs of MAPbI<sub>3</sub> layers after heating at 100 °C for the indicated time and the MAPbI<sub>3</sub> layers are deposited on the thermally pretreated ZnO films at 25, 100, 200, 300, 400 °C and SiO<sub>2</sub> film, respectively. (b) and (c) Reproduced with permission from Yang *et al.*, Chem. Mater. **27**, 4229 (2015). Copyright 2015 American Chemical Society. (d) The energy band diagram of TiO<sub>2</sub> and SnO<sub>2</sub> for MAPbI<sub>3</sub> and mixed perovskite. Reproduced with permission from Correa Baena *et al.*, Energy Environ. Sci. **8**, 2928 (2015). Copyright 2015 Royal Society of Chemistry. (e) Schematic of preparing interconnected SnO<sub>2</sub> layers. Reproduced with permission from Sun *et al.*, Sol. RRL **4**, 1900229 (2020). Copyright 2019 WILEY-VCH. (f) Schematic illustration of the dependence of energy level on particle size. Reproduced with permission from Shin *et al.*, J. Phys. Chem. Lett. **7**, 1845 (2016). Copyright 2016 American Chemical Society. (g) Schematic illustration of the FPSCs with the EVA interlayer could attain uniform PCBM layer, improved water resistance, inhibited ionic migration, and favorable interfacial contact. Reproduced with permission from Huang *et al.*, Adv. Funct. Mater. **29**, 1902629 (2019). Copyright 2019 WILEY-VCH.

of ZnO. Recently, there are research studies that introduced dopants such as cobalt and aluminum to further enhance the conductivity of ZnO thin films, and the FPSCs based on cobalt-doped ZnO film exhibited a fourfold higher current density than the pure ZnO film in FPSCs.<sup>141</sup> In addition, the ionic liquid is also introduced to modify ZnO ETL in FPSCs, demonstrating a positive effect on the charge mobility, perovskite morphology, and energy level alignment.<sup>145</sup>

Despite various advantages of ZnO material, the thermal instability of the ZnO/CH<sub>3</sub>NH<sub>3</sub>PbI<sub>3</sub> interface hinders the development of highly stable PSCs. It has been proved that the basic nature of ZnO

results in the degradation of the perovskite layer. As illustrated in Fig. 5(b), the proton-transfer reactions occur at the ZnO/perovskite interface and the released protons are absorbed by vicinal oxygen atoms.<sup>146–148</sup> In addition, the residual hydroxyl and acetate ligands on the surface of the ZnO layer will accelerate the perovskite decomposition and the related processes are described in Eqs. (1)–(3).<sup>147,149,150</sup> The hydroxyl reacts with CH<sub>3</sub>NH<sub>3</sub>I to form CH<sub>3</sub>NH<sub>3</sub>OH, which is easily decomposed to CH<sub>3</sub>NH<sub>2</sub> and H<sub>2</sub>O during the thermal annealing. Eventually, the consumption of CH<sub>3</sub>NH<sub>3</sub>OH would promote the reaction (2), resulting in the perovskite decomposition in the reverse process of reaction (1).



Research trials have been conducted to solve this decomposition problem. As shown in Fig. 5(c), Yang *et al.* reported that the pre-sintered ZnO films could retard the degradation process due to the removal of surface hydroxyl groups and residual acetate ligands.<sup>147</sup> Zhang *et al.* indicated that surface chlorination treatment could also slow down the  $\text{CH}_3\text{NH}_3\text{PbI}_3$  decomposition.<sup>151</sup> Furthermore, the most efficient strategy to suppress the perovskite decomposition is inserting a thin layer between the ZnO ETL and the perovskite layer to prevent their direct contact. The commonly used inserting layers include ultra-thin  $\text{Al}_2\text{O}_3$  insulating layer,<sup>146</sup> polyethylenimine,<sup>150</sup> polyethylenimine ethoxylated,<sup>149</sup> [6,6]-phenyl-C<sub>61</sub>-butyric acid methyl ester (PCBM), benzoic acid derivatives, and so on.<sup>148,152,153</sup> However, their poor electrical properties have an adverse effect on the device efficiency, and it has been reported that the commonly used buffer layer PCBM tends to aggregate and diffuse during the annealing process, leading to a slow but certain degradation.<sup>150</sup>

### C. $\text{SnO}_2$

$\text{SnO}_2$  ETL has been applied in PSCs since 2015,<sup>154,155</sup> and many studies have demonstrated high efficiencies exceeding 19% in the  $\text{SnO}_2$ -based FPSCs.<sup>66,156–158</sup>  $\text{SnO}_2$  is considered a promising ETL candidate mainly owing to the high electron conductivity with enhanced charge transportation and reduced charge accumulation at the interface.<sup>132,138,159,160</sup> In addition, the wideband gap of  $\text{SnO}_2$  (3.6–4.0 eV) leads to high optical transparency (97% optical transparency in the visible range at the thickness of 0.1–1  $\mu\text{m}$ ).<sup>99,155,161</sup> The deeper conduction band than  $\text{TiO}_2$  results in more efficient electron transfer and favorable band alignment with perovskite, especially with mixed perovskite as shown in Fig. 5(d).<sup>132,162–165</sup> Moreover, the low processing temperature, excellent chemical stability, and better photostability than  $\text{TiO}_2$  make  $\text{SnO}_2$  superior among the ETL candidates.<sup>138</sup> A large variety of techniques have been developed to fabricate  $\text{SnO}_2$  layer, such as ALD,<sup>162,166,167</sup> chemical bath deposition,<sup>167,168</sup> e-beam evaporation,<sup>169</sup> hydrothermal treatment,<sup>170</sup> and solution method.<sup>49,108,132,154,155,167,171</sup>

Among the  $\text{SnO}_2$  film preparation method, ALD is expected to produce the most compact thin films at the lowest deposition temperature, especially PEALD which requires even lower deposition temperature due to the enhanced reactivity. Via this deposition method, Wang *et al.* demonstrated a pinhole-free  $\text{SnO}_2$  ETL on the ITO/PET substrate at about 100 °C, realizing an effective hole-blocking capability and a minimized charge recombination. After passivating the  $\text{SnO}_2$  surface with a C<sub>60</sub>-self-assembled monolayer, the best PCE of 16.8% with fair flexibility has been achieved.<sup>166</sup> However, the amorphous nature of the as-prepared  $\text{SnO}_2$  shows inferior electron mobility, causing *J-V* hysteresis and reduced performance.<sup>172</sup> Later, they developed a water vapor treatment method to improve the electrical conductivity of PEALD processed  $\text{SnO}_2$  ETLs, which is attributed to the complete reaction of organic materials to pure  $\text{SnO}_2$  with the participation of water vapor during the annealing process. The enhanced charge transport of  $\text{SnO}_2$  ETL leads to an increase in open-circuit voltage ( $V_{oc}$ ) and fill factor (FF) for FPSCs, exhibiting the best PCE of 18.36% with reduced *J-V* hysteresis compared to the FPSCs which employ

as-deposited  $\text{SnO}_2$ .<sup>173</sup> Similarly, Liu *et al.* developed spin-coated  $\text{SnO}_2$  with a hydrothermal treatment process which promotes the complete removal of organic surfactants that attached on the surface of  $\text{SnO}_2$  nanoparticles, resulting in enhanced crystallization of  $\text{SnO}_2$  ETL due to the high vapor pressure of water. Finally, the best PCE of 18.1% was demonstrated for FPSCs on the ITO/PEN substrates.<sup>170</sup>

Nevertheless, the most frequently used preparation method is the solution process, including thermal decomposition deposition and crystallized  $\text{SnO}_2$  nanocrystals deposition directly. In the thermal decomposition method, the  $\text{SnO}_2$  layer is fabricated by spin-coating the precursor solution such as  $\text{SnCl}_2 \cdot 2\text{H}_2\text{O}$  and converting it to  $\text{SnO}_2$  films later by thermal annealing at low temperature.<sup>154,155,164,167,174</sup> It is worth noting that the high temperature (500 °C) annealing results in an inferior device performance due to the aggregation of nanoparticles, while the low temperature (180–200 °C) processed  $\text{SnO}_2$  layer exhibits preferable film coverage and lower charge recombination.<sup>164,174,175</sup> Especially, Dong *et al.* presented a wet chemical route to prepare crystallized  $\text{SnO}_2$  layer below 80 °C and followed a UV-Ozone treatment, which exhibited little dependence on thermal annealing.<sup>176</sup> Recently, there are many researchers deposited the  $\text{SnO}_2$  layer by using pre-synthesized and well-dispersed  $\text{SnO}_2$  nanocrystals which are commercially available. Thus, the deposition temperature could be lowered below 150 °C by skipping the sintering procedure.<sup>108,132,170,177,178</sup> However, the poor interconnection among  $\text{SnO}_2$  nanocrystals would result in insufficient film coverage, leading to the current leakage and surface defects.<sup>177</sup> Thus, the appropriate thickness of  $\text{SnO}_2$  ETL is required to completely cover the transparent electrode for effective hole blocking, while keeping a low series resistance for undiminished device performance.<sup>132</sup> In addition, Sun *et al.* recently adopted amorphous  $\text{SnO}_x$  on the  $\text{SnO}_2$  nanocrystal thin film, resulting in effectively interconnected nanocrystals as well as passivated surface defects of the  $\text{SnO}_2$  layer. As illustrated in Fig. 5(e), the smooth ETL leads to enhanced electron extraction and reduced charge carrier recombination, and a PCE of 16.29% was achieved based on ITO/PET substrates.<sup>177</sup>

Constant improvements of  $\text{SnO}_2$  film properties are necessary for better device performance. The electrical conductivity of  $\text{SnO}_2$  can be enhanced by element doping, such as Sb doped  $\text{SnO}_2$ ,<sup>179</sup> Li doped  $\text{SnO}_2$ ,<sup>164</sup> and Nb doped  $\text{SnO}_2$ ,<sup>174</sup> which can effectively improve the carrier concentration. In addition, zwitterion-modified  $\text{SnO}_2$ , LiF doped  $\text{SnO}_2$ , and  $\text{InCl}_3$  doped  $\text{SnO}_2$  *et al.* also demonstrate enhanced conductivity and improved carrier transportation.<sup>180–183</sup> However, external doping is not suitable to obtain proper carrier concentration, which is crucial for the efficient ETL application to balance the high electrical conductivity and the reduced interface carrier recombination. Yang *et al.* discovered that the carrier concentration of  $\text{SnO}_2$  quantum dot can be tuned by changing the annealing temperature and the relevant flexible device demonstrated a high PCE of 16.97% under optimized conditions.<sup>178</sup> In addition, the higher electron mobility is also helpful in improving the performance of  $\text{SnO}_2$ -based devices by promoting electron transfer and eliminating charge accumulation at the interface of the ETL/perovskite layer to improve efficiency and reduce *J-V* hysteresis. For example, the ethylene diamine tetraacetic acid (EDTA) complexed  $\text{SnO}_2$  developed by Shengzhong Liu and co-workers achieved a high PCE of 18.28% for FPSCs with negligible hysteresis and excellent stability. The outstanding performance is mainly attributed to the electron mobility of EDTA- $\text{SnO}_2$ , which is three times higher than that of normal  $\text{SnO}_2$ . Moreover, the high quality of the

perovskite films deposited on the EDTA-SnO<sub>2</sub> layer and the elevated Fermi level of EDTA-SnO<sub>2</sub> result in improved device performance.<sup>108</sup> NH<sub>4</sub>Cl has also been reported to improve the performance of SnO<sub>2</sub>-based PSCs with enhanced electron mobility and much aligned energy level as well as the passivated interface between the perovskite layer and SnO<sub>2</sub> ETL, attributing to the coagulation of SnO<sub>2</sub> colloid induced by acidic NH<sub>4</sub>Cl.<sup>184</sup>

There are also reports focused on interface engineering to improve device performance. The insertion of insulating metal oxide, also named tunnel oxide, such as HfO<sub>2</sub>,<sup>11,158</sup> MgO,<sup>185</sup> and Al<sub>2</sub>O<sub>3</sub><sup>186</sup> between the transparent electrode and ETL can suppress charge recombination by blocking holes and enabling the tunneling of electrons. Recently, Bingbing Cao and co-workers demonstrated Rb<sub>1</sub>K<sub>4</sub>CsFAMA-based FPSCs with an ultrathin HfO<sub>2</sub> layer inserted between the ITO electrode and SnO<sub>2</sub> ETL via the ALD method. They demonstrated that the insertion of HfO<sub>2</sub> almost does not affect the morphology of the SnO<sub>2</sub> layer and perovskite layer. Owing to the restricted charge recombination between the perovskite and ITO electrodes, the devices achieved a champion PCE of 19.11% with a high FF of 0.792, good thermal stability as well as good bending resistance.<sup>158</sup> Moreover, the interface passivation is also helpful in eliminating hysteresis.<sup>166</sup> Recently, Qu *et al.* introduced the KCl layer into low-temperature ( $\leq 100^\circ\text{C}$ ) processed FPSCs between the spin-coating SnO<sub>2</sub> ETL and perovskite film on the ITO/PET substrate. With the modification of K<sup>+</sup> ion and Cl<sup>-</sup> ion, the perovskite layer showed better crystallinity and decreased defect density, and the conduction band minimum of SnO<sub>2</sub> has been raised, leading to a promoted  $V_{oc}$ . Finally, the devices modified by KCl showed less hysteresis and a higher PCE of 18.53%.<sup>171</sup> In addition, various materials have been employed to modify the interface of SnO<sub>2</sub>/perovskite, such as 3-aminopropyltriethoxysilane self-assembled monolayer, carbon derivatives, and fullerenes, which are very promising in the application of flexible devices.<sup>187</sup>

#### D. Other ETLs

Apart from TiO<sub>2</sub>, ZnO, and SnO<sub>2</sub>, there are also plenty of materials with appealing properties employed as ETL in FPSCs, such as Zn<sub>2</sub>SnO<sub>4</sub>, Nb<sub>2</sub>O<sub>5</sub>, WO<sub>x</sub>, In<sub>2</sub>O<sub>3</sub>, and organic ETLs including fullerene derivatives, solid-state ionic-liquids (ss-IL), etc.<sup>188–190</sup> Nb<sub>2</sub>O<sub>5</sub> is a transparent and highly stable metal oxide with a bandgap of 3.4 eV, large than the 3.2 eV of TiO<sub>2</sub>.<sup>191,192</sup> Considering the high carrier mobility, appropriate conduction band position, diminished charge recombination and low-temperature processes, such as RF magnetron sputtering<sup>193</sup> and electron beam evaporation<sup>69,188</sup> Nb<sub>2</sub>O<sub>5</sub> is one of the most promising ETL candidates in FPSCs. Nb<sub>2</sub>O<sub>5</sub> can extract carriers effectively and reduce the carrier recombination between the electrode and the perovskite layer, both of which are beneficial to achieving high carrier collection efficiency.<sup>188</sup> In 2017, Ling *et al.* processed RF magnetron sputtered Nb<sub>2</sub>O<sub>5</sub> on ITO/PET substrates at room temperature for the application in FPSCs. They demonstrated that the as sputtered amorphous Nb<sub>2</sub>O<sub>5</sub> ETL without any heat treatment has a similar effect to the crystalline Nb<sub>2</sub>O<sub>5</sub> annealed at high temperature (500 °C) and the resultant FPSCs conducted the best conversion efficiency of 12.1%.<sup>193</sup> Shengzhong Liu and co-workers demonstrated an electron beam evaporated Nb<sub>2</sub>O<sub>5</sub> film as ETL without post-treatment and achieved an efficiency of 15.56% with an optimum Nb<sub>2</sub>O<sub>5</sub> thickness of 60 nm on the ITO/PET substrates.<sup>188</sup> Later, they raised the efficiency of Nb<sub>2</sub>O<sub>5</sub> based FPSCs to 18.40% by introducing dimethyl sulfide

additive into the light absorber layer to improve the film quality.<sup>69</sup> Moreover, they also applied Nb<sub>2</sub>O<sub>5</sub> ETL in the all-inorganic FPSCs based on CsPbI<sub>2</sub>Br and a PCE of 11.73% was realized with good stability and flexibility.<sup>194</sup>

Owing to the wideband gap (3.6 eV), the similar conduction band position with TiO<sub>2</sub>, the low refractive index in the visible range, and good chemical stability with respect to acid/base solution and polar organic solvents, Zn<sub>2</sub>SnO<sub>4</sub> is a promising candidate as ETL for the application of highly efficient FPSCs.<sup>98</sup> As early as 2015, Shin *et al.* prepared flat and uniform Zn<sub>2</sub>SnO<sub>4</sub> films below 100 °C, and the FPSCs based on the Zn<sub>2</sub>SnO<sub>4</sub> exhibit a steady-state PCE of 14.85%. Due to the anti-reflection effect, the low refractive index of Zn<sub>2</sub>SnO<sub>4</sub> leads to an improved optical transmittance of ITO/PEN substrates, which accounts for the enhanced short-circuit current density ( $J_{sc}$ ) and efficiency.<sup>98</sup> Later, by controlling the Zn<sub>2</sub>SnO<sub>4</sub> particle size, they tuned the energy level of Zn<sub>2</sub>SnO<sub>4</sub> nanoparticles and found that generally the smaller the particle size, the larger the bandgap. They exhibited that owing to the higher crystallization and work function, the large Zn<sub>2</sub>SnO<sub>4</sub> nanoparticles are favorable for electron transport and electron transfer at the ETL/ITO interface, which is beneficial for  $J_{sc}$  and FF. In comparison, the Zn<sub>2</sub>SnO<sub>4</sub> quantum dots with diameters below 10 nm are supposed to improve the built-in potential at the ETL/perovskite interface and result in a correspondingly enhanced  $V_{oc}$  [Fig. 5(f)]. Finally, the combined Zn<sub>2</sub>SnO<sub>4</sub> nanoparticles and Zn<sub>2</sub>SnO<sub>4</sub> quantum dots are employed as efficient ETLs in FPSCs for optimal performance and a steady-state efficiency of 16% was reported.<sup>195</sup> However, the devices based on the as-fabricated mesoporous Zn<sub>2</sub>SnO<sub>4</sub> ETL suffer from large  $J-V$  hysteresis, probably caused by the severe charge recombination at the ETL/perovskite interface.<sup>98,195</sup> Comparatively speaking, the low temperature fabricated compact Zn<sub>2</sub>SnO<sub>4</sub> layer has potential for the application of hysteresis-inhibited FPSCs. Through a new reflux condensation method, Dou *et al.* fabricated a compact Zn<sub>2</sub>SnO<sub>4</sub> layer that fully covered the TCO substrates and mesoporous Zn<sub>2</sub>SnO<sub>4</sub> was spin-coated above it later. The PSCs based on the bilayer ETL which is composed of compact Zn<sub>2</sub>SnO<sub>4</sub> and mesoporous Zn<sub>2</sub>SnO<sub>4</sub> layer demonstrated reduced charge recombination and much aligned band structure, resulting in high efficiency and decreased hysteresis.<sup>196</sup>

In addition to the bilayer structured Zn<sub>2</sub>SnO<sub>4</sub> ETL, other bilayer ETLs have been proposed in advanced FPSCs for the effectively enhanced blocking effect and avoided leakage current.<sup>197–201</sup> For example, the SnO<sub>2</sub> ETL bilayer is composed of amorphous SnO<sub>2</sub> prepared by the sol-gel method and crystalline SnO<sub>2</sub> nanoparticles from commercially available colloid dispersion as bottom and top metal oxide, respectively. Compared with the single SnO<sub>2</sub> layer, the bi-SnO<sub>2</sub> ETL demonstrated improved surface morphology with suppressed defects, and better band arrangement, realizing effective electron extraction.<sup>202,203</sup> Recently, inspired by mesoscopic PSCs, Chung *et al.* developed porous planar ETL which combined SnO<sub>2</sub> compact layer and porous Zn<sub>2</sub>SnO<sub>4</sub> layer via layer-by-layer coating. This bilayer ETL provides favorable energy level alignment and induces high quality perovskite due to the porous layer. The resultant FPSCs showed the best efficiency of 20.7% on ITO/PEN substrates.<sup>204</sup>

Except for the above-mentioned inorganic ETL materials, diverse organic materials with advantageous photoelectric characteristics have been explored as possible substitutes. Fullerene derivatives such as PCBM and C<sub>60</sub> have high electron mobility and conductivity and

could be processed simply by solution deposition or thermal evaporation. In addition, they are generally used in p-i-n FPSCs which is more desirable than the normal type PSCs from the aspect of *J-V* hysteresis. Furthermore, owing to the use of organic ETL and HTL, intrinsically better flexibility for devices could be realized. One of the drawbacks of fullerene based ETLs is the element diffusion which easily happens between the perovskite and the metal electrode through the organic materials since the PCBM layer is not pinhole free. In addition, the inappropriate energy level between the Ag electrode and PCBM or C<sub>60</sub> ETLs results in severally charge carrier recombination.<sup>205</sup> There are various solutions to address these obstacles by employing the bilayer-structured ETL such as PCBM/ZnO<sup>206,207</sup> PCBM/TiO<sub>x</sub><sup>109</sup> and double fullerene layer<sup>205,208,209</sup> or embedding the insert layer such as bathocuproine<sup>67,208,210–213</sup> and LiF<sup>214</sup> layer to inhibit ion diffusion and modify their work function at the same time for effective hole blocking. In addition, PCBM has a problem with the surface coverage due to the lack of chain entanglement. Heo *et al.* introduced a polymeric electron conductor poly([N,N'-bis(2-octyldodecyl)-1,4,5,8-naphthalene bis(dicarboximide)-2,6-diyl]-alt-5,5'-(2,2'-bithiophene)) (PNDI-2T) in PCBM and obtained enhanced photoelectric performance and flexibility in inverted FPSCs by relieving mechanical stress through the entangled polymeric matrix of PNDI-2T.<sup>214</sup> Chen and co-workers introduced an adhesive poly(ethylene-co-vinyl acetate) (EVA) interfacial layer between the perovskite film and PCBM layer as illustrated in Fig. 5(g). This glued interfacial layer results in uniform PCBM film and protective structure to suppress ion migration, weaken interface degradation, improve moisture impermeability and enhance mechanical flexibility.<sup>213</sup> In comparison, C<sub>60</sub> has a higher electrical conductivity than PCBM, while the solubility problem of C<sub>60</sub> inhibits the application in planar n-i-p architecture, since the C<sub>60</sub> easily dissolves by the solvents which are usually used in perovskite and HTL such as N, N-dimethylformamide and chlorobenzene, resulting in poor surface morphology and low reproducibility. Yoo *et al.* evaporated C<sub>60</sub> on ITO/PEN substrate with ethoxylated polyethylenimine as the interlayer to strengthen the adhesion of C<sub>60</sub> to the substrate and avoid the C<sub>60</sub> film being undermined during the deposition of the perovskite layer, achieving a PCE of 13.3%.<sup>215</sup> However, the C<sub>60</sub> molecules were still partially washed off during the subsequent spin-coating process. Song *et al.* treated C<sub>60</sub> film with 0.08 wt. % of poly(allylamine), leading to insoluble robust ETL and sufficient adhesion to substrates. Finally, a PCE of 15.2% was realized in FPSCs with negligible hysteresis.<sup>216</sup>

However, the fullerene derivates are very expensive and the performances of FPSCs based on organic ETLs have yet to be improved even though they display extremely low hysteresis.<sup>108</sup> Various novel materials have been applied in FPSCs as ETL. Polymeric ETL such as P(NDI2DT-TTCN) showed enhanced mechanical stability and excellent long-term stability against ambient conditions owing to the hydrophobicity.<sup>212</sup> The ss-IL is a promising candidate as ETL in FPSCs due to the wideband gap (4.59 eV), large electrical conductivity, suitable work function, anti-reflection, and good thermal stability. As early as 2016, ss-IL was used as ETL and realized a high efficiency of 16.09% for FPSCs.<sup>190</sup> In addition, Ryu *et al.* synthesized nanocrystalline Ti-based metal-organic framework (nTi-MOF) particles combining PCBM as ETL to provide efficient electron transfer as well as suppressed contact between the substrate and the perovskite layer directly, and an efficiency of 17.43% was achieved on ITO/PET substrates.<sup>60</sup> There are also new materials that have been applied in rigid

devices that could be developed on flexible substrates such as PFN-2TNDI<sup>217</sup> and In<sub>2</sub>S<sub>3</sub>,<sup>218</sup> which are low-temperature and solution-processable.

## V. LOW-TEMPERATURE PROCESSED HTL

The HTL plays the role of extracting the photo-generated holes from the light absorbing materials and transporting them to anodes, and it has been proved that a more efficient HTL is beneficial to achieving high-performance PSCs by raising  $J_{sc}$  due to the inferior hole transport than an electron.<sup>219</sup> The high hole mobility and conductivity, favorable electron blocking ability, good morphological contact with perovskite, and aligned band structure with electrode and perovskite are the essential requirements for HTL. Apart from that, the application of HTL in FPSCs also needs low-temperature processability, high mechanical flexibility, and high moisture resistance because of the high water vapor transmission rate of the polymer substrate.

### A. Organic HTL

Spiro-OMeTAD is the most frequently used HTL with high efficiency demonstrated in n-i-p type PSCs. However, the electrical conductivity of pristine Spiro-OMeTAD is barely satisfactory. Generally, the conductivity of Spiro-OMeTAD relies on the oxidation in the air in virtue of the addition of additives including tris(2-(1*H*-pyrazol-1-yl)-4-*tert*-butylpyridine)-cobalt(III) tris(bis(trifluoromethylsulfonyl)imide) (FK209), bis (trifluoromethane) sulfonimide lithium salt (LiTFSI) and 4-*tert*-butylpyridine which are corrosive and hygroscopic, leading to the diminished long-term stability of devices.<sup>66,118,148,156–158</sup> In addition, there is a work utilized spiro(TFSI)<sub>2</sub> with high conductivity to bypass the oxidation process.<sup>220</sup> Another popular organic HTL in n-i-p PSCs is poly(bis(4-phenyl)(2,4,6-tri-methylphenyl)amine) (PTAA), which is more thermally and mechanically stable than Spiro-OMeTAD, possibly owing to the lower dopant concentration.<sup>221</sup> However, the record high efficiency devices in both rigid and flexible are often based on Spiro-OMeTAD HTL.<sup>11,12</sup> For a detailed comparison of the dopants and device stability of Spiro-OMeTAD and PTAA could refer to the review by Macdonald *et al.*<sup>222</sup>

The normal type planar FPSCs usually suffer from notorious hysteresis behavior due to the unbalanced flux of electrons and holes. Conversely, inverted type planar FPSCs using organic materials such as PEDOT:PSS as HTL are more desirable in obtaining stable performance and avoiding the high-temperature sintering process. Moreover, owing to the use of organic ETL and HTL, the inverted FPSCs have intrinsically better flexibility than normal structures. PEDOT:PSS has been widely applied as HTL due to the good electrical conductivity, suitable energy level alignment, low temperature, and solution processibility.<sup>109,209,223–225</sup> Actually, since the aqueous solution of PEDOT:PSS is improper with perovskite layer, the PEDOT:PSS is only used in inverted PSCs, preparing by spin-coating,<sup>109,212–214,223,225,226</sup> blade-coating,<sup>205</sup> and meniscus-coating.<sup>227</sup>

Back in 2013, Docampo and co-workers developed low temperature ( $\leq 150^{\circ}\text{C}$ ) processed inverted FPSCs which employed spin-coated PEDOT:PSS and PCBM as HTL and ETL, respectively, on the ITO/PET substrates, realizing an efficiency of 6.4%.<sup>109</sup> Then, You *et al.* improved the efficiency to 9.2% with a similar procedure at a lower temperature ( $\leq 120^{\circ}\text{C}$ ).<sup>225</sup> However, the spin-coating method is a major hurdle to the upscaling of FPSCs. Yang and co-workers

demonstrated the fully printable FPSCs and showed a promising PCE of 7.14%.<sup>205</sup> The perovskite layer and the charge transport layers of PEDOT:PSS, PC<sub>61</sub>BM, and bis-C<sub>60</sub> are deposited via blade-coating with an annealing temperature below 100 °C. In addition, Song and co-workers printed PEDOT:EVA HTL on the ITO/PET substrates by meniscus-coating. The resultant FPSCs realized high PCEs of 19.87% and 17.55% with effective areas of 1.01 and 31.20 cm<sup>2</sup>, respectively.<sup>227</sup>

The work function of PEDOT:PSS ranges between 4.9 and 5.2 eV, lower than the ionization potential of perovskite, resulting in reduced built-in potential and possible energy loss at the interface of perovskite/PEDOT:PSS.<sup>228</sup> In addition, the moderate electrical conductivity of PEDOT:PSS is another concern in the application of HTL. Appropriate doping strategy in PEDOT:PSS HTL demonstrates higher electrical conductivity and reduced energy barrier between PEDOT:PSS and perovskite, leading to improved device performance, such as F4-TCNQ doped PEDOT:PSS,<sup>229</sup> PEO doped PEDOT:PSS,<sup>230</sup> PEDOT:GO composite film and the composition of PEDOT:PSS with MoO<sub>3</sub>.<sup>231</sup> Lim *et al.* applied perfluorinated ionomer modified PEDOT:PSS as HTL on the PET/ITO substrate. With the improved work function of PEDOT:PSS, they realized a PCE of 8.0% in FPSCs.<sup>228</sup> Gu *et al.* applied 3-aminopropanoic acid as a self-assembling monolayer on PEDOT:PSS layer in order to improve the work function of PEDOT:PSS from 5. to 5.2 eV and modify the morphology of perovskite materials as well, leading to better crystallinity and increased film coverage of perovskite layer.<sup>233</sup> Recently, Ding and co-workers used polymer electrolyte sodium polystyrene sulfonate additive to modify PEDOT:PSS.<sup>224</sup> The modified PEDOT:PSS exhibited a higher work function (5.2 eV) than pristine PEDOT:PSS

(4.9 eV) [Fig. 6(a)], and they further employed this PEDOT:PSS in one-step roll-to-roll processed FPSCs, leading to an enhanced PCE of 11.16% with negligible hysteresis.<sup>226</sup> Song *et al.* synthesized high conductivity and high adhesion HTL by blending PEDOT with graphene oxide, and this glued HTL could enhance the flexibility of FPSCs by adhering to the brittle ITO and perovskite layer.<sup>232</sup>

Novel strategies have been proposed to advance the performance of PEDOT:PSS HTL based FPSCs. Hu *et al.* introduced a polystyrene-doped nanocellular PEDOT:PSS (NC-PEDOT:PSS) HTL, which acts as a mechanical buffer layer and an optical resonant cavity to synchronously enhance the mechanical flexibility and light utilization as shown in Figs. 6(b) and 6(c). After dimethylformamide post-treatment, NC-PEDOT:PSS exhibits a higher work function of 5.3 eV because the polystyrene doping can effectively protect PSS during the perovskite coating. As a result, a PCE of 12.32% was achieved for large-scale FPSCs with excellent flexural endurance.<sup>74</sup> In comparison, the PEDOT:PSS HTL-based devices showed an efficiency of 7.16%. Recently, Wang *et al.* demonstrated FPSCs with a maximum PCE of 19.41% and an ultimate high FF of 81% on the ITO/PEN substrates by interface engineering and perovskite morphology control. The bilayer PEDOT:PSS/PTAA HTL provided good band structure alignment with ITO and perovskite, leading to efficient charge extraction and enhanced FF [see Fig. 6(d)]. Furthermore, this double layer interface strengthens the flexibility of the ITO electrodes, resulting in excellent mechanical durability of FPSCs, preserving over 90% of the initial PCE after 1000 bending cycles at a curvature radius of 3 mm.<sup>210</sup> In addition, the solvent treatment on PEDOT:PSS is also useful in improving the conductivity of PEDOT:PSS. For example, N,

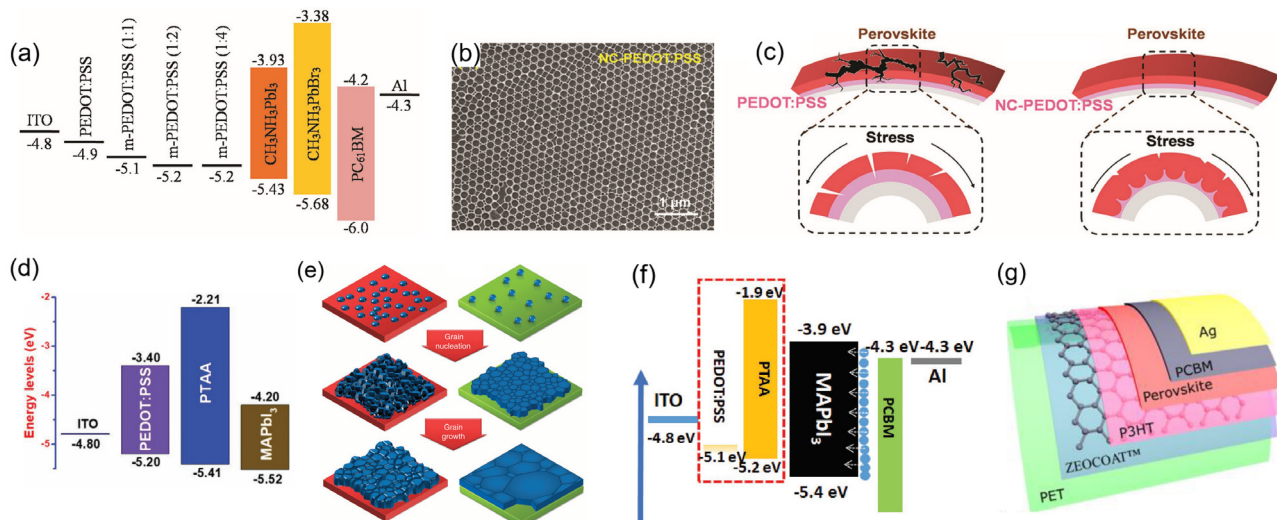


**FIG. 6.** (a) Energy level diagram of FPSCs with modified PEDOT:PSS HTL. Reproduced with permission from C. Zuo and L. Ding, *Adv. Energy Mater.* **7**, 1601193 (2017). Copyright 2016 WILEY-VCH. (b) SEM image of the NC-PEDOT:PSS film. (c) Illustration of mechanical stresses release for perovskite on the PEDOT:PSS layer (left) and NC-PEDOT:PSS (right). (b) and (c) Reproduced with permission from Hu *et al.*, *Adv. Mater.* **29**, 1703236 (2017). Copyright 2017 WILEY-VCH. (d) Energy level diagram of FPSCs with PEDOT:PSS/PTAA HTL. Reproduced with permission from Wang *et al.*, *Adv. Funct. Mater.* **30**, 2001240 (2020). Copyright 2020 WILEY-VCH. (e) Illustration of the nucleation and growth of perovskite grains on the hydrophilic and hydrophobic HTLs. Reproduced with permission from Bi *et al.*, *Nat. Commun.* **6**, 7747 (2015). Copyright 2015 Authors, licensed under a Creative Commons Attribution (CC BY) license. (f) Energy level diagram of FPSCs with PTAA HTL. Reproduced with permission from Xu *et al.*, *Adv. Energy Mater.* **8**, 1703054 (2018). Copyright 2018 WILEY-VCH. (g) The flexible device structure with P3HT HTL. Reproduced with permission from Liu *et al.*, *Nano Energy* **28**, 151 (2016). Copyright 2016 Elsevier.

N-dimethylformamide-treated PEDOT:PSS demonstrated increased electrical conductivity and a much smoother surface.<sup>233</sup>

In addition, the hygroscopicity of PEDOT:PSS has an adverse influence on the moisture sensitive perovskite, causing a fast degradation for PEDOT:PSS-based device. Its acidic nature is harmful to the ITO substrate and the perovskite layer when the PEDOT:PSS contacts with them, resulting in relatively low efficiency and reproducibility.<sup>234–236</sup> Chen *et al.* demonstrated a cryo-controlled quasi-congealing spin-coating to improve the quality of PEDOT:PSS film. By enhancing the hydrogen bonds between the solvent and PSS chains and inducing the interaction between the co-solvent and PEDOT chains through quasi-congealing at a low temperature, a uniform and smooth PEDOT:PSS film with a high moisture resistance was achieved, leading to a promising PCE of 15.13% on PET/ITO substrate.<sup>234</sup>

Replacing PEDOT:PSS with other p-type materials in p-i-n devices which possess better properties is feasible to overcome the above challenges. Various organic materials act as the replacement of PEDOT:PSS, such as organic small molecular PTAA which is hydrophobic, leading to enlarged grain size and improved crystallinity of perovskite as illustrated in Fig. 6(e). In addition, the higher work function of PTAA than PEDOT:PSS is favorable for the energy band alignment [Fig. 6(f)].<sup>208,237,238</sup> Many reports compared the performances of PEDOT:PSS and PTAA based devices, demonstrating that PTAA is a better choice for the significantly improved efficiency and long-term stability.<sup>237–239</sup> However, the high cost and the requirement of hygroscopic dopants for PTAA limit its mass production in FPSCs. In addition, the hydrophobic P3HT with advantages of matchable band structure, low-cost, low temperature fabrication process, is a likely alternative to hole transport material in FPSCs.<sup>240</sup> Liu *et al.* demonstrated FPSCs with P3HT as HTL on the graphene electrode with a PCE of 11.5% [Fig. 6(g)].<sup>241</sup> The doped P3HT exhibits better electrical properties than the pure P3HT, such as tetrafluoro-tetracyano-quinodimethan doped P3HT<sup>242</sup> and cobalt complex doped P3HT.<sup>243</sup> However, the P3HT based FPSCs demonstrated a lower efficiency due to the poor contact and additional recombination at the P3HT/perovskite interface. Seo *et al.* overcame this issue by inserting a wide-bandgap-halide between the narrow-bandgap-halide and P3HT, and demonstrated high efficiency on the rigid devices, illustrating the potential application prospects in the FPSCs.<sup>240</sup> Polymeric material based on 1,4-bis(4-sulfonatobutoxy)benzene and thiophene moieties (PhNa-1T) was introduced as HTL in low-temperature solution processed FPSCs by Jo *et al.* The PhNa-1T has several advantages as HTL, including high work function, high electrical conductivity, hole-transport ability in the out-of-plane direction and neutral property ( $\text{PH} = 7.12$ ). Moreover, owing to the smoother surface of PhNa-1T compared to PEDOT:PSS layer, the upper perovskite film showed improved morphology and better contact with HTL, which is expected to suppress the charge recombination. As a result, the FPSCs showed a noticeable PCE of 14.7% with good stability.<sup>244</sup> Lately, Reddy *et al.* synthesized an organic small molecular of N-(4-(9H-carbazol-9-yl)phenyl)-7-(4-(bis(4-methoxyphenyl)amino)phenyl)-N-(7-(4-(bis(4-methoxyphenyl)amino)phenyl)-9,9-diethyl-9H-fluoren-2-yl)-9,9-diethyl-9H-fluoren-2-amine via coupling reactions and applied it as HTL on ITO/PET substrates. The appropriate highest occupied molecular orbital (HOMO) level ( $-5.07 \text{ eV}$ ), high hole mobility, and the hydrophobic nature of this molecular lead to a PCE of 12.46% in FPSCs, which is higher than the device based on the PEDOT:PSS (10.52%).<sup>207</sup>

## B. Inorganic HTL

Despite organic HTL possessing high efficiency and reduced hysteresis, the high price and stability problem hinder its application. The cheap p-type inorganic semiconductor materials with excellent chemical and environmental adaptability such as  $\text{NiO}_x$  have been extensively investigated in FPSCs.<sup>211,245–247</sup>

As high efficiencies of over 20% have been achieved in  $\text{NiO}_x$  based FPSCs,  $\text{NiO}_x$  is undoubtedly a promising HTL for flexible devices with advantages of wide bandgap, good band alignment, good optical transparency, electron-blocking capability, and low-temperature preparation process.<sup>67,248</sup> Compared to the low intrinsic conductivity of  $\text{NiO}$ ,  $\text{NiO}_x$  exhibits better electrical conductivity induced by the self-doping of  $\text{Ni}^{3+}$  ions.<sup>249,250</sup> Several approaches have been adopted to fabricate the  $\text{NiO}_x$  layer, including sol-gel process,<sup>251</sup> sputtering,<sup>252</sup> spray pyrolysis,<sup>249,253</sup> pulsed laser deposition,<sup>254</sup> electro-deposition,<sup>255</sup> and ALD.<sup>256</sup> However, the above-mentioned preparation methods are not suitable for the low-cost manufacturing of FPSCs because of either the high temperature annealing process or the vacuum deposition technique. The solution combustion route is helpful to lower the  $\text{NiO}_x$  preparation temperature to  $150\text{--}250^\circ\text{C}$ , which is more compatible with flexible substrates.<sup>257,258</sup> In addition, depositing pre-synthesized  $\text{NiO}_x$  nanocrystals at low temperature ( $<150^\circ\text{C}$ ) is widely applied on the FPSCs via spin coating or meniscus coating.<sup>206,248,253,259,260</sup> In 2016, Yin *et al.* deposited  $\text{NiO}_x$  films by spin coating the presynthesized  $\text{NiO}_x$  nanoparticle solution and annealing at  $130^\circ\text{C}$ , and the corresponding device achieved a PCE of 13.34%. Han *et al.* utilized  $\text{NiO}_x$  as HTL in FPSCs with perovskite processed by low-temperature soft-cover deposition method and achieved an efficiency of 15.3%.<sup>253</sup> Recently, Najafi *et al.* employed pre-synthesized, solution-derived  $\text{NiO}_x$  nanoparticles films as HTL by spin-coating method without any additional annealing treatments. The resultant FPSCs based on triple cation perovskite attained a high PCE of 16.6% with excellent durability on the ITO/PEN substrates.<sup>206</sup> Han *et al.* found that the low temperature prepared  $\text{NiO}_x$  showed inferior stability, which could be ascribed to the addition of ligands absorbed on the  $\text{NiO}_x$  surface during the fabrication process. They synthesized  $\text{NiO}_x$  nanoparticles in ethanol rather than the normally used water to reduce the absorption of hydroxyl group and water molecules. High stability was realized with this ligand-free  $\text{NiO}_x$  layer, maintaining 90% of the original efficiency after 500 h damp-heat test ( $85^\circ\text{C}$  and 85% relative humidity).<sup>260</sup>

Nevertheless,  $\text{NiO}_x$  has relatively low hole mobility which can be improved by doping strategy with metal ions such as  $\text{Mg}^{2+}$ ,<sup>252</sup>  $\text{Cs}^+$ ,<sup>261</sup>  $\text{Li}^+$ ,<sup>249</sup> and  $\text{Cu}^{2+}$ .<sup>262–264</sup> Chen *et al.* demonstrated that the substitution of  $\text{Ni}^{2+}$  with  $\text{Cu}^{2+}$  favors the increase in carrier concentration, and they performed a high PCE of 17.41% for the flexible devices by employing spin-coated Cu:NiO HTL [Figs. 7(a) and 7(b)].<sup>262</sup> In addition, the surface defects, inherent brittleness, and poor contact with perovskite hinder the development of flexible devices based on  $\text{NiO}_x$ . Zhang *et al.* demonstrated a room-temperature solution-processed  $\text{NiO}_x$  film without post-treatment which is flawless with surface nanostructures, leading to reduced charge recombination at the interface and effective hole extraction for the large contact area between HTL and absorber layer [Figs. 7(c) and 7(d)]. Finally, a PCE of 14.53% with good stability and reproducibility was realized.<sup>245</sup> Benzoic acid self-assembly monolayers could also passivate the surface defects of the  $\text{NiO}_x$  layer. Wang *et al.* demonstrated that the benzoic acid

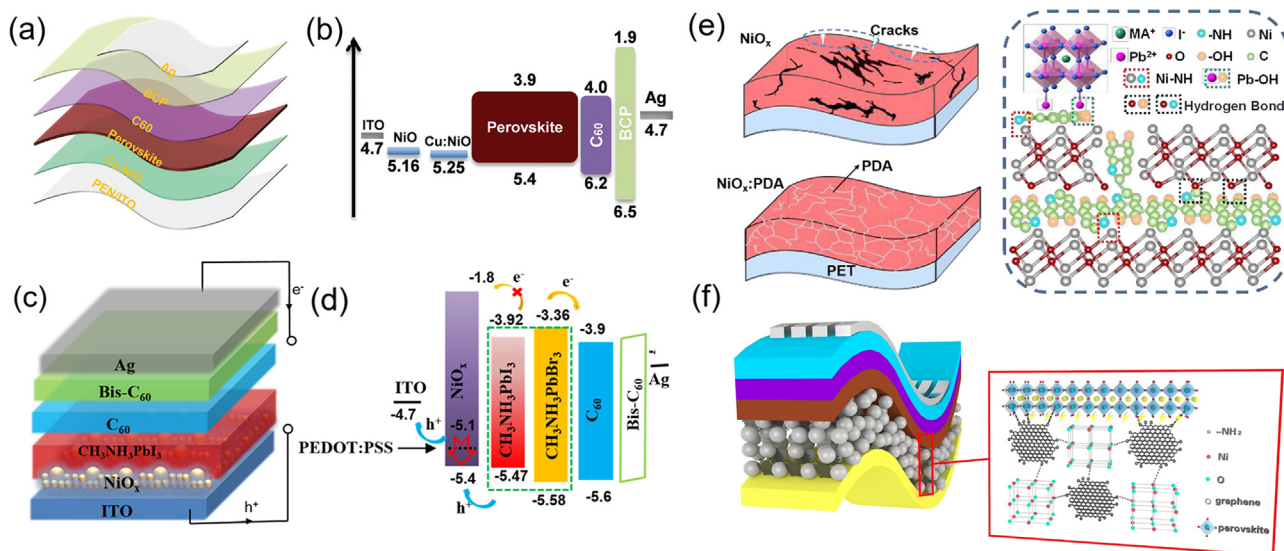


**FIG. 7.** Device configuration of FPSCs with Cu:NiO HTL (a) and nano-structured NiO<sub>x</sub> HTL (c), and the corresponding energy level diagram (b) and (d). (a) and (b) Reproduced with permission from Chen *et al.*, *Adv. Energy Mater.* **8**, 1703519 (2018). Copyright 2018 WILEY-VCH. (c) and (d) Reproduced with permission from Zhang *et al.*, *ACS Nano* **10**, 1503 (2016). Copyright 2016 American Chemical Society. (e) Illustration of NiO<sub>x</sub> film and NiO<sub>x</sub>:PDA film after constant bending, and the modification effect of NiO<sub>x</sub> HTL with PDA. Reproduced with permission from Duan *et al.*, *Chem. Commun.* **55**, 3666 (2019). Copyright 2019 Royal Society of Chemistry. (f) Schematic diagram of the NiO<sub>x</sub> HTL with the amino-functionalized graphene quantum dots as additive. Reproduced with permission from Wang *et al.*, *ACS Appl. Mater. Interfaces* **12**, 8342 (2020). Copyright 2020 American Chemical Society.

self-assembly monolayers could retard the trap-assisted recombination, minimize the energy offset between the NiO<sub>x</sub> nanoparticles and the perovskite, and change the HTL surface wettability, resulting in enhanced perovskite crystallization. Thus, a stable FPSC was realized with enhanced efficiency of 16.2% and a remarkable power-per-weight of 26.9 W/g.<sup>265</sup> Polydopamine (PDA) modified NiO<sub>x</sub> has also been employed as HTL in FPSCs via spin-coating. The modified NiO<sub>x</sub> with PDA displays a lower valence band than NiO<sub>x</sub>, and the more favorable energy level alignment between NiO<sub>x</sub>:PDA and the active layer is beneficial for gaining higher  $V_{oc}$  of FPSCs. The crosslinked NiO<sub>x</sub> with PDA could release the mechanical stress to overcome the brittleness of NiO<sub>x</sub> and realize excellent flexural endurance [Fig. 7(e)]. Thus, the device based on NiO<sub>x</sub>:PDA exhibits a PCE of 18.35% with negligible hysteresis and can maintain 70% of the initial PCE after 1000 bending cycles at a curvature radius of 5 mm.<sup>211</sup> Lately, Wang *et al.* adopted amino-functionalized graphene quantum dots as a dual-role additive in NiO<sub>x</sub> HTL, which can not only improve the crystallization of perovskite layer but also provide better energy level alignment between HTL and active layer to facilitate hole transport, leading to the best PCE of 18.10% with negligible hysteresis on the ITO/PEN substrate [Fig. 7(f)].<sup>266</sup> Chen *et al.* applied 3,6-difluoro-2,5,7,7,8,8-hexa cyanoquinodimethane molecules with high electron affinity to improve the conductivity of NiO<sub>x</sub>, resulting in enhanced hole separation and a champion efficiency of 20.01% for FPSCs.<sup>67</sup>

Moreover, other inorganic p-type semiconductor materials such as Cu<sub>2</sub>O, CuO, CuCrO<sub>2</sub>, CuSCN, CuI, and VO<sub>x</sub> were also investigated as HTL.<sup>46,267,268</sup> These low-cost materials are beneficial for HTL due to the high optical transparency and high electrical conductivity. However, the high processing temperature prohibits their extensive employment on temperature-sensitive polymer substrates. Qin *et al.*

demonstrated a low-temperature solution-processed CuCrO<sub>2</sub> HTL which has a larger bandgap compared to the copper oxides, and the resultant FPSCs performed the best efficiency of 15.53%.<sup>269</sup> Meanwhile, it is advisable to employ metal substrates such as copper foil for the easily formed copper based HTL as stated in the metal substrates section. For example, CuI HTL could be derived from Cu substrate by iodination.<sup>46</sup> In addition, some research utilized the bilayer structured HTL composed of VO<sub>x</sub> and copper phthalocyanine which exhibited excellent conductivity and suitable energy level. The room temperature preparation process is favorable for the application in FPSCs, performing an efficiency of 14.39%.<sup>270</sup>

### C. HTL-free FPSCs

It has been demonstrated that perovskite can act as both light absorber and hole transporter, thereby benefiting HTL-free PSCs.<sup>271,272</sup> HTL-free devices cannot only address the chemical stability issues which arise from unstable HTLs, but also simplify the fabrication process, reduce fabrication costs, and increase the flexibility of FPSCs. Gold has been first employed in HTL-free devices with a simple configuration of FTO/TiO<sub>2</sub>/perovskite/Au.<sup>273,274</sup> However, the ion diffusion of metal ions into the perovskite materials would cause device performance deterioration.<sup>102</sup> In addition, the high materials cost and vacuum-based deposition process of the gold electrode make it unsuitable for realizing low-cost roll-to-roll processed FPSCs.

Carbon paste is thought to be promising for electrode materials in HTL-free devices due to the capability of extracting photogenerated holes and approaching work function with Au electrodes. Moreover, carbon paste electrodes with low materials cost, high chemical stability, inertness to ion migration, and water resistance are advantageous for

highly stable devices. An opaque carbon electrode with a high temperature ( $400^{\circ}\text{C}$ ) sintering process has been employed in rigid HTL-free devices at the early edge.<sup>103</sup> With the development of low-temperature processable carbon paste electrodes, carbon-based HTL-free devices can be realized on flexible plastic substrates. Usually, the carbon paste electrode is directly printed on the pre-deposited perovskite layer, followed by drying at room temperature or heating at about  $100^{\circ}\text{C}$ .<sup>61,275,276</sup> With the blade-coated carbon pastes as the top electrode, Wang *et al.* realized an efficiency of 9.73% on the HTL-free FPSCs.<sup>276</sup> However, the poor carrier selectivity at the carbon/perovskite interface leads to high series resistance and significant charge recombination. A polymer interlayer is beneficial for adjusting interface properties and improving device performance. Qi *et al.* employed a poly-(ethylene oxide) interlayer to modify the perovskite/carbon interface, resulting in reduced energy level mismatch and enhanced charge transportation.<sup>105</sup>

In conclusion, although HTL-free devices seem advantageous in fabricating simple and stable flexible devices, there is still a significant efficiency gap between HTL-free devices and standard devices. It is still necessary to improve the efficiency of HTL-free FPSCs to enhance their competitiveness through interface modification and improvement of carbon paste compositions.

## VI. FLEXIBLE PEROVSKITE

For the flexible devices, past research paid much attention to the flexible substrate and electrode, while recently there is growing interest in the mechanical durability of perovskite films. Due to the inherent brittle nature of perovskite materials, stress-induced cracks are easily formed and propagated along the grain boundaries under repeated bending or stretching processes, resulting in diminished optoelectronic properties and environmental stability problems for the flexible devices, limiting the application potential of FPSCs.<sup>56,118,171,277</sup> In this section, a brief introduction for enhancing the perovskite film flexibility is presented.

Although there are scientists researched all inorganic perovskite and tin-based perovskite for FPSCs, the significant efficiency gap with FPSCs based on the organic-inorganic lead-based perovskite cannot be neglected.<sup>278,279</sup> From the nanoindentation measurements, organic-inorganic lead-based perovskite materials demonstrate a low Young's module with 13.5 GPa for film and 20.0 GPa for crystal, which is at a similar level to other organic layers in PSCs.<sup>56,73</sup> This is important in realizing ultra-flexible devices. The metal-halide bond would affect the elastic properties of perovskite materials and Young's module decreases on the order of  $\text{Cl} > \text{Br} > \text{I}$  determined by the electronegativity.<sup>32</sup> Nevertheless, the constituent of perovskite has a light influence on mechanical flexibility. And the common methods to improve the bending stability of perovskite film are the additive strategy and interface optimization. The normally used additives are polymers including soft elastomers, long alkyl chain polymers, cross-linking materials, self-polymerized molecules, self-healing polymers, and so on since the resilient polymer is capable of absorbing stresses to prevent the formation of cracks. Except functioned as a plasticizer in perovskite, these additives also play the role of crystal growth template in facilitating perovskite grain growth by suppressing crystallization speed and offering more nucleation sites. In addition, the polymers also act as the perovskite surface passivator by interspersing within grain boundaries to reduce defects, impede ionic migration, and against moisture

infiltration, which is important for the operational stability of PSCs.<sup>280</sup> In addition, additives with special groups could induce chemical interactions with the perovskite, leading to passivated grain boundaries and improved film flexibility. Moreover, inserting a sticky layer such as EVA would enhance the device's flexibility by bonding the adjacent layer and absorbing mechanical stress.<sup>227</sup>

### A. Additive doping

Previously, polymer additives such as poly(ethylene glycol)<sup>281,282</sup> poly(2-ethyl-2-oxazoline),<sup>283</sup> poly(4-vinylpyridine)<sup>284,285</sup> poly(ethylene oxide)<sup>286</sup> are introduced into the perovskite film to tune the perovskite grain size and optimize the film morphology, leading to significantly enhanced photovoltaic parameters and improved environmental stability for PSCs. Recently, advanced polymer doping strategies aiming at highly efficient and stable PSCs have been proposed. Yang *et al.* formed a perovskite-polymer composite cross-linker by introducing long chain polymers in perovskite precursors, which leads to the bridge of perovskite grains.<sup>287</sup> Huang *et al.* introduced sulfonic zwitterion in perovskite film, which plays dual roles in controlling crystallization and passivating defects.<sup>288</sup>

Usually, these polymer additives could simultaneously improve the device performance and enhance the environmental robustness including light, thermal, and moisture by constructing a continuous network or forming strong interactions such as hydrogen bonds with the perovskite to passivate grain boundaries. Furthermore, the above-mentioned polymers have potential in flexible device applications to enhance the device mechanical flexibility and durability. Various research has been reported to strengthen the perovskite film flexibility with polymer addition. Elastomer polyurethane (PU) was incorporated into the perovskite precursor by Chen *et al.*, and they demonstrated enhanced device performance of FPSCs with PU additive, ascribed to the large grained perovskite [Figs. 8(a) and 8(b)] and the effective charge extraction. In addition, the adjacent perovskite grain boundaries could be crosslinked by resilient PU, constructing an elastomer network to absorb mechanical stresses, realizing improved mechanical bendability.<sup>277</sup> Later, they introduced self-healing PU with a dynamic covalent oxime-carbamate structure into the perovskite layer. During severe mechanical deformation, the self-healing PU at perovskite grain boundaries would break ahead of the perovskite to release mechanical stress and subsequently repair the cracks after thermal treatment. Consequently, the stretchable PSCs they demonstrated upon PDMS substrates exhibited a high PCE of 19.15% with recoverable performance [Figs. 8(c)-8(e)].<sup>54</sup> Inspired by the elastic “brick-and-mortar structure,” Yanlin Song and co-workers employed an elastomer matrix filled into the grain boundaries, which is favorable for the flexural endurance of flexible devices. The insoluble matrix poly(styrene-co-butadiene) as a scaffold in the perovskite could facilitate the growth of large grain size by optimizing nucleation, and the soluble PU could realize a high quality perovskite film due to the retarded crystallization.<sup>55</sup> In conclusion, the functions of polymer additives in the perovskite film, including the templating effect on facilitating nucleation and crystal growth, passivate grain boundaries, suppressing ion migration, and impeding moisture invasion, could simultaneously improve device efficiency and operational stability. Moreover, the perovskite film embraced in the elastic and soft polymer could sustain server bending or stretching.<sup>248,280,289-296</sup>

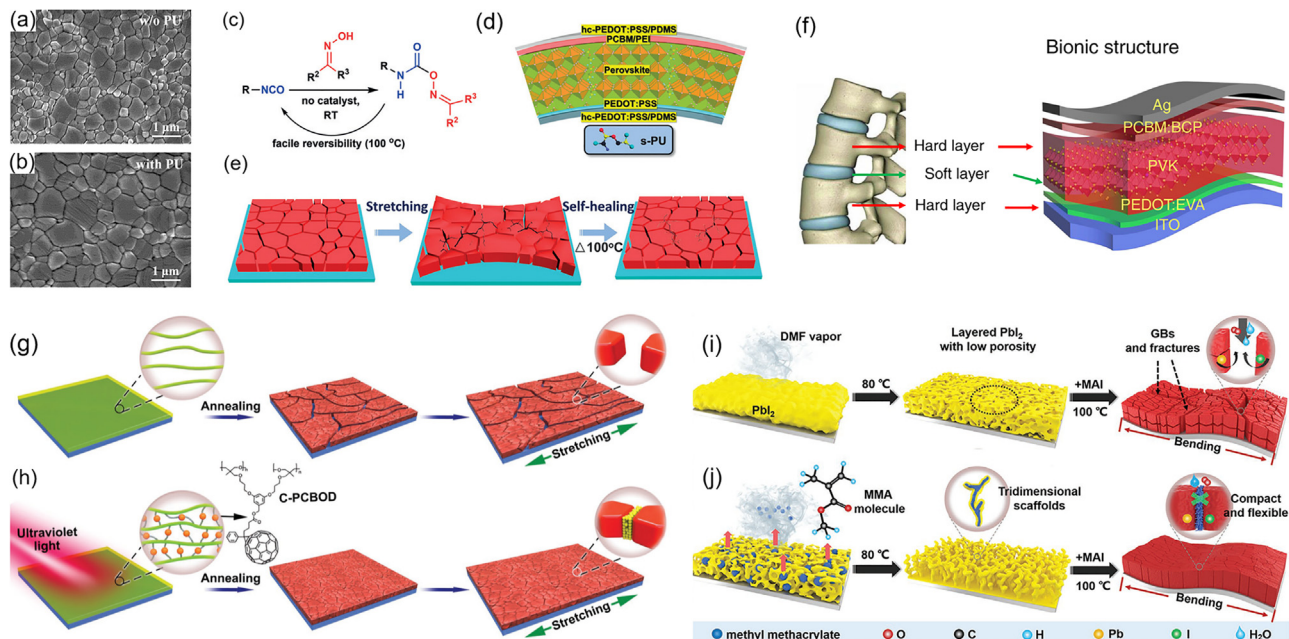


**FIG. 8.** SEM images of perovskite films without (a) and with 0.02 wt. % PU (b). (a) and (b) Reproduced with permission from Huang *et al.*, *Adv. Funct. Mater.* **27**, 1703061 (2017). Copyright 2017 WILEY-VCH. Preparation of self-healing PU (c) and device structure of the related self-healing device (d). (e) Schematic diagram of the self-healing process. (c)–(e) Reproduced with permission from Meng *et al.*, *Angew. Chem., Int. Ed.* **59**, 16602 (2020). Copyright 2020 WILEY-VCH. (f) Configuration of the device inspired by vertebra. Reproduced with permission from Meng *et al.*, *Nat. Commun.* **11**, 3016, 2020. Copyright 2020 Authors, licensed under a Creative Commons Attribution (CC BY) license. (g) Illustration of large cracks in the pristine perovskite film during bending or stretching. (h) Illustration of the mechanism of C-PCBOD doped perovskite, which is achieved by UV irradiation 5 min before film annealing. (g), (h) Reproduced with permission from Li *et al.*, *Adv. Mater.* **31**, 1901519 (2019). Copyright 2019 WILEY-VCH. (i) The typical  $\text{PbI}_2$  layer demonstrates low porosity, and the resulting perovskite layer show fractures during bending. (j) The sMMA- $\text{PbI}_2$  could form a scaffold network to facilitate MAI penetration, and the final perovskite layer is capable of releasing mechanical stress and improving environmental stability. (i) and (j) Reproduced with permission from Duan *et al.*, *Adv. Mater.* **32**, 2000617 (2020). Copyright 2020 WILEY-VCH.

In general, it has been reported that the additive with special function groups such as carbonyl or sulfonic group adhered on the perovskite grain boundary through chemical interaction with under-coordinated  $\text{Pb}^{2+}$  (also referred to as the polymer-perovskite interaction) could assist the perovskite grain growth, passivate surface defects and enhance the film ductility for the cracks often generated at the grain boundary.<sup>288</sup> The introduction of sulfonated graphene oxide in perovskite film could lead to cementitious perovskite grain boundaries due to the strong interaction that sulfonic groups and  $[\text{PbI}_6]^{4-}$  formed, which is reported by the Song group. In addition to the obviously increased waterproofness and reduced defects, the FPSCs treated with sulfonated graphene oxide demonstrated great flexibility by retaining 80% PCE after 10 000 cycles of bending test at a small radius of 3 mm.<sup>248</sup>

Novel strategies to improve the flexibility of the perovskite layer by self-cross-linking have emerged recently. The cross-linking materials which are triggered by light, heat, or moisture can form a soft network to embrace perovskite grains, enabling a more durable film to sustain bending or stretching. With the dimethyl itaconate monomers added in the precursor, Yang *et al.* developed a polymerization-assisted grain growth method in which the *in situ* polymerization process will be triggered by thermal treatment.<sup>295</sup> Similarly, trimethylolpropane triacrylate within perovskite film could anchor at the grain boundaries and *in situ* cross-links after the annealing process.<sup>296</sup> It is

rewarding to apply this method to the flexible device. Li *et al.* employed photo-crosslinked [6,6]-phenylC<sub>61</sub>-butyric oxetane dendron ester (C-PCBOD) in the perovskite film and the cross-link will take place under the ultraviolet radiation before the perovskite crystallizes. In addition to the improved environmental stability and raised efficiency due to the passivated defects at the grain boundaries, the perovskite film that embraced the soft C-PCBOD network demonstrated enhanced flexing and stretching stability [Figs. 8(g) and 8(h)].<sup>118</sup> In addition, *in situ* self-polymerized methyl methacrylate (sMMA) into  $\text{PbI}_2$ , which facilitates the perovskite crystallization by confining the precursor in the scaffold network and offering more nucleation sites. In addition, this cross-linking network formed by the sMMA oligomers is capable to release mechanical stress and prolong operational stability by passivating grain boundaries [Figs. 8(i) and 8(j)]. As a result, the flexible devices reserve 72% of the original efficiency after 5000 bending cycles at a radius of 8 mm.<sup>280</sup>

## B. Other methods

Apart from the additive assistant strategy, interfacial engineering is also useful in enhancing the mechanical flexibility of FPSCs by increasing the adhesion of the neighboring layer. Chen *et al.* have

introduced EVA into different positions in FPSCs. Except serving as a self-sealing additive in tin-based PSCs to improve environmental stability,<sup>297</sup> the conductive and glued EVA has also been employed as an interfacial layer underneath and upon the perovskite film, respectively. When the cohesive EVA layer is employed below the perovskite layer, it can stick the perovskite grains which could be ascribed to the Van Der Waals and hydrogen-bounding interaction. Hence, the mechanical stress could be absorbed and released through this sticky layer such as the spinal cartilage, leading to a mechanical robust perovskite film with no obvious cracks after 7000 bending cycles at a radius of 3 mm [Fig. 8(f)].<sup>227</sup> Correspondingly, the EVA layer placed on the perovskite film enables passivated surface defects of perovskite and favorable interfacial contact, which leads to a dense and uniform PC<sub>61</sub>BM layer on top. In addition, the adhesive interaction between the EVA-treated perovskite film and the PC<sub>61</sub>BM layer endows enhanced flexibility and moisture stability for FPSCs.<sup>213</sup> In addition, inorganic materials which could construct a cross-linking network are also effective in protecting the perovskite layer. For example, fluoro-silane deposited on top of the perovskite layer would cross-link by forming Si—O—Si bonds, which is triggered by the hydroxylation of silanes into silanols with a little water that exists in the perovskite.<sup>298</sup>

In addition, structure optimization is also profitable for FPSCs to simultaneously improve efficiency, long-term stability, and flexural endurance. Hu *et al.* prepared a nanocellular scaffold by PS microspheres before the perovskite deposition. And this scaffold acts as a mechanical buffer layer to release mechanical stresses, resulting in

highly flexible FPSCs with 93% of the initial efficiency maintained after 1000 cycles of bending test at a radius of 2 mm, which is more compelling than their counterparts with the flat interface.<sup>74</sup> Very recently, Shi *et al.* realized FPSCs with a high PCE of 20.1% with diffused ETL/perovskite interface, which could provide enhanced carrier extraction and transport. In addition, the interpenetrating structure could significantly improve mechanical reliability compared to the sharp interfaces.<sup>299</sup> They also grew low-dimensional perovskite materials as a capping layer above the 3D perovskite, which is effective in improving carrier separation, providing protection for FPSCs to resist water penetration, and enhancing mechanical reliability. An unprecedented efficiency of 21.0% was achieved and 81% of the original PCE could be retained after 20,000 tension-only bending cycles at a radius of 5 mm.<sup>12</sup>

## VII. CHALLENGES

### A. Higher efficiency

Although various flexible substrates and flexible electrodes have been developed in FPSCs, the polymer/ITO demonstrates the best overall performance in FPSCs with the highest efficiency of over 21%.<sup>11,12</sup> Nonetheless, the polymer/ITO based FPSCs still demonstrated an inferior efficiency compared to their rigid counterparts as shown in Fig. 9(a). There are several factors that may account for the reduced performance of flexible devices, and all of them are related to the flexible substrates and flexible electrodes.

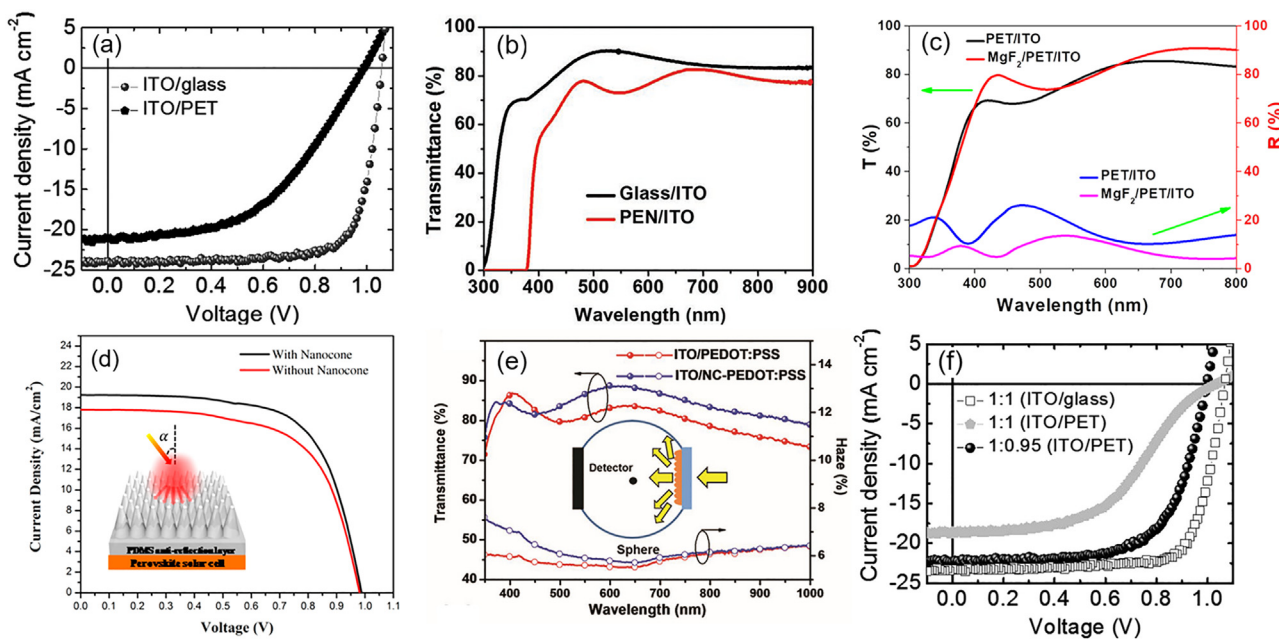


**FIG. 9.** (a) Typical J-V curves of devices based on ITO/glass and ITO/PET substrates. Reproduced with permission from Bi *et al.*, *Adv. Mater.* **29**, 1605900 (2017). Copyright 2017 WILEY-VCH. (b) The comparison of optical transmittance between glass/ITO and PEN/ITO substrates. Reproduced with permission from Huang *et al.*, *Adv. Energy Mater.* **9**, 1901419 (2019). Copyright 2019 WILEY-VCH. (c) Transmission and reflectance spectra of PET/ITO substrates with and without the MgF<sub>2</sub> layer. Reproduced with permission from Feng *et al.*, *Adv. Mater.* **30**, 1901418 (2018). Copyright 2018 WILEY-VCH. (d) J-V curves of devices with and without the nanocone PDMS layer and the inset shows the light scattering effect of the PDMS film. Reproduced with permission from Tavakoli *et al.*, *ACS Nano* **9**, 10287 (2015). Copyright 2015 American Chemical Society. (e) Transmittance and haze spectra of ITO/PEDOT:PSS and ITO/NC-PEDOT:PSS, and the inset illustrates the measurement of optical properties with an integrating sphere. Reproduced with permission from Hu *et al.*, *Adv. Mater.* **29**, 1703236 (2017). Copyright 2017 WILEY-VCH. (f) J-V curves of devices with different precursor ratios on the rigid and flexible substrates. Reproduced with permission from Bi *et al.*, *Adv. Mater.* **29**, 1605900 (2017). Copyright 2017 WILEY-VCH.

- (1) Higher sheet resistance.<sup>108,120,123,129,140,166,206,225</sup> The sheet resistance of ITO/PET or ITO/PEN substrates is about  $60 \Omega/\square$  which is apparently higher than that of the ITO/glass ( $10\text{--}15 \Omega/\square$ ) and FTO/glass ( $7 \Omega/\square$ ) substrates.<sup>123,205,206</sup> The higher series resistance would result in decreased  $J_{sc}$  and FF, and eventually poor efficiency for FPSCs.
- (2) Lower optical transparency [Fig. 9(b)].<sup>61,108,123,129,140</sup> Compared to the high light transmittance of 92% of the FTO/glass substrate, the flexible substrate such as ITO/PET substrate only exhibits 78% light transmittance,<sup>123</sup> resulting in less incident light reaching the absorbing layer. Consequently, the flexible devices showed decreased photo-generated electrons and limited performance. The antireflection layer such as MgF<sub>2</sub> or nanocone PDMS film for light scattering is desirable in reducing the optical reflection [Figs. 9(c) and 9(d)].<sup>51,69</sup> In addition, substrates or electrodes with a high haze ratio are also beneficial for light utilization. For example, nanopaper substrate and AgNW film electrode.<sup>36,93</sup> Moreover, the surface nano-structure of the functional layer could also improve the light harvest, for instance, the nanocellular PEDOT:PSS HTL as shown in Fig. 9(e).<sup>74</sup>
- (3) Rougher surface.<sup>157,171,208</sup> The polymer substrates have high surface roughness, which results in low conductivity of transparent electrodes that are deposited subsequently. In particular, the unevenness of the substrate will lead to inferior film morphology of the charge transport layer and perovskite film. Generally, polishing for metal foil substrates and coating planarization layer for polymer substrates can realize a smooth surface for depositing subsequent layers. For example, Liu *et al.* coated 2  $\mu\text{m}$  polymer on the PET substrate to decrease the surface roughness and improve the device performance.<sup>241</sup> Adjustments of the solution concentration or precursor ratio also work to control the morphology of functional layers. By varying the concentrations of SnO<sub>2</sub> solution, Ding and coworkers demonstrated a precisely controlled SnO<sub>2</sub> ETL which leads to increased photo transmittance of substrates and reduced trap density of perovskite materials.<sup>157</sup> Huang and coworkers fabricated a high-quality perovskite film on ITO/PET substrates by optimizing the precursor ratio of perovskite, leading to an efficiency of 18.1% [Fig. 9(f)].<sup>208</sup>

In addition, other potential causes have been raised, for example, the higher work function of ITO/PEN than ITO/glass substrate, which brings about a larger Schottky barrier at the ETL/ITO junction, resulting in poor FF in flexible devices.<sup>195</sup> Advanced electrodes with good optoelectrical qualities and surface morphology are urgently needed to develop high-performance FPSCs.

## B. Higher flexibility

In addition to achieving high efficiency, the most appealing thing for FPSCs is to realize better mechanical flexibility. In addition to the methods mentioned above to enhance the flexibility of perovskite materials through doping strategy and structural optimization, the geometrical engineering approach also helps to enhance the mechanical reliability of FPSCs during the bending process. Flexible devices would suffer severe mechanical stress ( $\sigma$ ) during the small radius ( $r$ ) bending test.<sup>30,56</sup> According to Eq. (4), Young's modulus ( $E$ ) of

perovskite film and the thickness of substrate would affect the maximum stress,<sup>299,300</sup>

$$\sigma = \frac{Et}{2r}. \quad (4)$$

Specifically, the concave and convex side of the device undergoes compressive and tensile stress upon bending, respectively. There is research revealed that convex bending (the perovskite film at the convex side) will lead to cracks on the perovskite film and decreased electrical conductivity of perovskite film, resulting in worse mechanical stability than concave bending.<sup>301</sup> Moderate concave bending (the perovskite film at the concave side) is beneficial to heal the perovskite cracks, while large compression stress (small concave bending radius) will result in peel-off and even delamination at the perovskite/ETL interface [Fig. 10(a)].<sup>12,299,300</sup> To enhance the mechanical stability and diminish the damage caused by flexing, there are two main strategies via the structure optimizing method. One is reducing the thickness of the substrate or bottom electrode, which is a reasonable method for lessening the strain applied on the perovskite layer as stated in Eq. (4).<sup>56,69</sup> Choi *et al.* displayed that neither device efficiencies nor surface morphology change could be observed in 2.5  $\mu\text{m}$  thick PET substrates after 1000 bending cycles at a teeny curvature radius of 0.5 mm. In comparison, the devices on the 30 and 100  $\mu\text{m}$  thick PET substrates demonstrated cracks in the perovskite film and large performance degradation as displayed in Figs. 10(b<sub>1</sub>)–10(b<sub>3</sub>).<sup>56</sup>

The other is to apply a mechanical design to shift the perovskite layer to the neutral plane where the compressive and tensile stress is compensated as described in Fig. 10(c).<sup>56</sup> And this method could realize ultra-flexibility along with foldability. Usually, placing a proper layer such as parylene or PDMS above the device is a wise choice to simultaneously shift the mechanical neutral plane from substrate to perovskite layer and protect the device against environmental threats [Fig. 10(d)].<sup>51,55,56,73,302</sup> Song *et al.* fabricated ultra-flexible FPSCs with negligible decrease performance after 5000 bending cycles at a curvature radius of 2 mm, which is mainly attributed to the introduction of the top PDMS layer by shifting the perovskite layer to the mechanical neutral plane.<sup>55</sup> In addition, ultrathin substrates could also achieve the purpose of tuning the perovskite layer to the neutral plane.<sup>37</sup>

## C. Higher stability

The unsatisfactory operational and long-term stability of FPSCs limits their applications, which are mainly caused by the decomposition of sensitive perovskite layers under ambient conditions. In addition, the unstable organic charge transporting materials and electrode materials are corrosive for FPSCs under thermal stress or moisture invasion. Encapsulation is a feasible and universal strategy to extend the lifetime of FPSCs by preventing oxygen and moisture invasion. Unlike rigid devices which can be effectively encapsulated with glass sheets and epoxy, flexible devices require lightweight, flexible sealing materials. Film packaging with organic materials such as PDMS is more suitable but has a high water vapor transmission rate and cannot be employed alone for effective encapsulation. The multilayer in which the organic layer is combined with the inorganic layer has a low water vapor transmission rate and small oxygen infiltration and is more promising to improve device stability. Upon the PDMS barrier layer (with synthesized CdSe/ZnS-QD), Park *et al.* spin-coated an inorganic perhydropolysilazane layer, which could convert into dense SiO<sub>2</sub> film

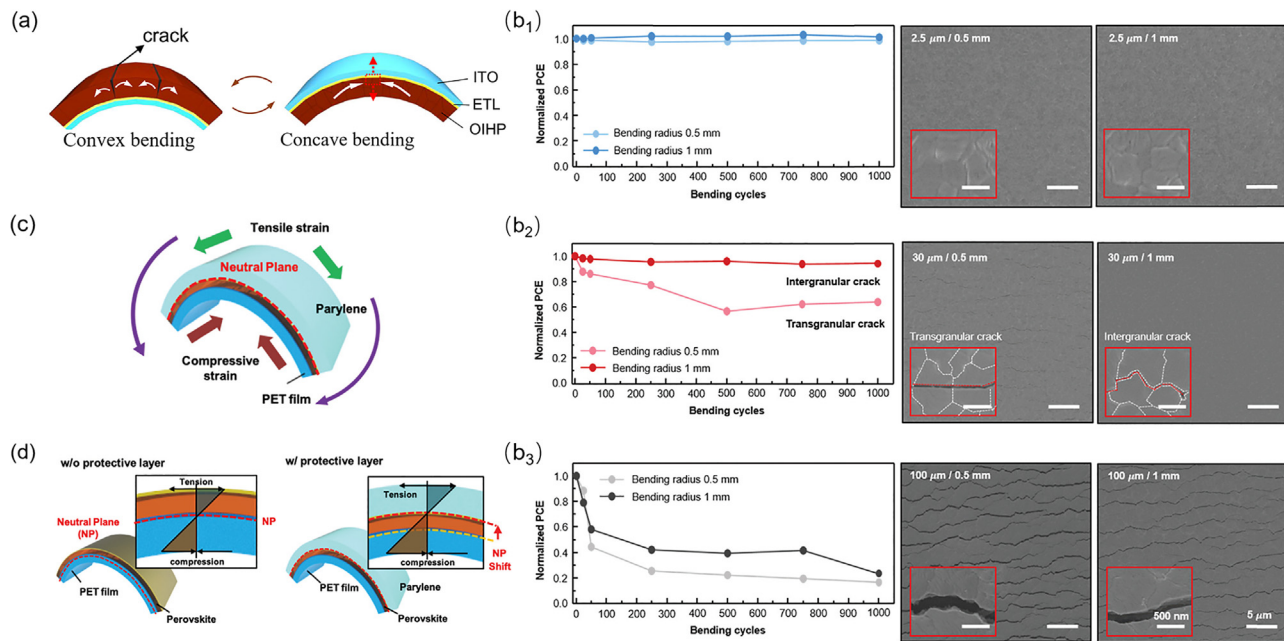


**FIG. 10.** (a) The demonstration of convex bending and concave bending of FPSCs. Reproduced with permission from Dong *et al.*, Nat. Commun. **12**, 973, 2021. Copyright 2021 Authors, licensed under a Creative Commons Attribution (CC BY) license. (b) Normalized PCEs as a function of bending cycles and the corresponding SEM images of the perovskite layer after bending at 0.5 and 1 mm curvature radius on the 2.5  $\mu\text{m}$  thick (b<sub>1</sub>), 30  $\mu\text{m}$  thick (b<sub>2</sub>), and 100  $\mu\text{m}$  thick (b<sub>3</sub>) substrates. (c) Demonstration of the neutral plane. (d) Illustrations of devices without and with a protective layer. (b<sub>1</sub>)–(b<sub>3</sub>), (c), and (d) Reproduced with permission from Lee *et al.*, Energy Environ. Sci. **12**, 3182 (2019). Copyright 2019 Royal Society of Chemistry.

against moisture. The resulting encapsulation layer showed a very low water vapor transmission rate of  $8.63 \times 10^{-3} \text{ gm}^{-2} \text{ d}^{-1}$  ( $37.8^\circ\text{C}/100 \text{ RH}\%$ ) and the encapsulated FPSCs maintained the initial efficiency for more than 400 h under ambient conditions.<sup>303</sup> Simple encapsulation methods using flexible barrier film could enhance the operational stability of FPSCs. However, Weerasinghe *et al.* revealed that moisture invasion through the adhesive films and the electrical wire contacts will limit the long-term stability of the encapsulated devices.<sup>304</sup>

Preventing the ingress of environmental threats by external physical encapsulation can effectively improve the device stability, and besides, forming a protective layer on the perovskite film also helps to achieve better device stability. Huang *et al.* introduced a fluoro-silane film on the perovskite layer, which can be cross-linked by forming Si–O–Si bonds, thereby resulting in a waterproof layer to prevent moisture erosion.<sup>298</sup> In addition, low-dimensional perovskite could improve the operational stability of devices due to their hydrophobic nature. Shi *et al.* applied *in situ*-grown low dimensional perovskite capping layer on top of the three-dimensional perovskite layer. Except for the improved device efficiency, the FPSCs with a low-dimensional perovskite layer retained 90% of the original efficiency after 800 h under continuous 1-sun illumination, while the control FPSCs dropped to 79% after 475 h, as demonstrated in Fig. 11(a).<sup>12</sup>

The above strategies can effectively improve the device stability by preventing the decomposition of perovskite caused by moisture and air intrusion, but cannot avoid the decomposition inside the device caused by ions migration, chemical reactions, light, and thermal stress. For perovskite materials, some studies have made efforts on passivating grain boundaries to suppress ions migration, thereby

improving device operational stability.<sup>292,305</sup> As illustrated in Fig. 11(b), Bai *et al.* wrapped perovskite grains within oligomeric silica matrix to passivate defects, leading to extended operational stability for PSCs.<sup>305</sup> For transparent metallic electrodes such as AgNW, metal meshes, and UTMF, the diffusion and chemical reaction of halide ions and metal atoms would decompose perovskite materials and electrodes, resulting in severe device deterioration. As discussed in Sec. IIID, combining unstable metallic electrodes with isolation layers such as TCO, conducting polymer and carbon nanomaterials is an effective strategy to improve chemical stability. For opaque metal film (Au, Ag film) that has generally been applied as top electrodes, an inorganic isolation layer such as Cr<sub>2</sub>O<sub>3</sub>/Cr is effective to inhibit ions diffusion and suppress detrimental reactions between the metallic electrode and perovskite materials.<sup>8</sup> Moreover, replacing metallic electrodes with opaque carbon paste is favorable in realizing ultra-stable FPSCs due to the excellent chemical and moisture resistance of carbon materials. Wojciechowski *et al.* employed commercial carbon paste as the top electrode and the corresponding FPSCs performed outstanding operational (at the maximum power point) and thermal (inside the nitrogen-filled glovebox at 85 °C) stability over 1000 h of aging.<sup>306</sup> For the commonly applied HTL such as spiro-OMeTAD, the used dopants are usually corrosive and hygroscopic, leading to the degradation of moisture-sensitive perovskite film.<sup>157</sup> In addition, the water absorption and acidity of PEDOT:PSS are detrimental to perovskite materials and ITO electrode, resulting in accelerated deterioration of device.<sup>234,236</sup> Therefore, developing alternative HTL materials with comparable performance but with better long-term stability is required in FPSCs. For the ETL used in FPSCs, TiO<sub>2</sub> suffers from the inherent instability

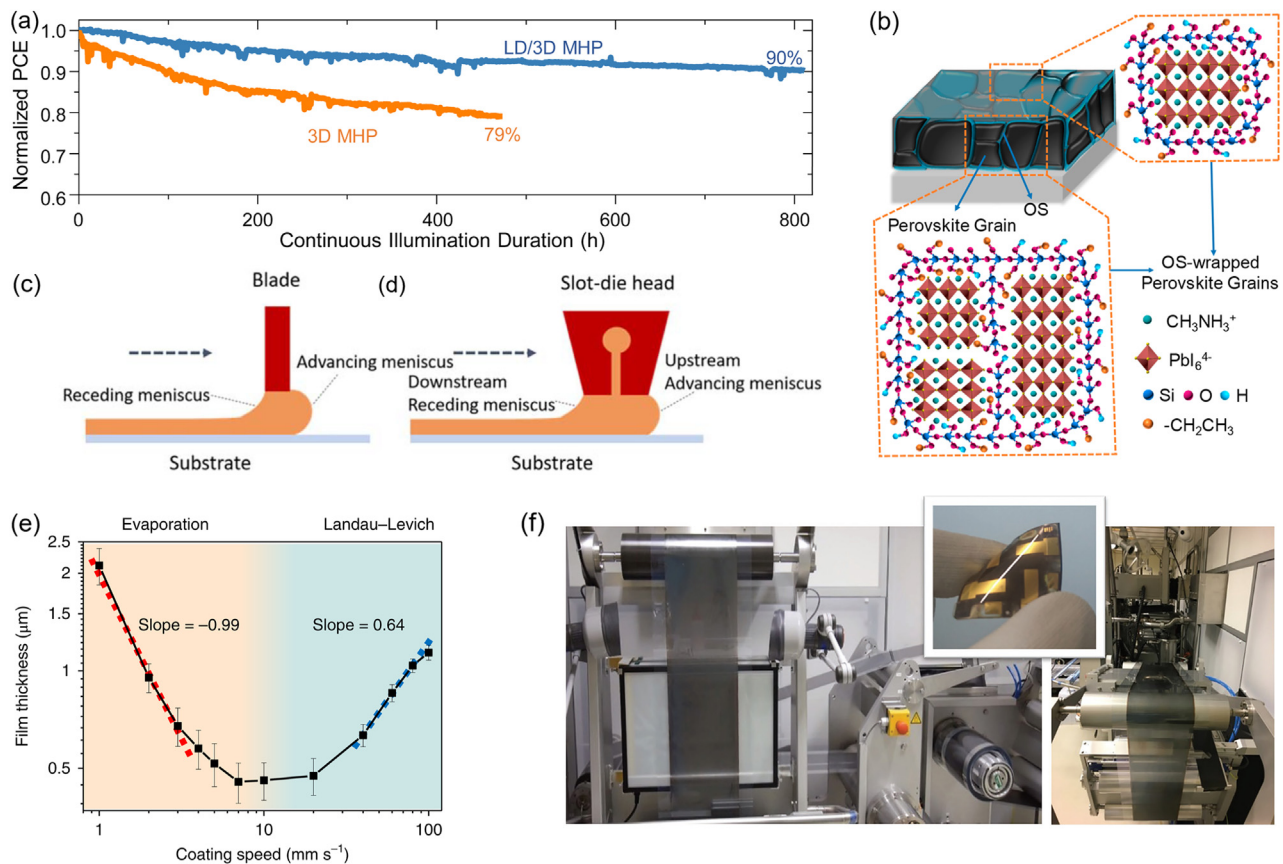


**FIG. 11.** (a) Normalized efficiencies of FPSCs with and without low-dimensional perovskite capping layers as a function of time. (1-sun illumination, MPP tracking, flowing N<sub>2</sub> atmosphere,  $\sim 45^\circ\text{C}$ ). Reproduced with permission from Dong *et al.*, Joule 5, 1587 (2021). Copyright 2021 Elsevier. (b) Schematic illustration of oligomeric silica-wrapped perovskite grains. Reproduced with permission from Bai *et al.*, ACS Energy Lett. 4, 1231 (2019). Copyright 2019 American Chemical Society. Schematic diagram of blade coating (c) and slot-die coating (d). Dai *et al.*, Int. J. Extrem. Manuf. 1, 22004 (2019). Copyright 2019 Authors, licensed under a Creative Commons Attribution (CC BY) license. (e) The thickness of the perovskite film as a function of blade-coating speed. Reproduced with permission from Deng *et al.*, Nat. Energy 3, 560 (2018). Copyright 2018 Springer Nature. (f) Photograph images of the roll-to-roll coated perovskite film and an example of FPSC. Reproduced with permission from Galagan *et al.*, Adv. Energy Mater. 8, 1801935 (2018). Copyright 2018 WILEY-VCH.

upon UV exposure.<sup>137</sup> In addition, the thermal instability of the ZnO/ $\text{CH}_3\text{NH}_3\text{PbI}_3$  interface caused by the proton-transfer reactions hinders the application of ZnO ETL.<sup>147</sup> Proper passivation of TiO<sub>2</sub> and ZnO surface is efficient for stabilizing devices, and the most efficient way is to replace them with other ETLs such as SnO<sub>2</sub>, as discussed in Sec. IV.

In conclusion, to comprehensively improve the long-term stability of FPSCs, multiple improvements are required, including external packaging, barrier isolation, grain stabilization, and selection of stable electrodes, ETL and HTL.

#### D. Scalable fabrication

In terms of commercialization, FPSCs are more promising than rigid devices due to the low-cost and continuous roll-to-roll processing capabilities. In addition, FPSCs have achieved efficiencies of over 21% in small areas ( $\sim 0.1 \text{ cm}^2$ )<sup>10,11</sup> but the efficiency in large-area devices is poor. For example, Meng *et al.* achieved a PCE of 17.55% for FPSCs on an effective area of  $31.20 \text{ cm}^2$ .<sup>227</sup> The main reasons for the

decreased efficiency of large-area FPSCs are the amplification of the electrode series resistance and film defects when the effective area is increased. Methods to fabricate large-area functional layers with conformality and fewer pinholes are needed to minimize the efficiency loss when scaling up the fabrication of FPSCs. This section briefly summarized different coating methods which have been applied in FPSCs and focused on scalable deposition methods.

The vapor deposition method can form a conformal film on an uneven surface. However, the requirement of vacuum conditions increases the complexity and cost of the fabrication process, which is not suitable for mass production. In comparison, solution methods are low-cost strategies for fabricating thin films under ambient conditions. Spin-coating is a widely used method to conveniently produce high-quality functional layers in the laboratory with a small area. However, it is difficult to control the film morphology over a large area in the spin coating method. The low material usage and low throughput of spin coating are not suitable for scalable production.

Continuous roll-to-roll processes are profitable for commercialization due to low materials wasting and high production rates, which is efficient and cost-effective. Spray coating, inkjet printing, screen printing, and meniscus coating have been widely employed in flexible printed electronics and are compatible with the roll-to-roll process. Meniscus coating is considered the most promising technique to realize scalable fabrication of FPSCs. As illustrated in Figs. 11(c) and 11(d), scalable meniscus coating refers to the formation of the meniscus shape during coating of the solution, and mainly includes blade coating and slot-die coating.<sup>307</sup> Blade coating has been widely applied in PSCs due to its simplicity and versatility.<sup>205,210</sup> The challenge in the blade-coated films is the non-uniformity surface which is mainly caused by the inherent solution flow dynamics.<sup>308</sup> In addition, the non-wetting issue of perovskite solution to substrates will result in incomplete coverage of perovskite film. Huang and co-workers reported tiny surfactant additive (for example, l- $\alpha$ -phosphatidylcholine) in bladed coated perovskite film which could impact the surface tension and improve the affinity of perovskite solution to flexible substrates, resulting in a uniform and smooth perovskite films.<sup>308</sup> Except for additive engineering, substrates' pre-heating, and proper coating speed are also significant for producing continuous and compact perovskite films. Huang *et al.* demonstrated that the blade-coating speed will result in different deposition modules and varied film thickness as shown in Fig. 11(e).<sup>308</sup> In addition, gas-assisted blade coating enables high-speed deposition, which incorporates an N<sub>2</sub> knife to accelerate solvent evaporation rate. With the perovskite films deposited by gas-assisted blade coating, Huang *et al.* obtained FPSCs with a PCE of 19.72% on a small area and 15.86% on an area of 42.9 cm<sup>2</sup>.<sup>309</sup>

Slot-die coating is a large-scale industry-compatible technology, which requires optimization of layer uniformity and fast crystallization kinetics to obtain high-quality films.<sup>310</sup> In addition to the organic function layers which are relatively favorable for slot-die coating,<sup>87</sup> researchers have also fabricated inorganic charge transport materials via slot-die coating. Bu *et al.* performed slot-die-coated large-area SnO<sub>2</sub> film with the assistance of hot air blowing, and the corresponding flexible modules (5 × 6 cm<sup>2</sup>) obtained an efficiency of over 15%.<sup>159</sup> Galagan *et al.* demonstrated the commercial feasibility of upscaling FPSCs using a roll-to-roll slot-die coating technique, as demonstrated in Fig. 11(f). With the slot-die coated SnO<sub>2</sub> and perovskite layers, they realized an efficiency of 13.5% in FPSCs.<sup>310</sup>

With advantages such as contactless, high throughput, conformal film coverage, and compatibility with various substrates, ultrasonic spray coating is a cost-effective roll-to-roll compatible technique. Das *et al.* employed the ultrasonic spray-coated perovskite layer in FPSCs and achieved a PCE of 8.1%.<sup>311</sup> In addition, inkjet printing with the advantage of very low material waste is suitable for mass production. Moreover, the inkjet printing method allows for customization due to computer-programmed patterns. Vedraine *et al.* inkjet printed WO<sub>x</sub>, perovskite, and spiro-OMeTAD layers under low-temperature ambient conditions, demonstrating the prospects of large-scale flexible devices.<sup>312</sup>

It has been proved that all functional layers in FPSCs are capable of being printed with a roll-to-roll process, except for the top metal film electrodes, which are deposited in vacuum conditions.<sup>205,313</sup> To address this problem, replacing metal film electrodes with printable carbon pastes is promising, due to the compatibility with scalable fabrication methods such as screen printing and blade coating.<sup>306</sup>

However, scalable printing methods in FPSCs are in the preliminary stage and large-area FPSCs still demonstrate low efficiency. Further improvements in film uniformity and crystallization kinetics need to be developed to enhance the efficiency of large-size FPSCs for commercialization.

## VIII. SUMMARY AND FUTURE PERSPECTIVES

In this review, recent breakthroughs of FPSCs have been summarized through different functional layers: (i) Flexible substrate: critically assessments of various flexible substrates are given, including polymers (PET, PEN, and PI), metals (Ti, Cu), biomass (paper, cellulose, and chitin), and other materials such as flexible glass and photoresist. In addition, the handling problem of FPSCs that are based on the ultra-thin substrate is also provided. (ii) Flexible electrode: broadly used flexible electrodes are discussed, including ITO, PEDOT:PSS, CNT, graphene, metal nanowires, metal meshes, and UTMFs, focusing on the optical transparency and electrical resistance. (iii) Charge transporting layer: the low temperature processed ETL, such as TiO<sub>2</sub>, ZnO, SnO<sub>2</sub>, Nb<sub>2</sub>O<sub>5</sub>, and HTL including Spiro-OMeTAD, PTAA, PEDOT:PSS, NiO<sub>x</sub>, etc. are reviewed from the perspective of optoelectrical properties, fabrication method, doping strategy, interface engineering and structure optimization. (iv) Flexible perovskite layer: the strategies in making more durable perovskite film are summarized, such as addition of doping and interface engineering, which could induce high-quality perovskite films and absorb mechanical stress to prevent cracks. Additionally, fiber-shaped FPSCs and mesoporous FPSCs are also introduced apart from the mainstream planar FPSCs. In the end, we highlight the major obstacles in realizing high-efficient ultra-flexible devices and present future development trends in FPSCs.

The gap between polymer substrates and rigid glass substrates needs to be minimized in terms of light transmittance, electrical resistance, and surface roughness to improve the efficiency of FPSCs. The advanced FPSCs with the highest efficiency are usually fabricated upon PET/ITO or PEN/ITO substrates, but the inferior flexibility and the high cost of ITO impede their applications in flexible devices. Other flexible electrodes with unique properties have different weaknesses in mechanical and chemical stability, optical clarity, electrical conductivity, etc. By combining the advantages of different materials, the composite electrode will be the most promising electrode in FPSCs to realize both high efficiency and good mechanical durability. Better additives, interface, and structure optimization should be employed in the low temperature processed charge transporting layers and perovskite layers in pursuing highly efficient and mechanical durable FPSCs.

In addition, the toxicity of the Pb-based FPSCs is a major hurdle in the application of portable and wearable electronics, which are possible to directly contact human skins and are difficult to recycle. A lead-free absorber and reliable encapsulation could mitigate this problem. The higher water vapor transmission rate of polymer substrates than glass substrates results in worse environmental stability of FPSCs. Apart from the proper encapsulation, replacing metal electrodes with stable carbon electrodes is also helpful in reducing the ion migration and improving device stability. In addition, the manufacturing cost and the scalability issues of FPSCs are also important in commercialization. Flexible devices are relatively cost-effective than rigid counterparts due to their suitability for roll-to-roll manufacturing. The expensive materials such as electrodes (ITO, Au) and HTL

(Spiro-OMeTAD, PTAA) could be replaced by developing cheaper materials. Printing methods with roll-to-roll processes are attractive for fabricating large-area FPSCs, while the low device efficiency could be increased by improving film quality. Efficiency improvement along with the study of flexibility enhancement of FPSCs is ongoing. We believe that FPSCs will play a major role in the future flexible PV market.

## ACKNOWLEDGMENTS

This work was financially supported by the National Natural Science Foundation of China (No. 52192610), the National Key Research and Development Program of China (Grant No. 2021YFA0715600), and the Fundamental Research Funds for the Central Universities and the Innovation Fund of Xidian University.

## AUTHOR DECLARATIONS

### Conflict of Interest

The authors have no conflicts to disclose.

## DATA AVAILABILITY

The data that support the findings of this study are available within the article.

## NOMENCLATURE

AgNWs	Silver nanowires
ALD	Atomic layer deposition
AZO	Aluminum doped zinc oxide
CNTs	Carbon nanotubes
C-PCBOD	[6,6]-phenylC <sub>61</sub> -butyric oxetane dendron ester
CPI	Colorless polyimide
DSSCs	Dye-sensitized solar cells
e-beam	Electron beam
EDTA	Ethylene diamine tetraacetic acid
ETL	Electron transport layer
EVA	Poly(ethylene-co-vinyl acetate)
FF	Fill factor
FK209	Tris(2-(1 <i>H</i> -pyrazol-1-yl)-4- <i>tert</i> -butylpyridine)-cobalt(III) tris(bis(trifluoromethylsulfonyl)imide)
FPSCs	Flexible perovskite solar cells
FTO	Fluorine doped tin oxide
GW	Gigawatts
HOMO	Highest occupied molecular orbital
HTL	Hole transport layer
ITO	Indium tin oxide
IZO	Indium zinc oxide
J-V	Density–voltage
<i>J<sub>sc</sub></i>	Short-circuit current density
LiTFSI	Bis (trifluoromethane) sulfonimide lithium salt
nTi-MOF	Nanocrystalline Ti-based metal-organic framework
NC-PEDOT:PSS	Nanocellular PEDOT:PSS
NOA63	Norland Optical Adhesive 63
OPV	Organic photovoltaic
PCBM	[6,6]-phenyl-C <sup>61</sup> -butyric acid methyl ester

PCE	Power conversion efficiency
PDA	Polydopamine
PDMS	Polydimethylsiloxane
PEALD	Plasma enhanced atomic layer deposition
PEDOT:PSS	Poly(3,4-ethylenedioxythiophene):poly(styrenesulfonate)
PEN	Polyethylene naphthalate
PET	Polyethylene terephthalate
PhNa-1T	1,4-bis(4-sulfonatobutoxy) benzene and thiophene moieties
PI	Polyimide
PMMA	Polymethyl methacrylate
PNDI-2T	Poly([N,N'-bis(2-octyldodecyl)-1,4,5,8-naphthalene bis(dicarboximide)-2,6-diyl]-alt-5,5'-(2,2'-bithiophene))
PSCs	Perovskite solar cells
PTAA	Poly(bis(4-phenyl)(2,4,6-trimethylphenyl)amine)
PU	Polyurethane
PV	Photovoltaic
RMS	Root mean square
sMMA	Self-polymerized methyl methacrylate
ss-IL	Solid-state ionic-liquids
TCO	Transparent conductive oxide
UTMFs	Ultra-thin metal films
<i>V<sub>oc</sub></i>	Open-circuit voltage

## REFERENCES

- <sup>1</sup>REN21, *Renewables 2021 Global Status Report* (REN21 Secretariat, Paris, 2021).
- <sup>2</sup>National Energy Administration, see [http://zfxgk.nea.gov.cn/2021-05/11/c\\_139958210.htm](http://zfxgk.nea.gov.cn/2021-05/11/c_139958210.htm) “Notice of the National Energy Administration on Matters Relating to the Development and Construction of Wind Power and Photovoltaic Power Generation in 2021.”
- <sup>3</sup>OXFORD PV, see <https://www.oxfordpv.com/tandem-cell-production>, for information about Tandem cell production.
- <sup>4</sup>NREL, see <https://www.nrel.gov/pv/cell-efficiency.html> “Best Research-Cell Efficiency Chart (2021)”
- <sup>5</sup>H. S. Jung, G. S. Han, N.-G. G. Park, and M. J. Ko, *Joule* **3**, 1850 (2019).
- <sup>6</sup>J. Di, J. Du, Z. Lin, S. (Frank) Liu, J. Ouyang, and J. Chang, *InfoMat* **3**, 293 (2021).
- <sup>7</sup>L. Yang, M. Singh, S. Shen, K. Chih, S. Liu, C. Wu, C. Chu, and H. Lin, *Adv. Funct. Mater.* **31**, 2008259 (2021).
- <sup>8</sup>M. Kaltenbrunner, G. Adam, E. D. Głowacki, M. Drack, R. Schwödauer, L. Leonat, D. H. Apaydin, H. Groiss, M. C. Scharber, M. S. White, N. S. Sariciftci, and S. Bauer, *Nat. Mater.* **14**, 1032 (2015).
- <sup>9</sup>J. Zhang, W. Zhang, H.-M. Cheng, and S. R. P. Silva, *Mater. Today* **39**, 66 (2020).
- <sup>10</sup>S. Wu, Z. Li, J. Zhang, X. Wu, X. Deng, Y. Liu, J. Zhou, C. Zhi, X. Yu, W. C. H. Choy, Z. Zhu, and A. K. Y. Jen, *Adv. Mater.* **33**, 2105539 (2021).
- <sup>11</sup>L. Yang, Q. Xiong, Y. Li, P. Gao, B. Xu, H. Lin, X. Li, and T. Miyasaka, *J. Mater. Chem. A* **9**, 1574 (2021).
- <sup>12</sup>Q. Dong, M. Chen, Y. Liu, F. T. Eickemeyer, W. Zhao, Z. Dai, Y. Yin, C. Jiang, J. Feng, S. Jin, S. Liu, S. M. Zakeeruddin, M. Grätzel, N. P. Padture, and Y. Shi, *Joule* **5**, 1587 (2021).
- <sup>13</sup>M. H. Kumar, N. Yantara, S. Dharani, M. Graetzel, S. Mhaisalkar, P. P. Boix, and N. Mathews, *Chem. Commun.* **49**, 11089 (2013).
- <sup>14</sup>F. D. Giacomo, V. Zardetto, A. D’Epifanio, S. Pescetelli, F. Matteocci, S. Razza, A. D. Carlo, S. Licoccia, W. M. M. Kessels, M. Creatore, and T. M. Brown, *Adv. Energy Mater.* **5**, 1401808 (2015).

- <sup>15</sup>V. Zardetto, F. D. Giacomo, G. Lucarelli, W. M. M. Kessels, T. M. Brown, and M. Creatore, *Sol. Energy* **150**, 447 (2017).
- <sup>16</sup>B. Feleki, G. Bex, R. Andriessen, Y. Galagan, and F. Di Giacomo, *Mater. Today Commun.* **13**, 232 (2017).
- <sup>17</sup>J. Dagar, S. Castro-Hermosa, M. Gasbarri, A. L. Palma, L. Cina, F. Matteocci, E. Calabro, A. D. Carlo, and T. M. Brown, *Nano Res.* **11**, 2669 (2018).
- <sup>18</sup>J. Troughton, D. Bryant, K. Wojciechowski, M. J. Carnie, H. Snaith, D. A. Worsley, and T. M. Watson, *J. Mater. Chem. A* **3**, 9141 (2015).
- <sup>19</sup>L. Qiu, J. Deng, X. Lu, Z. Yang, and H. Peng, *Angew. Chem., Int. Ed.* **53**, 10425 (2014).
- <sup>20</sup>H. Hu, K. Yan, M. Peng, X. Yu, S. Chen, B. Chen, B. Dong, X. Gao, and D. Zou, *J. Mater. Chem. A* **4**, 3901 (2016).
- <sup>21</sup>L. Qiu, S. He, J. Yang, J. Deng, and H. Peng, *Small* **12**, 2419 (2016).
- <sup>22</sup>S. He, L. Qiu, X. Fang, G. Guan, P. Chen, Z. Zhang, and H. Peng, *J. Mater. Chem. A* **3**, 9406 (2015).
- <sup>23</sup>M. Lee, Y. Ko, and Y. Jun, *J. Mater. Chem. A* **3**, 19310 (2015).
- <sup>24</sup>B. Dong, J. Hu, X. Xiao, S. Tang, X. Gao, Z. Peng, and D. Zou, *Adv. Mater. Technol.* **4**, 1900131 (2019).
- <sup>25</sup>R. Li, X. Xiang, X. Tong, J. Zou, and Q. Li, *Adv. Mater.* **27**, 3831 (2015).
- <sup>26</sup>L. Qiu, S. He, J. Yang, F. Jin, J. Deng, H. Sun, X. Cheng, G. Guan, X. Sun, H. Zhao, and H. Peng, *J. Mater. Chem. A* **4**, 10105 (2016).
- <sup>27</sup>Q. Li, A. Balilonda, A. Ali, R. Jose, F. Zabidi, S. Yang, S. Ramakrishna, and M. Zhu, *Sol. RRL* **4**, 2000269 (2020).
- <sup>28</sup>J.-Y. Lam, J.-Y. Chen, P.-C. Tsai, Y.-T. Hsieh, C.-C. Chueh, S.-H. Tung, and W.-C. Chen, *RSC Adv.* **7**, 54361 (2017).
- <sup>29</sup>J. W. Jung, J. H. Bae, J. H. Ko, and W. Lee, *J. Power Sources* **402**, 327 (2018).
- <sup>30</sup>J.-I. Park, J. H. Heo, S.-H. Park, K. Il Hong, H. G. Jeong, S. H. Im, and H.-K. Kim, *J. Power Sources* **341**, 340 (2017).
- <sup>31</sup>J. Y. Kim, J.-W. Lee, H. S. Jung, H. Shin, and N.-G. Park, *Chem. Rev.* **120**, 7867 (2020).
- <sup>32</sup>S. Sun, Y. Fang, G. Kieslich, T. J. White, and A. K. Cheetham, *J. Mater. Chem. A* **3**, 18450 (2015).
- <sup>33</sup>V. Zardetto, T. M. Brown, A. Reale, and A. D. Carlo, *J. Polym. Sci., Part B* **49**, 638 (2011).
- <sup>34</sup>W. A. MacDonald, M. K. Looney, D. MacKerron, R. Eveson, and K. Rakos, *Plast. Rubber Compos.* **37**, 41 (2008).
- <sup>35</sup>S. Castro-Hermosa, J. Dagar, A. Marsella, and T. M. Brown, *IEEE Electron Device Lett.* **38**, 1278 (2017).
- <sup>36</sup>M.-H. Jung, N. Park, and S. Lee, *Sol. Energy* **139**, 458 (2016).
- <sup>37</sup>H. Li, X. Li, W. Wang, J. Huang, J. Li, S. Huang, B. Fan, J. Fang, and W. Song, *Sol. Energy* **188**, 158 (2019).
- <sup>38</sup>C. Gao, S. Yuan, K. Cui, Z. Qiu, S. Ge, B. Cao, and J. Yu, *Sol. RRL* **2**, 1800175 (2018).
- <sup>39</sup>H. Li, X. Li, W. Wang, J. Huang, J. Li, Y. Lu, J. Chang, J. Fang, and W. Song, *Sol. RRL* **3**, 1800317 (2019).
- <sup>40</sup>K. Zhu, Z. Lu, S. Cong, G. Cheng, P. Ma, Y. Lou, J. Ding, N. Yuan, M. H. Rümmeli, and G. Zou, *Small* **15**, 1902878 (2019).
- <sup>41</sup>Z. Lu, Y. Lou, P. Ma, K. Zhu, S. Cong, C. Wang, X. Su, and G. Zou, *Sol. RRL* **4**, 2000320 (2020).
- <sup>42</sup>P. Ma, Y. Lou, S. Cong, Z. Lu, K. Zhu, J. Zhao, and G. Zou, *Adv. Energy Mater.* **10**, 1903357 (2020).
- <sup>43</sup>J. Jin, D. Lee, H.-G. Im, Y. C. Han, E. G. Jeong, M. Rolandi, K. C. Choi, and B.-S. Bae, *Adv. Mater.* **28**, 5169 (2016).
- <sup>44</sup>M. Lee, Y. Jo, D. S. Kim, and Y. Jun, *J. Mater. Chem. A* **3**, 4129 (2015).
- <sup>45</sup>M. Lee, Y. Ko, B. K. Min, and Y. Jun, *ChemSusChem* **9**, 31 (2016).
- <sup>46</sup>B. Abdollahi Nejand, P. Nazari, S. Gharibzadeh, V. Ahmadi, and A. Moshaii, *Chem. Commun.* **53**, 747 (2017).
- <sup>47</sup>M. Lee, Y. Jo, D. S. Kim, H. Y. Jeong, and Y. Jun, *J. Mater. Chem. A* **3**, 14592 (2015).
- <sup>48</sup>J. M. Burst, W. L. Rance, D. M. Meysing, C. A. Wolden, W. K. Metzger, in S. M. Garner, P. Cimo, T. M. Barnes, T. A. Gessert, and M. O. Reese, in *IEEE 40th Photovoltaic Specialist Conference (PVSC)* (IEEE, 2014), pp. 1589–1592.
- <sup>49</sup>B. Dou, E. M. Miller, J. A. Christians, E. M. Sanehira, T. R. Klein, F. S. Barnes, S. E. Shaheen, S. M. Garner, S. Ghosh, A. Mallick, D. Basak, and M. F. A. M. van Hest, *J. Phys. Chem. Lett.* **8**, 4960 (2017).
- <sup>50</sup>S. Garner, S. Glaesemann, and X. Li, *Appl. Phys. A* **116**, 403 (2014).
- <sup>51</sup>M. M. Tavakoli, K.-H. Tsui, Q. Zhang, J. He, Y. Yao, D. Li, and Z. Fan, *ACS Nano* **9**, 10287 (2015).
- <sup>52</sup>S. W. Jin, Y. H. Lee, K. M. Yeom, J. Yun, H. Park, Y. R. Jeong, S. Y. Hong, G. Lee, S. Y. Oh, J. H. Lee, J. H. Noh, and J. S. Ha, *ACS Appl. Mater. Interfaces* **10**, 30706 (2018).
- <sup>53</sup>S. Ke, C. Chen, N. N. Fu, H. Zhou, M. Ye, P. Lin, W. Yuan, X. Zeng, L. Chen, and H. Huang, *ACS Appl. Mater. Interfaces* **8**, 28406 (2016).
- <sup>54</sup>X. Meng, Z. Xing, X. Hu, Z. Huang, T. Hu, L. Tan, F. Li, and Y. Chen, *Angew. Chem., Int. Ed.* **59**, 16602 (2020).
- <sup>55</sup>X. Hu, Z. Huang, F. Li, M. Su, Z. Huang, Z. Zhao, Z. Cai, X. Yang, X. Meng, P. Li, Y. Wang, M. Li, Y. Chen, and Y. Song, *Energy Environ. Sci.* **12**, 979 (2019).
- <sup>56</sup>G. Lee, M. C. Kim, Y. W. Choi, N. Ahn, J. Jang, J. Yoon, S. M. Kim, J. G. Lee, D. Kang, H. S. Jung, and M. Choi, *Energy Environ. Sci.* **12**, 3182 (2019).
- <sup>57</sup>M. Xu, J. Feng, Z.-J. Fan, X.-L. Ou, Z.-Y. Zhang, H.-Y. Wang, and H.-B. Sun, *Sol. Energy Mater. Sol. Cells* **169**, 8 (2017).
- <sup>58</sup>Y. Li, M. Lei, Y. Yang, X. Guiying, H. Ziruo, C. Qi, Y. Jingbi, L. Gang, Y. Yang, and L. Yongfang, *Nat. Commun.* **7**, 10214 (2016).
- <sup>59</sup>S. Kang, J. Jeong, S. Cho, Y. J. Yoon, S. Park, S. Lim, J. Y. Kim, and H. Ko, *J. Mater. Chem. A* **7**, 1107 (2019).
- <sup>60</sup>U. J. Ryu, S. Jee, J. S. Park, I. K. Han, J. H. Lee, M. Park, and K. M. Choi, *ACS Nano* **12**, 4968 (2018).
- <sup>61</sup>S. Jon, G. Sin, G. Kim, G. Jong, and J. Ri, *Synth. Met.* **262**, 116286 (2020).
- <sup>62</sup>M. Dianetti, F. D. Giacomo, G. Polino, C. Ciceroni, A. Liscio, A. D'Epifanio, S. Licoccia, T. M. Brown, A. Di Carlo, and F. Brunetti, *Sol. Energy Mater. Sol. Cells* **140**, 150 (2015).
- <sup>63</sup>J. Poorkazem, D. Liu, and T. L. Kelly, *J. Mater. Chem. A* **3**, 9241 (2015).
- <sup>64</sup>T. Kawashima, T. Ezure, K. Okada, H. Matsui, K. Goto, and N. Tanabe, *J. Photochem. Photobiol. A* **164**, 199 (2004).
- <sup>65</sup>W.-H. Baek, M. Choi, T.-S. Yoon, H. H. Lee, and Y.-S. Kim, *Appl. Phys. Lett.* **96**, 133506 (2010).
- <sup>66</sup>L. Yang, Y. Li, L. Wang, Y. Pei, Z. Wang, Y. Zhang, H. Lin, and X. Li, *ACS Appl. Mater. Interfaces* **12**, 22992 (2020).
- <sup>67</sup>P. Ru, E. Bi, Y. Zhang, Y. Wang, W. Kong, Y. Sha, W. Tang, P. Zhang, Y. Wu, W. Chen, X. Yang, H. Chen, and L. Han, *Adv. Energy Mater.* **10**, 1903487 (2020).
- <sup>68</sup>E. Cho, Y. Yun, D. Seok, J. Heung, J. Park, J. Seo, and S. Lee, *Nano Energy* **82**, 105737 (2021).
- <sup>69</sup>J. Feng, X. Zhu, Z. Yang, X. Zhang, J. Niu, Z. Wang, S. Zuo, S. Priya, S. (Frank) Liu, and D. Yang, *Adv. Mater.* **30**, 1801418 (2018).
- <sup>70</sup>X. Hu, X. Meng, L. Zhang, Y. Zhang, Z. Cai, Z. Huang, M. Su, Y. Wang, M. Li, F. Li, X. Yao, F. Wang, W. Ma, Y. Chen, and Y. Song, *Joule* **3**, 2205 (2019).
- <sup>71</sup>K. Sun, P. Li, Y. Xia, J. Chang, and J. Ouyang, *ACS Appl. Mater. Interfaces* **7**, 15314 (2015).
- <sup>72</sup>N. Kim, H. Kang, J. H. Lee, S. Kee, S. H. Lee, and K. Lee, *Adv. Mater.* **27**, 2317 (2015).
- <sup>73</sup>M. Park, H. J. Kim, I. Jeong, J. Lee, H. Lee, H. J. Son, D. E. Kim, and M. J. Ko, *Adv. Energy Mater.* **5**, 1501406 (2015).
- <sup>74</sup>X. Hu, Z. Huang, X. Zhou, P. Li, Y. Wang, Z. Huang, M. Su, W. Ren, F. Li, M. Li, Y. Chen, and Y. Song, *Adv. Mater.* **29**, 1703236 (2017).
- <sup>75</sup>B. Vaagensmith, K. M. Reza, M. D. N. N. Hasan, H. Elbohy, N. Adhikari, A. Dubey, N. Kantack, E. Gaml, and Q. Qiao, *ACS Appl. Mater. Interfaces* **9**, 35861 (2017).
- <sup>76</sup>I. Jeon, J. Yoon, U. Kim, C. Lee, R. Xiang, A. Shawky, J. Xi, J. Byeon, H. M. Lee, M. Choi, S. Maruyama, and Y. Matsuo, *Adv. Energy Mater.* **9**, 1901204 (2019).
- <sup>77</sup>X. Wang, Z. Li, W. Xu, S. A. Kulkarni, S. K. Batabyal, S. Zhang, A. Cao, and L. H. Wong, *Nano Energy* **11**, 728 (2014).
- <sup>78</sup>Q. Luo, H. Ma, Q. Hou, Y. Li, J. Ren, X. Dai, Z. Yao, Y. Zhou, L. Xiang, H. Du, H. He, N. Wang, K. Jiang, H. Lin, H. Zhang, and Z. Guo, *Adv. Funct. Mater.* **28**, 1706777 (2018).
- <sup>79</sup>I. Jeon, T. Chiba, C. Delacou, Y. Guo, A. Kaskela, O. Reynaud, E. I. Kauppinen, S. Maruyama, and Y. Matsuo, *Nano Lett.* **15**, 6665 (2015).
- <sup>80</sup>I. Jeon, J. Yoon, N. Ahn, M. Atwa, C. Delacou, A. Anisimov, E. I. Kauppinen, M. Choi, S. Maruyama, and Y. Matsuo, *J. Phys. Chem. Lett.* **8**, 5395 (2017).
- <sup>81</sup>Z. Liu, S. P. Lau, and F. Yan, *Chem. Soc. Rev.* **44**, 5638 (2015).

- <sup>82</sup>J. H. Heo, D. H. Shin, M. H. Jang, M. L. Lee, M. G. Kang, and S. H. Im, *J. Mater. Chem. A* **5**, 21146 (2017).
- <sup>83</sup>J. Yoon, H. Sung, G. Lee, W. Cho, N. Ahn, H. S. Jung, and M. Choi, *Energy Environ. Sci.* **10**, 337 (2017).
- <sup>84</sup>J. H. Heo, D. H. Shin, M. L. Lee, M. G. Kang, and S. H. Im, *ACS Appl. Mater. Interfaces* **10**, 31413 (2018).
- <sup>85</sup>J. H. Heo, D. H. Shin, D. H. Song, D. H. Kim, S. J. Lee, and S. H. Im, *J. Mater. Chem. A* **6**, 8251 (2018).
- <sup>86</sup>F. Guo, H. Azimi, Y. Hou, T. Przybilla, M. Hu, C. Bronnbauer, S. Langner, E. Spiecker, K. Forberich, and C. J. Brabec, *Nanoscale* **7**, 1642 (2015).
- <sup>87</sup>K. K. Sears, M. Fievez, M. Gao, H. C. Weerasinghe, C. D. Easton, and D. Vak, *Sol. RRL* **1**, 1700059 (2017).
- <sup>88</sup>H. Im, S. Jeong, J. Jin, J. Lee, D. Youn, W. Koo, S. Kang, H.-J. Kim, J. Jang, D. Lee, H.-K. Kim, I. Kim, J. Lee, and B. Bae, *NPG Asia Mater.* **8**, e282 (2016).
- <sup>89</sup>J. Han, S. Yuan, L. Liu, X. Qiu, H. Gong, X. Yang, C. Li, Y. Hao, and B. Cao, *J. Mater. Chem. A* **3**, 5375 (2015).
- <sup>90</sup>J. Kang, K. Han, X. Sun, L. Zhang, R. Huang, I. Ismail, J. Lin, C. Ma, Z. Wang, C. Ding, W. Zha, F. Li, Q. Luo, Y. Li, J. Lin, and C. Ma, *Org. Electron.* **82**, 105714 (2020).
- <sup>91</sup>H. Lu, J. Sun, H. Zhang, S. Lu, and W. C. H. H. Choy, *Nanoscale* **8**, 5946 (2016).
- <sup>92</sup>Y. Liu, J. Zhang, H. Gao, Y. Wang, Q. Liu, S. Huang, C. F. Guo, and Z. Ren, *Nano Lett.* **17**, 1090 (2017).
- <sup>93</sup>W. Shin, W. Cho, and S. J. Baik, *Mater. Res. Express* **5**, 15050 (2018).
- <sup>94</sup>M. Li, W. Zuo, A. G. Ricciardulli, Y. Yang, Y. Liu, Q. Wang, K. Wang, G. Li, M. Saliba, D. D. Girolamo, A. Abate, and Z. Wang, *Adv. Mater.* **32**, 2003422 (2020).
- <sup>95</sup>G. Jeong, D. Koo, J. Seo, S. Jung, Y. Choi, J. Lee, and H. Park, *Nano Lett.* **20**, 3718 (2020).
- <sup>96</sup>C. Hammandlu, C.-C. Liu, C.-Y. Chen, K. M. Boopathi, S.-H. Wu, M. Singh, A. Mohapatra, H.-W. Lin, Y.-C. Chang, Y.-C. Chang, C.-S. Lai, and C.-W. Chu, *ACS Appl. Mater. Interfaces* **10**, 17973 (2018).
- <sup>97</sup>C. Roldán-Carmona, O. Malinkiewicz, A. Soriano, G. Mínguez Espallargas, A. García, P. Reinecke, T. Kroyer, M. I. Dar, M. K. Nazeeruddin, and H. J. Bolink, *Energy Environ. Sci.* **7**, 994 (2014).
- <sup>98</sup>S. S. Shin, W. S. Yang, J. H. Noh, J. H. Suk, N. J. Jeon, J. H. Park, J. S. Kim, W. M. Seong, and S. Il Seok, *Nat. Commun.* **6**, 7410 (2015).
- <sup>99</sup>L. Zhou, X. Guo, Z. Lin, J. Ma, J. Su, Z. Hu, C. Zhang, S. (Frank) Liu, J. Chang, and Y. Hao, *Nano Energy* **60**, 583 (2019).
- <sup>100</sup>J. Yoon, U. Kim, Y. Yoo, J. Byeon, S. K. Lee, J. S. Nam, K. Kim, Q. Zhang, E. I. Kauppinen, S. Maruyama, P. Lee, and I. Jeon, *Adv. Sci.* **8**, 2004092 (2021).
- <sup>101</sup>J. Li, Q. Dong, N. Li, and L. Wang, *Adv. Energy Mater.* **7**, 1602922 (2017).
- <sup>102</sup>K. Domanski, J.-P. Correa-Baena, N. Mine, M. K. Nazeeruddin, A. Abate, M. Saliba, W. Tress, A. Hagfeldt, and M. Grätzel, *ACS Nano* **10**, 6306 (2016).
- <sup>103</sup>Z. Ku, Y. Rong, M. Xu, T. Liu, and H. Han, *Sci. Rep.* **3**, 3132 (2013).
- <sup>104</sup>Y. Xu, Z. Lin, W. Wei, Y. Hao, S. Liu, J. Ouyang, and J. Chang, *Nano-Micro Lett.* **14**, 117 (2021).
- <sup>105</sup>Z. Wu, Z. Liu, Z. Hu, Z. Hawash, L. Qiu, Y. Jiang, L. K. Ono, and Y. Qi, *Adv. Mater.* **31**, 1804284 (2019).
- <sup>106</sup>D. Liu, J. Yang, T. L. Kelly, D. Liu, J. Yang, and T. L. Kelly, *J. Am. Chem. Soc.* **136**, 17116 (2014).
- <sup>107</sup>W. Ke, G. Fang, J. Wan, H. Tao, Q. Liu, L. Xiong, P. Qin, J. Wang, H. Lei, G. Yang, M. Qin, X. Zhao, and Y. Yan, *Nat. Commun.* **6**, 6700 (2015).
- <sup>108</sup>D. Yang, R. Yang, K. Wang, C. Wu, X. Zhu, J. Feng, X. Ren, G. Fang, S. Priya, and S. (Frank) Liu, *Nat. Commun.* **9**, 3239 (2018).
- <sup>109</sup>P. Docampo, J. M. Ball, M. Darwiche, G. E. Eperon, and H. J. Snaith, *Nat. Commun.* **4**, 2761 (2013).
- <sup>110</sup>H. Kim, C.-R. Lee, J.-H. Im, K.-B. Lee, T. Moehl, A. Marchioro, S.-J. Moon, R. Humphrey-baker, J.-H. Yum, J. E. Moser, M. Grätzel, and N.-G. Park, *Sci. Rep.* **2**, 591 (2012).
- <sup>111</sup>M. M. Lee, J. Teuscher, T. Miyasaka, T. N. Murakami, and H. J. Snaith, *Science* **338**, 643 (2012).
- <sup>112</sup>K. Wojciechowski, M. Saliba, T. Leijtens, A. Abate, and H. J. Snaith, *Energy Environ. Sci.* **7**, 1142 (2014).
- <sup>113</sup>J. T.-W. Wang, J. M. Ball, E. M. Barea, A. Abate, J. A. Alexander-Webber, J. Huang, M. Saliba, I. Mora-Sero, J. Bisquert, H. J. Snaith, and R. J. Nicholas, *Nano Lett.* **14**, 724 (2014).
- <sup>114</sup>A. Yella, L.-P. P. Heiniger, P. Gao, M. K. Nazeeruddin, M. Grätzel, and M. Grätzel, *Nano Lett.* **14**, 2591 (2014).
- <sup>115</sup>H. Zhou, Q. Chen, G. Li, S. Luo, T. B. Song, H. S. Duan, Z. Hong, J. You, Y. Liu, and Y. Yang, *Science* **345**, 542 (2014).
- <sup>116</sup>Y. Dkhissi, F. Huang, S. Rubanov, M. Xiao, U. Bach, L. Spiccia, R. A. Caruso, and Y.-B. Cheng, *J. Power Sources* **278**, 325 (2015).
- <sup>117</sup>Z. Yang, W. Chen, A. Mei, Q. Li, and Y. Liu, *J. Alloys Compd.* **854**, 155488 (2021).
- <sup>118</sup>M. Li, Y. Yang, Z. Wang, T. Kang, Q. Wang, S. Turren-Cruz, X. Gao, C. Hsu, L. Liao, and A. Abate, *Adv. Mater.* **31**, 1901519 (2019).
- <sup>119</sup>B. Conings, L. Baeten, T. Jacobs, R. Dera, J. D'Haen, J. Manca, and H.-G. Boyen, *APL Mater.* **2**, 081505 (2014).
- <sup>120</sup>W. Qiu, U. W. Paetzold, R. Gehlhaar, V. Smirnov, H.-G. Boyen, J. G. Tait, B. Conings, W. Zhang, C. B. Nielsen, I. McCulloch, L. Froyen, P. Heremans, and D. Cheyns, *J. Mater. Chem. A* **3**, 22824 (2015).
- <sup>121</sup>I. Jeong, H. Jung, M. Park, J. S. Park, H. J. Son, J. Joo, J. Lee, and M. J. Ko, *Nano Energy* **28**, 380 (2016).
- <sup>122</sup>Q. Wang, Z. Lin, J. Su, Z. Hu, J. Chang, and Y. Hao, *Nano Sel.* **2**, 1055 (2021).
- <sup>123</sup>C. Chen, Y. Cheng, Q. Dai, and H. Song, *Sci. Rep.* **5**, 17684 (2015).
- <sup>124</sup>S. M. George, *Chem. Rev.* **110**, 111 (2010).
- <sup>125</sup>A. K. Chandiran, A. Yella, M. T. Mayer, P. Gao, M. K. Nazeeruddin, and M. Grätzel, *Adv. Mater.* **26**, 4309 (2014).
- <sup>126</sup>Y. Wu, X. Yang, H. Chen, K. Zhang, C. Qin, J. Liu, W. Peng, A. Islam, E. Bi, F. Ye, M. Yin, P. Zhang, and L. Han, *Appl. Phys. Express* **7**, 052301 (2014).
- <sup>127</sup>B. J. Kim, D. H. Kim, Y.-Y. Lee, H.-W. Shin, G. S. Han, J. S. Hong, K. Mahmood, T. K. Ahn, Y.-C. Joo, K. S. Hong, N.-G. Park, S. Lee, and H. S. Jung, *Energy Environ. Sci.* **8**, 916 (2015).
- <sup>128</sup>S. S. Mali, C. K. Hong, A. I. Inamdar, H. Im, and S. E. Shim, *Nanoscale* **9**, 3095 (2017).
- <sup>129</sup>D. Yang, R. Yang, J. Zhang, Z. Yang, S. F. Liu, and C. Li, *Energy Environ. Sci.* **8**, 3208 (2015).
- <sup>130</sup>B. Chen, M. Yang, S. Priya, and K. Zhu, *J. Phys. Chem. Lett.* **7**, 905 (2016).
- <sup>131</sup>K. H. Jung, J. Y. Seo, S. Lee, H. Shin, and N. G. Park, *J. Mater. Chem. A* **5**, 24790 (2017).
- <sup>132</sup>Q. Jiang, L. Zhang, H. Wang, X. Yang, J. Meng, H. Liu, Z. Yin, J. Wu, X. Zhang, and J. You, *Nat. Energy* **2**, 16177 (2016).
- <sup>133</sup>X. He, J. Wu, Y. Tu, J. Jia, J. Dong, R. Xu, Q. Guo, T. Wu, Z. Lan, J. Lin, and Y. Xie, *J. Power Sources* **365**, 83 (2017).
- <sup>134</sup>C. Liu, K. Wang, P. Du, T. Meng, X. Yu, S. Z. D. Cheng, and X. Gong, *ACS Appl. Mater. Interfaces* **7**, 1153 (2015).
- <sup>135</sup>D. Liu, S. Li, P. Zhang, Y. Wang, R. Zhang, H. Sarvari, F. Wang, J. Wu, Z. Wang, and Z. D. Chen, *Nano Energy* **31**, 462 (2017).
- <sup>136</sup>H.-S. Kim, I.-H. Jang, N. Ahn, M. Choi, A. Guerrero, J. Bisquert, and N.-G. Park, *J. Phys. Chem. Lett.* **6**, 4633 (2015).
- <sup>137</sup>T. Leijtens, G. E. Eperon, S. Pathak, A. Abate, M. M. Lee, and H. J. Snaith, *Nat. Commun.* **4**, 2885 (2013).
- <sup>138</sup>Q. Jiang, X. Zhang, and J. You, *Small* **14**, 1801154 (2018).
- <sup>139</sup>J. H. Heo, M. H. Lee, H. J. Han, B. R. Patil, J. S. Yu, and S. H. Im, *J. Mater. Chem. A* **4**, 1572 (2016).
- <sup>140</sup>D. Liu and T. L. Kelly, *Nat. Photonics* **8**, 133 (2014).
- <sup>141</sup>F. Bouhjar, L. Derbali, and B. Mari, *Nano Res.* **13**, 2546 (2020).
- <sup>142</sup>J. Ma, J. Su, Z. Lin, L. Zhou, J. He, J. Zhang, S. Liu, J. Chang, and Y. Hao, *Nano Energy* **67**, 104241 (2020).
- <sup>143</sup>D.-Y. Son, J.-H. Im, H.-S. Kim, and N.-G. Park, *J. Phys. Chem. C* **118**, 16567 (2014).
- <sup>144</sup>H. Liu, Z. Huang, S. Wei, L. Zheng, L. Xiao, and Q. Gong, *Nanoscale* **8**, 6209 (2016).
- <sup>145</sup>W. Chu, J. Yang, Q. Jiang, X. Li, and J. Xin, *Appl. Surf. Sci.* **440**, 1116 (2018).
- <sup>146</sup>H. Si, Q. Liao, Z. Zhang, Y. Li, X. Yang, G. Zhang, Z. Kang, and Y. Zhang, *Nano Energy* **22**, 223 (2016).
- <sup>147</sup>J. Yang, B. D. Siempelkamp, E. Mosconi, F. De Angelis, and T. L. Kelly, *Chem. Mater.* **27**, 4229 (2015).
- <sup>148</sup>Q. An, P. Fassl, Y. J. Hofstetter, D. Becker-Koch, A. Bausch, P. E. Hopkinson, and Y. Vaynzof, *Nano Energy* **39**, 400 (2017).
- <sup>149</sup>J. W. Lim, H. Wang, C. H. Choi, L. N. Quan, K. Chung, W.-T. Park, Y.-Y. Noh, and D. H. Kim, *J. Power Sources* **438**, 226956 (2019).

- <sup>150</sup>Y. Cheng, Q. Yang, J. Xiao, Q. Xue, H.-W. Li, Z. Guan, H.-L. Yip, and S.-W. Tsang, *ACS Appl. Mater. Interfaces* **7**, 19986 (2015).
- <sup>151</sup>D. Zhang, X. Zhang, S. Bai, C. Liu, Z. Li, W. Guo, and F. Gao, *Sol. RRL* **3**, 1900154 (2019).
- <sup>152</sup>J. Han, H. Kwon, E. Kim, D. W. Kim, H. J. Son, and D. H. Kim, *J. Mater. Chem. A* **8**, 2105 (2020).
- <sup>153</sup>R. Azmi, W. T. Hadmojo, S. Sinaga, C. L. Lee, S. C. Yoon, I. H. Jung, and S. Y. Jang, *Adv. Energy Mater.* **8**, 1701683 (2018).
- <sup>154</sup>Q. Dong, Y. Shi, K. Wang, Y. Li, S. Wang, H. Zhang, Y. Xing, Y. Du, X. Bai, and T. Ma, *J. Phys. Chem. C* **119**, 10212 (2015).
- <sup>155</sup>W. Ke, G. Fang, Q. Liu, L. Xiong, P. Qin, H. Tao, J. Wang, H. Lei, B. Li, J. Wan, G. Yang, and Y. Yan, *J. Am. Chem. Soc.* **137**, 6730 (2015).
- <sup>156</sup>C. Wu, D. Wang, Y. Zhang, F. Gu, G. Liu, N. Zhu, W. Luo, D. Han, X. Guo, B. Qu, S. Wang, Z. Bian, Z. Chen, and L. Xiao, *Adv. Funct. Mater.* **29**, 1902974 (2019).
- <sup>157</sup>K. Huang, Y. Peng, Y. Gao, J. Shi, H. Li, X. Mo, H. Huang, Y. Gao, L. Ding, and J. Yang, *Adv. Energy Mater.* **9**, 1901419 (2019).
- <sup>158</sup>B. Cao, L. Yang, S. Jiang, H. Lin, N. Wang, and X. Li, *J. Mater. Chem. A* **7**, 4960 (2019).
- <sup>159</sup>T. Bu, J. Li, F. Zheng, W. Chen, X. Wen, Z. Ku, Y. Peng, J. Zhong, Y. B. Cheng, and F. Huang, *Nat. Commun.* **9**, 4609 (2018).
- <sup>160</sup>S. Zhang, J. Su, Z. Lin, K. Tian, X. Guo, J. Zhang, J. Chang, and Y. Hao, *Adv. Mater. Interfaces* **6**, 1900400 (2019).
- <sup>161</sup>C. Kılıç and A. Zunger, *Phys. Rev. Lett.* **88**, 095501 (2002).
- <sup>162</sup>J. P. Correa Baena, L. Steier, W. Tress, M. Saliba, S. Neutzner, T. Matsui, F. Giordano, T. J. Jacobsson, A. R. Srimath Kandada, S. M. Zakeeruddin, A. Petrozza, A. Abate, M. K. Nazeeruddin, M. Grätzel, and A. Hagfeldt, *Energy Environ. Sci.* **8**, 2928 (2015).
- <sup>163</sup>H. J. Snaith and C. Ducati, *Nano Lett.* **10**, 1259 (2010).
- <sup>164</sup>M. Park, J.-Y. Kim, H. J. Son, C.-H. Lee, S. S. Jang, and M. J. Ko, *Nano Energy* **26**, 208 (2016).
- <sup>165</sup>X.-F. Wang, L. Wang, N. Tamai, O. Kitao, H. Tamiaki, and S. Sasaki, *J. Phys. Chem. C* **115**, 24394 (2011).
- <sup>166</sup>C. Wang, D. Zhao, C. R. Grice, W. Liao, Y. Yu, A. Cimaroli, N. Shrestha, P. J. Roland, J. Chen, Z. Yu, P. Liu, N. Cheng, R. J. Ellingson, X. Zhao, and Y. Yan, *J. Mater. Chem. A* **4**, 12080 (2016).
- <sup>167</sup>E. H. Anaraki, A. Kermanpur, L. Steier, K. Domanski, T. Matsui, W. Tress, M. Saliba, A. Abate, M. Grätzel, A. Hagfeldt, and J.-P. Correa-Baena, *Energy Environ. Sci.* **9**, 3128 (2016).
- <sup>168</sup>J. Barbé, M. L. Tietze, M. Neophytou, B. Murali, E. Alarousu, A. El Labban, M. Abulikemu, W. Yue, O. F. Mohammed, I. McCulloch, A. Amassian, and S. Del Gobbo, *ACS Appl. Mater. Interfaces* **9**, 11828 (2017).
- <sup>169</sup>J. Ma, X. Zheng, H. Lei, W. Ke, C. Chen, Z. Chen, G. Yang, and G. Fang, *Sol. RRL* **1**, 1700118 (2017).
- <sup>170</sup>C. Liu, L. Zhang, X. Zhou, J. Gao, W. Chen, X. Wang, and B. Xu, *Adv. Funct. Mater.* **29**, 1807604 (2019).
- <sup>171</sup>N. Zhu, X. Qi, Y. Zhang, G. Liu, C. Wu, D. Wang, X. Guo, W. Luo, X. Li, H. Hu, Z. Chen, L. Xiao, and B. Qu, *ACS Appl. Energy Mater.* **2**, 3676 (2019).
- <sup>172</sup>C. Wang, C. Xiao, Y. Yu, D. Zhao, R. A. Awni, C. R. Grice, K. Ghimire, I. Constantiou, W. Liao, A. J. Cimaroli, P. Liu, J. Chen, N. J. Podraza, C. Jiang, M. M. Al-Jassim, X. Zhao, and Y. Yan, *Adv. Energy Mater.* **7**, 1700414 (2017).
- <sup>173</sup>C. Wang, L. Guan, D. Zhao, Y. Yu, C. R. Grice, Z. Song, R. A. Awni, J. Chen, J. Wang, X. Zhao, and Y. Yan, *ACS Energy Lett.* **2**, 2118 (2017).
- <sup>174</sup>X. Ren, D. Yang, Z. Yang, J. Feng, X. Zhu, J. Niu, Y. Liu, W. Zhao, and S. F. Liu, *ACS Appl. Mater. Interfaces* **9**, 2421 (2017).
- <sup>175</sup>W. Ke, D. Zhao, A. J. Cimaroli, C. R. Grice, P. Qin, Q. Liu, L. Xiong, Y. Yan, and G. Fang, *J. Mater. Chem. A* **3**, 24163 (2015).
- <sup>176</sup>Q. Dong, Y. Shi, C. Zhang, Y. Wu, and L. Wang, *Nano Energy* **40**, 336 (2017).
- <sup>177</sup>Q. Sun, H. Li, X. Gong, H. Ban, Y. Shen, and M. Wang, *Sol. RRL* **4**, 1900229 (2020).
- <sup>178</sup>G. Yang, C. Chen, F. Yao, Z. Chen, Q. Zhang, X. Zheng, J. Ma, H. Lei, P. Qin, L. Xiong, W. Ke, G. Li, Y. Yan, and G. Fang, *Adv. Mater.* **30**, 1706023 (2018).
- <sup>179</sup>Y. Bai, Y. Fang, Y. Deng, Q. Wang, J. Zhao, X. Zheng, Y. Zhang, and J. Huang, *ChemSusChem* **9**, 2686 (2016).
- <sup>180</sup>K. Choi, J. Lee, H. Il Kim, C. W. Park, G. W. Kim, H. Choi, S. Park, S. A. Park, and T. Park, *Energy Environ. Sci.* **11**, 3238 (2018).
- <sup>181</sup>X. Guo, X. Huang, J. Su, Z. Lin, J. Ma, J. Chang, and Y. Hao, *Chem. Eng. J.* **417**, 129184 (2021).
- <sup>182</sup>X. Guo, J. Du, Z. Lin, J. Su, L. Feng, J. Zhang, Y. Hao, and J. Chang, *Chem. Eng. J.* **407**, 127997 (2021).
- <sup>183</sup>X. Huang, J. Du, X. Guo, Z. Lin, J. Ma, J. Su, L. Feng, C. Zhang, J. Zhang, J. Chang, and Y. Hao, *Sol. RRL* **4**, 1900336 (2020).
- <sup>184</sup>Z. Liu, K. Deng, J. Hu, and L. Li, *Angew. Chem. Int. Ed.* **58**, 11497 (2019).
- <sup>185</sup>J. Ma, G. Yang, M. Qin, X. Zheng, H. Lei, C. Chen, Z. Chen, Y. Guo, H. Han, X. Zhao, and G. Fang, *Adv. Sci.* **4**, 1700031 (2017).
- <sup>186</sup>J. Zhang, A. Hultqvist, T. Zhang, L. Jiang, C. Ruan, L. Yang, Y. Cheng, M. Edoff, and E. M. J. Johansson, *ChemSusChem* **10**, 3810 (2017).
- <sup>187</sup>G. Yang, C. Wang, H. Lei, X. Zheng, P. Qin, L. Xiong, X. Zhao, Y. Yan, and G. Fang, *J. Mater. Chem. A* **5**, 1658 (2017).
- <sup>188</sup>J. Feng, Z. Yang, D. Yang, X. Ren, X. Zhu, Z. Jin, W. Zi, Q. Wei, and S. (Frank) Liu, *Nano Energy* **36**, 1–8 (2017).
- <sup>189</sup>X. Guo, Z. Lin, J. Ma, Z. Hu, J. Su, C. Zhang, J. Zhang, J. Chang, and Y. Hao, *J. Power Sources* **438**, 226981 (2019).
- <sup>190</sup>D. Yang, R. Yang, X. Ren, X. Zhu, Z. Yang, C. Li, and S. (Frank) Liu, *Adv. Mater.* **28**, 5206 (2016).
- <sup>191</sup>S. Guo, X. Zhang, Z. Zhou, G. Gao, and L. Liu, *J. Mater. Chem. A* **2**, 9236 (2014).
- <sup>192</sup>B. Gu, Y. Zhu, H. Lu, W. Tian, and L. Li, *Sol. Energy* **166**, 187 (2018).
- <sup>193</sup>X. Ling, J. Yuan, D. Liu, Y. Wang, Y. Zhang, S. Chen, H. Wu, F. Jin, F. Wu, G. Shi, X. Tang, J. Zheng, S. (Frank) Liu, Z. Liu, and W. Ma, *ACS Appl. Mater. Interfaces* **9**, 23181 (2017).
- <sup>194</sup>H. Jiang, J. Feng, H. Zhao, G. Li, G. Yin, Y. Han, F. Yan, Z. Liu, and S. (Frank) Liu, *Adv. Sci.* **5**, 1801117 (2018).
- <sup>195</sup>S. S. Shin, W. S. Yang, E. J. Yeom, S. J. Lee, N. J. Jeon, Y.-C. Joo, I. J. Park, J. H. Noh, and S. Il Seok, *J. Phys. Chem. Lett.* **7**, 1845 (2016).
- <sup>196</sup>J. Dou, D. Shen, Y. Li, A. Abate, and M. Wei, *ACS Appl. Mater. Interfaces* **11**, 36553 (2019).
- <sup>197</sup>J. He, J. Su, Z. Lin, J. Ma, L. Zhou, S. Zhang, S. Liu, J. Chang, and Y. Hao, *Adv. Sci.* **8**, 2101367 (2021).
- <sup>198</sup>J. Ma, J. Su, Z. Lin, J. He, L. Zhou, T. Li, J. Zhang, S. Liu, J. Chang, and Y. Hao, *Energy Environ. Mater.* **2021**, eem2.12212.
- <sup>199</sup>J. Ma, Z. Lin, X. Guo, J. He, Z. Hu, J. Su, J. Zhang, J. Chang, and Y. Hao, *Mater. Today Energy* **14**, 100351 (2019).
- <sup>200</sup>M. Yue, J. Su, P. Zhao, Z. Lin, J. Zhang, J. Chang, and Y. Hao, *Nano-Micro Lett.* **11**, 91 (2019).
- <sup>201</sup>J. Ma, Z. Lin, X. Guo, L. Zhou, J. Su, C. Zhang, Z. Yang, J. Chang, S. Liu, and Y. Hao, *Sol. RRL* **3**, 1900096 (2019).
- <sup>202</sup>H. B. Lee, N. Kumar, M. M. Ovhal, Y. J. Kim, Y. M. Song, and J. Kang, *Adv. Funct. Mater.* **30**, 2001559 (2020).
- <sup>203</sup>H. Yi, D. Wang, M. A. Mahmud, F. Haque, M. B. Upama, C. Xu, L. Duan, and A. Uddin, *ACS Appl. Energy Mater.* **1**, 6027 (2018).
- <sup>204</sup>J. Chung, S. S. Shin, K. Hwang, G. Kim, K. W. Kim, D. S. Lee, W. Kim, B. S. Ma, Y.-K. Kim, T.-S. Kim, and J. Seo, *Energy Environ. Sci.* **13**, 4854 (2020).
- <sup>205</sup>Z. Yang, C. C. Chueh, F. Zuo, J. H. Kim, P. W. Liang, and A. K. Y. Jen, *Adv. Energy Mater.* **5**, 1500328 (2015).
- <sup>206</sup>M. Najafi, F. D. Giacomo, D. Zhang, S. Shanmugam, A. Senes, W. Verhees, A. Hadipour, Y. Galagan, T. Aernouts, S. Veenstra, and R. Andriessen, *Small* **14**, 1702775 (2018).
- <sup>207</sup>S. S. Reddy, S. Shin, U. K. Aryal, R. Nishikubo, A. Saeki, M. Song, and S.-H. Jin, *Nano Energy* **41**, 10 (2017).
- <sup>208</sup>C. Bi, B. Chen, H. Wei, S. DeLuca, and J. Huang, *Adv. Mater.* **29**, 1605900 (2017).
- <sup>209</sup>J. W. Jung, S. T. Williams, and A. K.-Y. K.-Y. Jen, *RSC Adv.* **4**, 62971 (2014).
- <sup>210</sup>Z. Wang, L. Zeng, C. Zhang, Y. Lu, S. Qiu, C. Wang, C. Liu, L. Pan, S. Wu, J. Hu, G. Liang, P. Fan, H. Egelhaaf, C. J. Brabec, F. Guo, and Y. Mai, *Adv. Funct. Mater.* **30**, 2001240 (2020).
- <sup>211</sup>X. Duan, Z. Huang, C. Liu, J. Yang, L. Tan, and Y. Chen, *Chem. Commun.* **55**, 3666 (2019).
- <sup>212</sup>H. Il Kim, M. J. Kim, K. Choi, C. Lim, Y. H. Kim, S. K. Kwon, and T. Park, *Adv. Energy Mater.* **8**, 1702872 (2018).
- <sup>213</sup>Z. Huang, X. Hu, C. Liu, X. Meng, Z. Huang, J. Yang, X. Duan, J. Long, Z. Zhao, L. Tan, Y. Song, and Y. Chen, *Adv. Funct. Mater.* **29**, 1902629 (2019).

- <sup>214</sup>J. H. Heo, M. Jahandar, S.-J. J. Moon, C. E. Song, and S. H. Im, *J. Mater. Chem. C* **5**, 2883 (2017).
- <sup>215</sup>J. Ha, H. Kim, H. Lee, K. G. Lim, T. W. Lee, and S. Yoo, *Sol. Energy Mater. Sol. Cells* **161**, 338 (2017).
- <sup>216</sup>S. Song, R. Hill, K. Choi, K. Wojciechowski, S. Barlow, J. Leisen, H. J. Snaith, S. R. Marder, T. Park, J. Leisen, H. J. Snaith, S. R. Marder, and T. Park, *Nano Energy* **49**, 324 (2018).
- <sup>217</sup>C. Sun, Z. Wu, H. Yip, H. Zhang, X. Jiang, Q. Xue, Z. Z. Hu, Z. Z. Hu, Y. Shen, M. Wang, F. Huang, and Y. Cao, *Adv. Energy Mater.* **6**, 1501534 (2016).
- <sup>218</sup>Y. Hou, X. Chen, S. Yang, Y. L. Zhong, C. Li, H. Zhao, and H. G. Yang, *Nano Energy* **36**, 102 (2017).
- <sup>219</sup>J. Chang, J. Xiao, Z. Lin, H. Zhu, Q. Xu, K. Zeng, Y. Hao, and J. Ouyang, *J. Mater. Chem. A* **4**, 17464 (2016).
- <sup>220</sup>W. H. Nguyen, C. D. Bailie, E. L. Unger, and M. D. McGehee, *J. Am. Chem. Soc.* **136**, 10996 (2014).
- <sup>221</sup>D. Bi, G. Boschloo, and A. Hagfeldt, *Nano* **9**, 1440001 (2014).
- <sup>222</sup>F. M. Rombach, S. A. Haque, and T. J. Macdonald, *Energy Environ. Sci.* **14**, 5161 (2021).
- <sup>223</sup>Z. Gu, L. Zuo, T. T. Larsen-Olsen, T. Ye, G. Wu, F. C. Krebs, and H. Chen, *J. Mater. Chem. A* **3**, 24254 (2015).
- <sup>224</sup>C. Zuo and L. Ding, *Adv. Energy Mater.* **7**, 1601193 (2017).
- <sup>225</sup>J. You, Z. Hong, Y. ( Yang, Q. Chen, M. Cai, T. Song, C. Chen, S. Lu, Y. Liu, H. Zhou, and Y. (Michael) Yang, *ACS Nano* **8**, 1674 (2014).
- <sup>226</sup>C. Zuo, D. Vak, D. Angmo, L. Ding, and M. Gao, *Nano Energy* **46**, 185 (2018).
- <sup>227</sup>X. Meng, Z. Cai, Y. Zhang, X. Hu, Z. Xing, Z. Huang, Z. Huang, Y. Cui, T. Hu, M. Su, X. Liao, L. Zhang, F. Wang, Y. Song, and Y. Chen, *Nat. Commun.* **11**, 3016 (2020).
- <sup>228</sup>K. G. Lim, H. B. Kim, J. Jeong, H. Kim, J. Y. Kim, and T. W. Lee, *Adv. Mater.* **26**, 6461 (2014).
- <sup>229</sup>D. Liu, Y. Li, J. Yuan, Q. Hong, G. Shi, D. Yuan, J. Wei, C. Huang, J. Tang, and M.-K. Fung, *J. Mater. Chem. A* **5**, 5701 (2017).
- <sup>230</sup>X. Huang, K. Wang, C. Yi, T. Meng, and X. Gong, *Adv. Energy Mater.* **6**, 1501773 (2016).
- <sup>231</sup>D. Bin Kim, J. C. Yu, Y. S. Nam, D. W. Kim, E. D. Jung, S. Y. Lee, S. Lee, J. H. Park, A.-Y. Lee, B. R. Lee, D. D. Nuzzo, R. H. Friend, and M. H. Song, *J. Mater. Chem. C* **4**, 8161 (2016).
- <sup>232</sup>T. Xue, G. Chen, X. Hu, M. Su, Z. Huang, X. Meng, Z. Jin, J. Ma, Y. Zhang, and Y. Song, *ACS Appl. Mater. Interfaces* **13**, 19959 (2021).
- <sup>233</sup>K. Chen, Q. Hu, T. Liu, L. Zhao, D. Luo, J. Wu, Y. Zhang, W. Zhang, F. Liu, T. P. Russell, R. Zhu, and Q. Gong, *Adv. Mater.* **28**, 10718 (2016).
- <sup>234</sup>W.-H. Chen, L. Qiu, P. Zhang, P.-C. Jiang, P. Du, L. Song, J. Xiong, and F. Ko, *J. Mater. Chem. C* **7**, 10247 (2019).
- <sup>235</sup>J. C. Yu, J. A. Hong, E. D. Jung, D. Bin Kim, S. Baek, S. Lee, S. S. Cho, S. Park, K. J. Choi, and M. H. Song, *Sci. Rep.* **8**, 1070 (2018).
- <sup>236</sup>H. Choi, C. K. Mai, H. B. Kim, J. Jeong, S. Song, G. C. Bazan, J. Y. Kim, and A. J. Heeger, *Nat. Commun.* **6**, 7348 (2015).
- <sup>237</sup>C. Bi, Q. Wang, Y. Shao, Y. Yuan, Z. Xiao, and J. Huang, *Nat. Commun.* **6**, 7747 (2015).
- <sup>238</sup>G. Xu, R. Xue, W. Chen, J. Zhang, M. Zhang, H. Chen, C. Cui, H. Li, Y. Li, and Y. Li, *Adv. Energy Mater.* **8**, 1703054 (2018).
- <sup>239</sup>C. Xu, Z. Liu, and E.-C. Lee, *J. Mater. Chem. C* **6**, 6975 (2018).
- <sup>240</sup>E. H. Jung, N. J. Jeon, E. Y. Park, C. S. Moon, T. J. Shin, T.-Y. Yang, J. H. Noh, and J. Seo, *Nature* **567**, 511 (2019).
- <sup>241</sup>Z. Liu, P. You, C. Xie, G. Tang, and F. Yan, *Nano Energy* **28**, 151 (2016).
- <sup>242</sup>Y. Zhang, M. Elawad, Z. Yu, X. Jiang, J. Lai, and L. Sun, *RSC Adv.* **6**, 108888 (2016).
- <sup>243</sup>J. W. Jung, J. Park, I. K. Han, Y. Lee, C. Park, W. Kwon, and M. Park, *J. Mater. Chem. A* **00**, 12158 (2017).
- <sup>244</sup>J. W. Jo, M.-S. Seo, M. Park, J. Kim, J. S. Park, I. K. Han, H. Ahn, J. W. Jung, B. Sohn, M. J. Ko, and H. J. Son, *Adv. Funct. Mater.* **26**, 4464 (2016).
- <sup>245</sup>H. Zhang, J. Cheng, F. Lin, H. He, J. Mao, K. S. Wong, A. K.-Y. Jen, and W. C. H. Choy, *ACS Nano* **10**, 1503 (2016).
- <sup>246</sup>Q. Wang, Z. Lin, J. Su, Z. Hu, J. Chang, and Y. Hao, *Nano Sel.* **2**, 1055 (2021).
- <sup>247</sup>S. Zhang, H. Wang, X. Duan, L. Rao, C. Gong, B. Fan, Z. Xing, X. Meng, B. Xie, and X. Hu, *Adv. Funct. Mater.* **31**, 2106495 (2021).
- <sup>248</sup>X. Hu, X. Meng, X. Yang, Z. Huang, Z. Xing, P. Li, L. Tan, M. Su, F. Li, Y. Chen, and Y. Song, *Sci. Bull.* **66**, 527 (2021).
- <sup>249</sup>W. Chen, Y. Wu, Y. Yue, J. Liu, W. Zhang, X. Yang, H. Chen, E. Bi, I. Ashraful, M. Grätzel, and L. Han, *Science* **350**, 944 (2015).
- <sup>250</sup>C. Yang and C. Wu, *Sol. Energy Mater. Sol. Cells* **132**, 492 (2015).
- <sup>251</sup>X. Yin, Z. Yao, Q. Luo, X. Dai, Y. Zhou, Y. Zhang, Y. Zhou, S. Luo, J. Li, N. Wang, and H. Lin, *ACS Appl. Mater. Interfaces* **9**, 2439 (2017).
- <sup>252</sup>G. Li, Y. Jiang, S. Deng, A. Tam, P. Xu, M. Wong, and H. Kwok, *Adv. Sci.* **4**, 1700463 (2017).
- <sup>253</sup>F. Ye, W. Tang, F. Xie, M. Yin, J. He, Y. Wang, H. Chen, Y. Qiang, X. Yang, and L. Han, *Adv. Mater.* **29**, 1701440 (2017).
- <sup>254</sup>J. H. Park, J. Seo, S. Park, S. S. Shin, Y. C. Kim, N. J. Jeon, H. W. Shin, T. K. Ahn, J. H. Noh, S. C. Yoon, C. S. Hwang, and S. Il Seok, *Adv. Mater.* **27**, 4013 (2015).
- <sup>255</sup>I. J. Park, G. Kang, M. A. Park, J. S. Kim, S. W. Seo, D. H. Kim, K. Zhu, T. Park, and J. Y. Kim, *ChemSusChem* **10**, 2660 (2017).
- <sup>256</sup>Q. Luo, H. Ma, F. Hao, Q. Hou, J. Ren, L. Wu, Z. Yao, Y. Zhou, N. Wang, K. Jiang, H. Lin, and Z. Guo, *Adv. Funct. Mater.* **27**, 1703068 (2017).
- <sup>257</sup>Z. Liu, J. Chang, Z. Lin, L. Zhou, Z. Yang, D. Chen, C. Zhang, S. (Frank) Liu, and Y. Hao, *Adv. Energy Mater.* **8**, 1703432 (2018).
- <sup>258</sup>B. Zhang, J. Su, X. Guo, L. Zhou, Z. Lin, L. Feng, J. Zhang, J. Chang, and Y. Hao, *Adv. Sci.* **7**, 1903044 (2020).
- <sup>259</sup>X. Yin, P. Chen, M. Que, Y. Xing, W. Que, C. Niu, and J. Shao, *ACS Nano* **10**, 3630 (2016).
- <sup>260</sup>J. He, E. Bi, W. Tang, Y. Wang, Z. Zhou, X. Yang, H. Chen, and L. Han, *Sol. RRL* **2**, 1800004 (2018).
- <sup>261</sup>W. Chen, F. Z. Liu, X. Y. Feng, A. B. Djurišić, W. K. Chan, and Z. B. He, *Adv. Energy Mater.* **7**, 1700722 (2017).
- <sup>262</sup>W. Chen, Y. Wu, J. Fan, A. B. Djurišić, F. Liu, H. W. Tam, A. Ng, C. Surya, W. K. Chan, D. Wang, and Z. He, *Adv. Energy Mater.* **8**, 1703519 (2018).
- <sup>263</sup>J. H. Kim, P. W. Liang, S. T. Williams, N. Cho, C. C. Chueh, M. S. Glaz, D. S. Ginger, and A. K.-Y. K. Y. Jen, *Adv. Mater.* **27**, 695 (2015).
- <sup>264</sup>J. W. Jung, C.-C. Chueh, and A. K. Y. Jen, *Adv. Mater.* **27**, 7874 (2015).
- <sup>265</sup>Q. Wang, C.-C. Chueh, T. Zhao, J. Cheng, M. Eslamian, W. C. H. Choy, and A. K. Y. Jen, *ChemSusChem* **10**, 3794 (2017).
- <sup>266</sup>Z. Wang, X. Rong, L. Wang, W. Wang, H. Lin, and X. Li, *ACS Appl. Mater. Interfaces* **12**, 8342 (2020).
- <sup>267</sup>P. Qin, S. Tanaka, S. Ito, N. Tetreault, K. Manabe, H. Nishino, M. K. Nazeeruddin, and M. Grätzel, *Nat. Commun.* **5**, 3834 (2014).
- <sup>268</sup>J. A. Christians, R. C. M. Fung, and P. V. Kamat, *J. Am. Chem. Soc.* **136**, 758 (2014).
- <sup>269</sup>P. Qin, Q. He, C. Chen, X. Zheng, G. Yang, H. Tao, L.-B. Xiong, L. Xiong, G. Li, and G. Fang, *Sol. RRL* **1**, 1700058 (2017).
- <sup>270</sup>T. Lei, H. Dong, J. Xi, Y. Niu, J. Xu, F. Yuan, B. Jiao, W. Zhang, X. Hou, and Z. Wu, *Chem. Commun.* **54**, 6177 (2018).
- <sup>271</sup>S. D. Stranks, G. E. Eperon, G. Grancini, C. Menelaou, M. J. P. Alcocer, T. Leijtens, L. M. Herz, A. Petrozza, and H. J. Snaith, *Science* **342**, 341 (2013).
- <sup>272</sup>L. Etgar, P. Gao, Z. Xue, Q. Peng, A. K. Chandiran, B. Liu, M. K. Nazeeruddin, and M. Grätzel, *J. Am. Chem. Soc.* **134**, 17396 (2012).
- <sup>273</sup>W. A. Laban and L. Etgar, *Energy Environ. Sci.* **6**, 3249 (2013).
- <sup>274</sup>J. Shi, J. Dong, S. Lv, Y. Xu, L. Zhu, J. Xiao, X. Xu, H. Wu, D. Li, Y. Luo, and Q. Meng, *Appl. Phys. Lett.* **104**, 63901 (2014).
- <sup>275</sup>H. Zhou, Y. Shi, K. Wang, Q. Dong, X. Bai, Y. Xing, Y. Du, and T. Ma, *J. Phys. Chem. C* **119**, 4600 (2015).
- <sup>276</sup>J. Jin, J. Li, Q. Tai, Y. Chen, D. D. Mishra, W. Deng, J. Xin, S. Guo, B. Xiao, and X. Wang, *J. Power Sources* **482**, 228953 (2021).
- <sup>277</sup>Z. Huang, X. Hu, C. Liu, L. Tan, and Y. Chen, *Adv. Funct. Mater.* **27**, 1703061 (2017).
- <sup>278</sup>Y. Tan, B. Xiao, P. Xu, Y. Luo, Q. Jiang, and J. Yang, *ACS Appl. Mater. Interfaces* **13**, 20034 (2021).
- <sup>279</sup>L. Rao, X. Meng, S. Xiao, Z. Xing, Q. Fu, H. Wang, C. Gong, T. Hu, X. Hu, R. Guo, and Y. Chen, *Angew. Chem., Int. Ed.* **60**, 14693 (2021).
- <sup>280</sup>X. Duan, X. Li, L. Tan, Z. Huang, J. Yang, G. Liu, Z. Lin, and Y. Chen, *Adv. Mater.* **32**, 2000617 (2020).
- <sup>281</sup>C. Y. Chang, C. Y. Chu, Y. C. Huang, C. W. Huang, S. Y. Chang, C. A. Chen, C. Y. Chao, and W. F. Su, *ACS Appl. Mater. Interfaces* **7**, 4955 (2015).
- <sup>282</sup>Y. Zhao, J. Wei, H. Li, Y. Yan, W. Zhou, D. Yu, and Q. Zhao, *Nat. Commun.* **7**, 10228 (2016).

- <sup>283</sup>Q. Xue, Z. Hu, C. Sun, Z. Chen, F. Huang, H. L. Yip, and Y. Cao, *RSC Adv.* **5**, 775 (2015).
- <sup>284</sup>L. Zuo, H. Guo, D. W. DeQuilettes, S. Jariwala, N. D. Marco, S. Dong, R. DeBlock, D. S. Ginger, B. Dunn, M. Wang, and Y. Yang, *Sci. Adv.* **3**, e1700106 (2017).
- <sup>285</sup>Y. Guo, K. Shoyama, W. Sato, and E. Nakamura, *Adv. Energy Mater.* **6**, 1502317 (2016).
- <sup>286</sup>M. Kim, S. G. Motti, R. Sorrentino, and A. Petrozza, *Energy Environ. Sci.* **11**, 2609 (2018).
- <sup>287</sup>T. Han, J.-W. Lee, C. Choi, S. Tan, C. Lee, Y. Zhao, Z. Dai, N. De Marco, S.-J. Lee, S. Bae, Y. Yuan, H. M. Lee, Y. Huang, and Y. Yang, *Nat. Commun.* **10**, 520 (2019).
- <sup>288</sup>X. Zheng, Y. Deng, B. Chen, H. Wei, X. Xiao, Y. Fang, Y. Lin, Z. Yu, Y. Liu, Q. Wang, and J. Huang, *Adv. Mater.* **30**, 1803428 (2018).
- <sup>289</sup>D. Bi, C. Yi, J. Luo, J. Décopet, F. Zhang, S. M. Zakeeruddin, X. Li, A. Hagfeldt, and M. Grätzel, *Nat. Energy* **1**, 16142 (2016).
- <sup>290</sup>K. Kim, J. Han, S. Maruyama, M. Balaban, and I. Jeon, *Sol. RRL* **5**, 2000783 (2021).
- <sup>291</sup>C. Wang, Z. Song, D. Zhao, R. A. Awani, C. Li, N. Shrestha, C. Chen, X. Yin, D. Li, R. J. Ellingson, X. Zhao, X. Li, and Y. Yan, *Sol. RRL* **3**, 1900078 (2019).
- <sup>292</sup>Y. Ma, Y. Cheng, X. Xu, M. Li, C. Zhang, S. H. Cheung, Z. Zeng, D. Shen, Y. Xie, K. L. Chiu, F. Lin, S. K. So, C. Lee, and S. Tsang, *Adv. Funct. Mater.* **31**, 2006802 (2021).
- <sup>293</sup>Y. Zhou, Y. Yin, X. Zuo, L. Wang, T. Li, Y. Zhou, N. P. Padture, Z. Yang, Y. Guo, Y. Xue, K. Kisslinger, M. Cotlet, C. Nam, and M. H. Rafailovich, *Chem. Mater.* **32**, 5104 (2020).
- <sup>294</sup>J. Jiang, Q. Wang, Z. Jin, X. Zhang, J. Lei, H. Bin, Z. Zhang, Y. Li, and S. F. Liu, *Adv. Energy Mater.* **8**, 1701757 (2018).
- <sup>295</sup>Y. Zhao, P. Zhu, M. Wang, S. Huang, Z. Zhao, S. Tan, T. Han, J. Lee, T. Huang, R. Wang, J. Xue, D. Meng, Y. Huang, J. Marian, J. Zhu, and Y. Yang, *Adv. Mater.* **32**, 1907769 (2020).
- <sup>296</sup>X. Li, W. Zhang, Y. Wang, W. Zhang, H.-Q. Wang, and J. Fang, *Nat. Commun.* **9**, 3806 (2018).
- <sup>297</sup>G. Liu, C. Liu, Z. Lin, J. Yang, Z. Huang, L. Tan, and Y. Chen, *ACS Appl. Mater. Interfaces* **12**, 14049 (2020).
- <sup>298</sup>Q. Wang, Q. Dong, T. Li, A. Gruverman, and J. Huang, *Adv. Mater.* **28**, 6734 (2016).
- <sup>299</sup>Q. Dong, C. Zhu, M. Chen, C. Jiang, J. Guo, Y. Feng, Z. Dai, S. K. Yadavalli, M. Hu, X. Cao, Y. Li, Y. Huang, Z. Liu, Y. Shi, L. Wang, N. P. Padture, and Y. Zhou, *Nat. Commun.* **12**, 973 (2021).
- <sup>300</sup>S. K. Yadavalli, Z. Dai, H. Zhou, Y. Zhou, and N. P. Padture, *Acta Mater.* **187**, 112 (2020).
- <sup>301</sup>L. Pei, H. Yu, Q. Zhang, J. Li, K. Wang, and B. Hu, *J. Phys. Chem. C* **124**, 2340 (2020).
- <sup>302</sup>L. Gao, L. Chen, S. Huang, N. Chen, and G. Yang, *ACS Appl. Mater. Interfaces* **11**, 17475 (2019).
- <sup>303</sup>J. Kim, J. H. Jang, J. H. Kim, K. Park, J. S. Jang, J. Park, and N. Park, *ACS Appl. Energy Mater.* **3**, 9257 (2020).
- <sup>304</sup>H. C. Weerasinghe, Y. Dkhissi, A. D. Scully, R. A. Caruso, and Y.-B. B. Cheng, *Nano Energy* **18**, 118 (2015).
- <sup>305</sup>Y. Bai, Y. Lin, L. Ren, X. Shi, E. Strounina, Y. Deng, Q. Wang, Y. Fang, X. Zheng, Y. Lin, Z. Chen, Y. Du, L. Wang, and J. Huang, *ACS Energy Lett.* **4**, 1231 (2019).
- <sup>306</sup>V. Babu, R. Fuentes Pineda, T. Ahmad, A. O. Alvarez, L. A. Castriotta, A. D. Carlo, F. Fabregat-Santiago, and K. Wojciechowski, *ACS Appl. Energy Mater.* **3**, 5126 (2020).
- <sup>307</sup>X. Dai, Y. Deng, C. H. Van Brackle, and J. Huang, *Int. J. Extreme Manuf.* **1**, 22004 (2019).
- <sup>308</sup>Y. Deng, X. Zheng, Y. Bai, Q. Wang, J. Zhao, and J. Huang, *Nat. Energy* **3**, 560 (2018).
- <sup>309</sup>X. Dai, Y. Deng, C. H. Van Brackle, S. Chen, P. N. Rudd, X. Xiao, Y. Lin, B. Chen, and J. Huang, *Adv. Energy Mater.* **10**, 1903108 (2020).
- <sup>310</sup>Y. Galagan, F. D. Giacomo, H. Gorter, G. Kirchner, I. de Vries, R. Andriessen, and P. Groen, *Adv. Energy Mater.* **8**, 1801935 (2018).
- <sup>311</sup>S. Das, B. Yang, G. Gu, P. C. Joshi, IN. Ivanov, C. M. Rouleau, T. Aytug, D. B. Geohegan, and K. Xiao, *ACS Photonics* **2**, 680 (2015).
- <sup>312</sup>A. Gheno, Y. Huang, J. Bouclé, B. Ratier, A. Rolland, J. Even, and S. Vedrine, *Sol. RRL* **2**, 1800191 (2018).
- <sup>313</sup>X. Meng, X. Hu, Y. Zhang, Z. Huang, Z. Xing, C. Gong, L. Rao, H. Wang, F. Wang, T. Hu, L. Tan, Y. Song, and Y. Chen, *Adv. Funct. Mater.* **31**, 2106460 (2021).
- <sup>314</sup>S. M. F. Cruz, L. A. Rocha, and J. C. Viana, in *Flexible Electronics* (InTech, 2018), pp. 60–61.
- <sup>315</sup>Y. H. Yeh, C. C. Cheng, M. J. Yu, C. Y. Lin, B. C. M. Lai, H. T. Lin, H. C. Ku, C. M. Leu, and Y. L. Tseng, in *Digest Technical Papers-SID International Symposium (SID Symposium Digest of Technical Papers, 2012)*, Vol. 43, p. 345.
- <sup>316</sup>K. Fukuda, K. Yu, and T. Someya, *Adv. Energy Mater.* **10**, 2000765 (2020).
- <sup>317</sup>J. Huang, H. Zhu, Y. Chen, C. Preston, K. Rohrbach, J. Cummings, and L. Hu, *ACS Nano* **7**, 2106 (2013).